INVESTIGATION OF THE HOT DEFORMATION OF SINTERED TITANIUM COMPACTS PRODUCED FROM DIRECT REDUCTION POWDER

A thesis submitted to the Faculty of Engineering and the Built Environment, University of Cape Town, in fulfilment of the requirements for the degree of Master of Science in Engineering

By: Shaheeda Petersen

Centre for Materials Engineering

2010

ABSTRACT

The focus of this study was the use of powder metallurgy to produce low cost titanium with comparative mechanical properties to wrought titanium. The objectives of this investigation was to produce sintered titanium compacts that represented metal made by the Direct Powder Rolling method. The critical strain (ε_C) required to induce recrystallization following deformation was determined by hot compressing wrought titanium samples. Finally sintered titanium samples were hot compressed at ε_C and the changes to the microstructure, porosity and mechanical properties was assessed.

A testing facility was designed and assembled to simulate uniaxial hot compression which allowed a study of the deformation and microstructural response under specific conditions to be done. The testing facility consisted of an induction heating system and alumina ceramic compression platens enclosed by a quartz glass cylinder which was sealed with a stainless steel base and cover plate. The system was operated under vacuum. Commercially pure titanium (CP-Ti) in wrought and sintered powder forms underwent hot compression testing. The sintered powder samples were produced from direct reduction powder which was uniaxially compacted in an air environment and sintered separately in a vacuum furnace at 1200°C to obtain partial density. Hot compression was limited to uniaxial compression and thus did not directly simulate the plane strain condition that occurs in conventional rolling. The wrought CP-Ti samples were hot compressed at 800°C, 900°C and 1000°C to a nominal strain of 0, 0.2 and 0.5. The sintered CP-Ti samples were hot compressed at 900°C to a nominal strain of 0.2, 0.5 and 0.65. The deformed microstructures were rapidly cooled to room temperature and subsequently annealed at 870°C. Microstructural analysis using optical light microscopy and microhardness testing was performed on all deformed samples before and after post deformation annealing. The microstructures of both the wrought and the sintered CP-Ti samples were observed to have a strain gradient through the sample after deformation. Microhardness testing was performed on the hot compressed samples through the midsection where the highest amount of internal strain was retained.

The hot compression testing of the wrought CP-Ti was performed in order to determine the testing parameters for the sintered CP-Ti. The results of the hot compression testing and the analysis of the deformed microstructures showed that the best combination of temperature and strain that resulted in the highest amount of retained internal strain was at a temperature of 900°C and a nominal strain =0.5.The initiation of recrystallization could not be observed in the as deformed wrought CP-Ti samples but were clearly observed after post deformation annealing. The hot compression testing of the sintered CP-Ti compacts at 900°C and various nominal strains resulted in the reduction of porosity in the samples as well as the deformation of the microstructure which resulted in an increase in hardness. It was also found that partial recrystallization was occurring in the samples which had undergone hot compression testing under the nominal strains of 0.5 and 0.65. Microhardness testing showed that there was an increase in the hardness of the hot compressed sintered CP-Ti samples with increasing nominal strain due to work hardening, the collapse and subsequent reduction in porosity and/or the refinement of grain structure by recrystallization. In the sintered CP-Ti samples the post deformation annealing resulted in the further recrystallization of the grains which were deformed during hot compression. Thus the investigation concluded that the hot compressing of sintered CP-Ti is an excellent method of improving the microstructure and hence the mechanical properties of sintered CP-Ti. This could lead to increase in the use of sintered CP-Ti products made from direct reduction powders in many industries which need the lightweight properties of CP-Ti without the cost.

ACKNOWLEDGEMENTS

I would like to thank everyone who assisted and supported me throughout the duration of this project:

- The Advanced Manufacturing Technology Strategy (AMTS) and the National Research Foundation (NRF) for their financial support
- My supervisor – Prof R.D Knutsen and my co-supervisor – Prof C Lang for their supervision and guidance
- Dr D Blaine of the University of Stellenbosch for assistance in sourcing material and for providing technical assistance with the pressing of samples
- Ms Penelope Park-Ross for advice and technical assistance in the laboratory
- Mr Glen Newins, Mr Horst Emrich, Mr Hubert Tomlinson and all the staff of the workshop for preparing my samples and helping with the design and assembly of my testing rig
- Ms Miranda Waldron from the Electron Microscope Unit for assisting me with the SEM analysis
- Mr Chetan Chhiba for assistance with the mechanical drawings
- All the students and staff at the Centre for Materials Engineering for their support, assistance and friendship

To my family and friends who stood by me throughout this thesis project. Without their support none of this would be possible

DECLARATION

I, Shaheeda Petersen, know the meaning of plagiarism and declare that all the work in this document, save for that which is properly acknowledged, is my own.

Signature:_____

Date:_____

TABLE OF CONTENTS

1 INTRODUCTION

1.1 Subject of thesis

The subject of this thesis is the investigation of the hot deformation of sintered titanium compacts made from direct reduction powder.

1.2 Background to thesis

Titanium and its alloys are amongst the most important advanced materials used in aerospace and terrestrial systems today. This is because of the excellent combinations of specific mechanical properties and corrosion resistance of titanium alloys.

Table 1.1 Properties of Commercially Pure titanium [1]

Property	**Value**
Density	4.51 g/cm^3
Minimum Yield Stress	480 MPa
Minimum Ultimate Tensile Strength	550 MPa
Young's Modulus of Elasticity	102.7 GPa
Hardness	265 (Brinell)
Coefficient of Thermal Expansion	8.64 x 10^{-6}/°C
Solidus/Liquidus	1725°C
Melting Point	1668±10°C
Specific Heat (25°C)	0.518 J/kg K

Table 1.2 Composition of Commercially Pure (CP) titanium [2]

Element	**Weight %**
Titanium	99.67
Carbon	0.08
Iron	0.03
Nitrogen	0.03
Oxygen	0.18
Hydrogen	0.015

Titanium is not as widely used as other competing materials due to the high cost of producing titanium metal. This has led to the development of more cost effective methods of producing titanium mainly through powder metallurgy. There are many types of titanium powder metallurgy processes but the process which we will be simulating experimentally is that of Direct Powder Rolling (DPR).

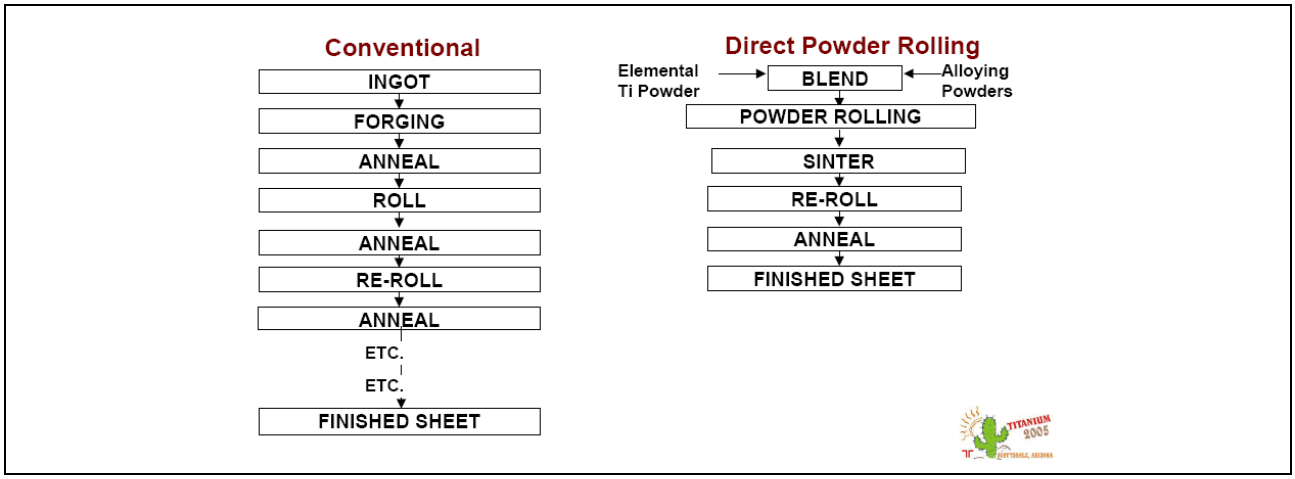

Figure 1.1 Comparison of the conventional titanium sheet making process with the Direct Powder Rolling process [3]

From figure 1.1 it can be seen that the Direct Powder rolling process has significantly less steps than the conventional ingot process. This results in the DPR titanium sheet being substantially less expensive than the conventionally made titanium sheet. However the mechanical properties of titanium made via powder metallurgical processes are lower than that of conventionally made titanium. [3]

In order to improve these properties the material has to undergo thermal processing such as hot rolling. During hot rolling the microstructure of the material evolves and porosity is reduced. A phenomenon known as Dynamic Recrystallization (DRX) occurs which results in refinement of the microstructure and therefore an improvement of the mechanical properties. [4] DPR uses direct reduction titanium powder also known as titanium sponge fines. This type of powder is the product of the Kroll Process of titanium extraction from Rutile (TiO_2). This powder is cheaper to use than other forms of titanium powder as it has not undergone a melting step which is quite costly as titanium has a high melting temperature.

1.3 Objectives of thesis

The objectives of the thesis are therefore to:

- Design and build a hot compression testing rig to simulate the hot deformation process
- Produce sintered titanium compacts that represent metal made by the Direct Powder Rolling method
- Determine the critical strain (ε_c) needed to induce dynamic, metadynamic or static (following the deformation event) recrystallization
- Hot compress samples at ε_c and evaluate the changes in microstructure, porosity and mechanical properties

1.4 Scope and limitations

This thesis only refers to sintered titanium compacts made from Commercially Pure titanium powder produced from sponge fines. The green compacts were made via uniaxial pressing in an air environment and not under vacuum. The sintering occurred as a separate process under a high vacuum to prevent oxidation. The sintered compacts are not fully dense and do contain porosity. The hot compression of the sintered titanium compacts occurs under high vacuum. Hot compression is limited to uniaxial compression and thus does not directly simulate the plain strain condition that occurs during conventional "rolling".

1.5 Plan of development

The thesis begins with a literature review of important topics related to the manufacture of titanium powder, powder metallurgy and hot deformation. It then provides detail of the design of the testing rig and the compaction and sintering of the sample. This is then followed by a detailed account of the testing methodology used. The results of the testing are then analysed and discussed. Comparison of the results of the testing to that of the calibration standards and the original sintered compact follows and the microstructural evolution is assessed. The changes in hardness measurements of the sintered samples are then compared to the samples which had been hot compressed. The report will be concluded with recommendations for future work.

2 LITERATURE REVIEW

2.1 Titanium

2.1.1 Introduction

Titanium is a structural metal and is both corrosion resistant and lightweight. It has many advantages as a structural material due to its low density (4.51 $g.cm^{-3}$), low coefficient of thermal expansion, good corrosion resistance and a good strength to weight ratio [5]. Titanium also has good oxidation resistance at intermediate temperatures which do not exceed 400°C. Titanium has a melting point of 1670°C but it is known to combust at temperatures exceeding 400°C. This makes pure titanium unsuitable for components which would experience harsh environments where the titanium component would be in contact with other metals at high temperature. The global production of titanium and its alloys is very small in comparison to that of steel and 80% of all titanium produced is used by aerospace industries. [6]

2.1.2 Alpha (α) and Beta (β) titanium

Titanium has two stable allotropic forms namely alpha (α) and beta (β). At ambient temperature and pressure, the crystal structure is close packed hexagonal with a/c ratio of 1.587. [6]

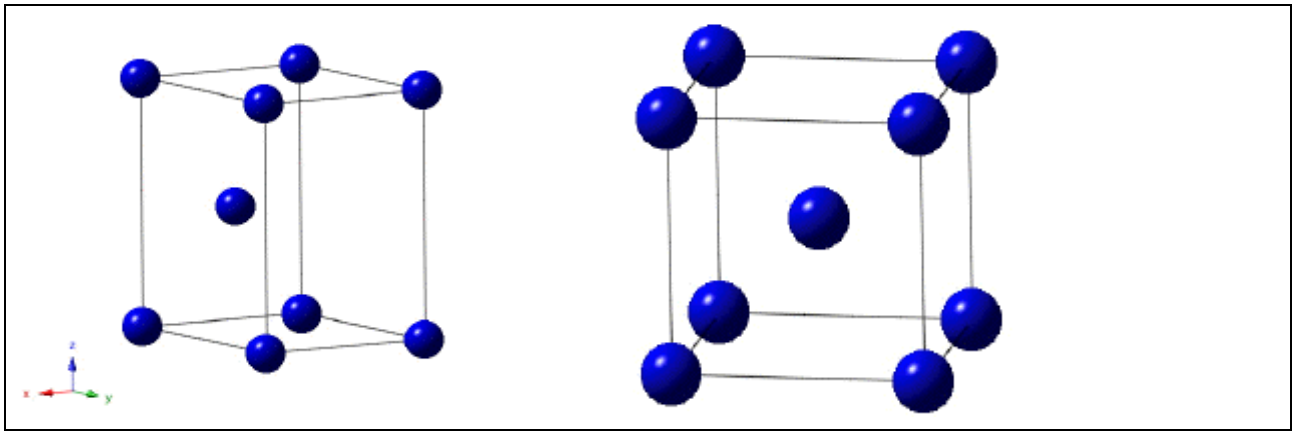

Figure 2.1.Crystal structure of α-titanium [6]

Figure 2.2. Crystal structure of β-titanium [6]

At approximately 890°C, the titanium crystal structure undergoes an allotropic transformation to a body-centred cubic β phase, which is stable up to the melting temperature. [7]

2.2 Titanium powder metallurgy

2.2.1 Introduction

Titanium alloys are considered to be the most important of the advanced materials and are essential to the manufacture of high performance aerospace components. This is due to the specific mechanical properties (normalised by density) and outstanding corrosion resistance provided by titanium alloys. The high cost of the titanium alloys in comparison with other structural metals limits their use. This has led to the investigation of cost reducing processes such as powder metallurgy techniques. [8]

2.2.2 Production of titanium powders

The titanium powders that are currently available are formed via four distinctive processing methods. These are: Atomised powders which are generally prealloyed and spherical in shape; Hydride-dehydride powders which are generally prealloyed and are angular in nature; Sponge fines are “sponge-like” in nature and contain remnant salts which prevent the achievement of full density and negatively affect weldability and powders produced by Reverse Electrolysis process. [8]

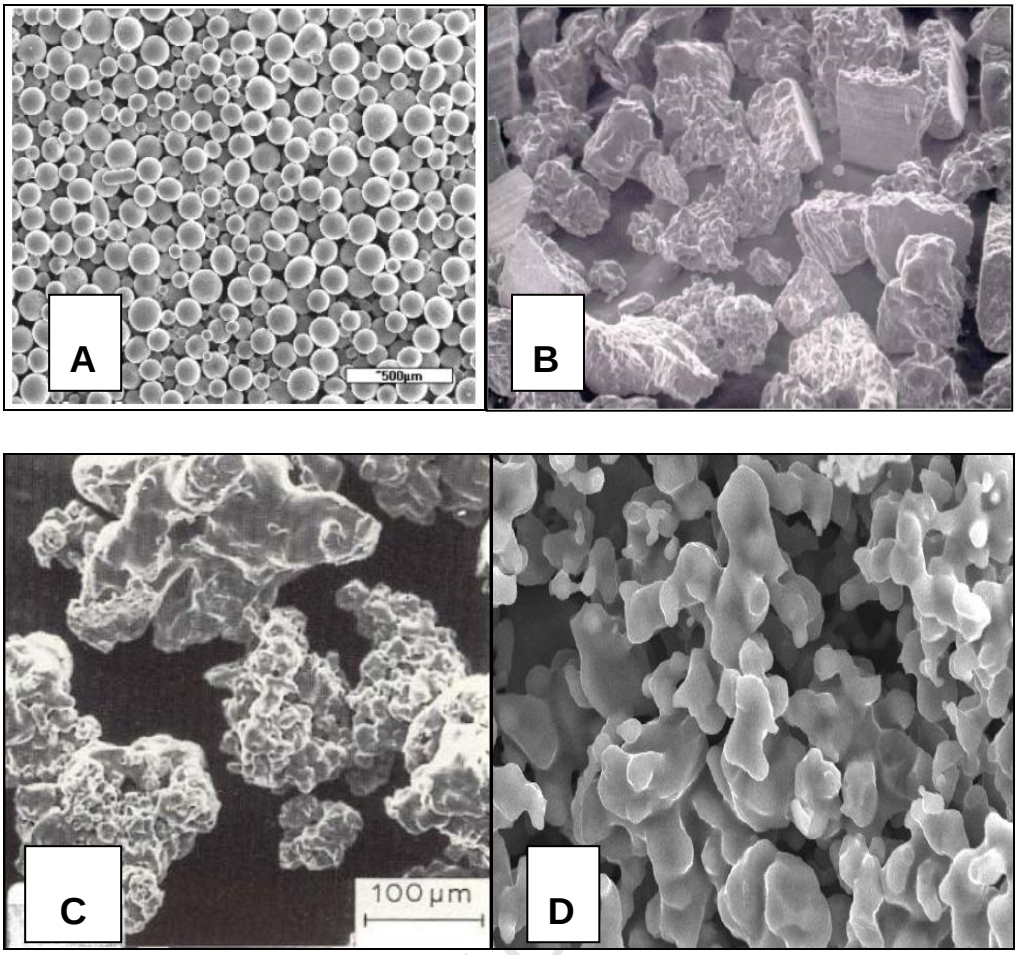

Figure 2.3A: SEM photomicrograph of gas atomised spherical prealloyed Ti-6Al-4V; 2.3B. SEM photomicrograph of the powder produced by Ti sponge fines (Hydride-dehydride process); 2.3C: Al-Ti process sponge and 2.3D. SEM photomicrograph of titanium powder produced by the FFC reversed electrolytic process [8]

Atomised powders

In water and gas atomisation the starting material is melted, metallurgically treated in a separate furnace and then fed into a tundish. [9] The tundish acts as a reservoir which supplies a constant controlled flow of molten metal to the atomisation chamber. As the metal stream exits the tundish it is struck by a high velocity stream of atomising medium which can be water, air or an inert gas. The molten metal stream is disintegrated into fine droplets which fall through the atomisation tank and collect at the bottom. Another alternative method would be to use centrifugal force to break up the liquid as it is removed from the periphery of a rotating electrode or spinning disk/cup. [10]

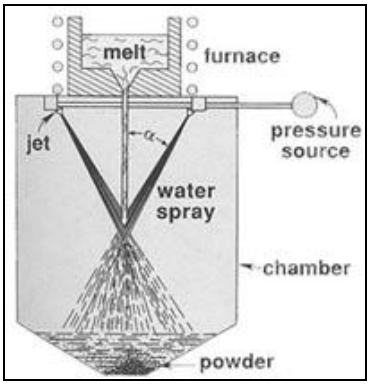

Figure 2.4: Water atomisation process [10]

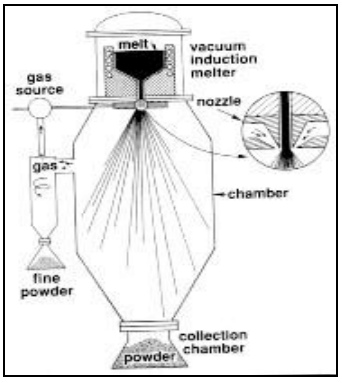

Figure 2.5 Gas atomisation [10]

Hydride-dehydride processes

The hydride processing route enables very fine and highly reactive powders to be produced from metals which are capable of forming solid hydrides. The hydrides are obtained by the reaction of metal with molecular hydrogen at elevated temperatures under a suitable partial pressure. They are brittle, can be powdered easily and dissociated in a vacuum at similar or higher temperatures than that at which they were formed. [9]In the hydride-dehydride (H/D) process, the alloy material is converted to a hydride by absorbing a significant amount of hydrogen gas, thus embrittling the material so that it can be easily crushed or ground to a fine particle size. The powder is then reheated slowly and the hydrogen is pumped off under vacuum. This process also yields the possibility of obtaining powders from secondary raw material. [11] The metal powders produced from hydrides are highly reactive and often pyrophoric; depending on the dissociation conditions. Special precautions, such as inert gas absorption on the powder surfaces, are needed in order to avoid instantaneous ignition on exposure to air. [9]

Sponge fines

The conventional process for producing titanium from titanium oxide is a multistep process involving the conversion of the oxide to a chloride followed by the reduction of the chloride to a metal. [12] Currently all titanium metal production begins with Rutile (TiO_2). Rutile is combined with petroleum coke and chlorinated in a fluid bed reactor at 1000°C to produce $TiCl_4$. [13]

$$TiO_2 + 2Cl_2 + C \leftrightarrow TiCl_4 + CO_2$$

Conventionally, titanium sponge is produced using the Kroll process. The Kroll process starts with the reduction of $TiCl_4$ by magnesium at a temperature above 800°C. [12]

$$TiCl_4 + 2Mg \rightarrow Ti + 2MgCl_2$$

$MgCl_2$ is periodically tapped off as the reduction proceeds. This by-product is leached out to obtain sponge titanium with chloride contamination levels of 1,500 ppm or less.

The cost of titanium production is high because of the large consumption of energy, problems associated with the elevated temperatures involved and difficulties associated with the removal of $MgCl_2$. [12] Titanium sponge fines can also be made via the Hunter process. The Hunter process is very similar to the Kroll process except that magnesium is replaced by sodium. Even though the processes are similar, the Hunter process is slightly more expensive and the process exists only to supply a small speciality high purity powder market. [13]

Fray Farthing Chen (FFC Cambridge) reverse electrolytic process

In this process, TiO_2 is pressed into pellets and becomes the cathode in a 950°C calcium chloride ($CaCl_2$) bath. A graphite electrode is the anode. When a current is applied, the oxygen is ionized and dissolves into the $CaCl_2$ bath. Because the monovalent oxygen is in the solution, the problem of divalent titanium ions is eliminated. This method can produce titanium with only 60 ppm oxygen even when the titanium is produced on a kilogram scale. Since the route begins with Rutile it appears that this process will produce titanium at significantly lower cost than the other processes. [10]

2.2.3 Powder preparation

Specific properties of powders affect the ease of shaping, handling, compaction and sintering. The operations that can occur in the precompaction stage are classification, blending, mixing, agglomeration, de-agglomeration, annealing, cleaning and lubrication. The precompaction steps are designed to adjust the powders for easier processing. [14]

Classification of a powder is done using screens or air classifiers which remove selective size fractions. Classification is also used in the sizing of powders. Mixing and blending are two common precompaction steps, they both combine powders into a homogenous mass. Blending is a combining of different sized particles of the same chemistry and mixing implies different powder chemistries. Powders are blended to achieve control of the particle size distribution. Powders with a small particle size are often added to a coarser particle size powder to aid sintering as the coarse powder is easier to compact but exhibits poor sinter strength. Powders can be mixed to form new compositions. Mixed powders provide a basis for forming alloys by diffusional homogenization during sintering or for the incorporation of second phase. Prealloyed powders are much more difficult to press than elemental powders because of their high work hardening rate and high hardness. The prealloyed powders require higher compaction pressures which result in rapid tool wear. Mixed powders are not as hard and do not work harden as quickly during compaction thus making the pressing operation easier. Mixed powders undergo homogenization during sintering. [14]

In some shaping operations a binder is used to mould the powders. This binder must be homogenously mixed with the powder. Organic lubricants are mixed with the powders to provide easier part ejection from compaction tooling and longer die life.

With very hard powders binders are added to improve green strength, which is the strength of the compact before sintering. The lubricants and/or binders are evaporated out of the compacts during the sintering process. [14]

Attritioning of powders before compaction is only necessary for powders which have formed diffusion bonds during fabrication. Attritioning and de-agglomeration are useful when a fine, discrete powder is needed. Alternatively small powders which exhibit a high interparticle friction can be agglomerated into clusters for better flow in automatic forming equipment. Many powder handling procedures either contaminate or damage the powder. To remove the surface or microstructural damage it is appropriate to thermally reduce the surface oxides and anneal the particles. [14]

Safety considerations

Certain powders have harmful effects on workers exposed to them. Powder handling requires safety precautions and cleanliness. Respirable powders are a major health concern and can cause disease and lung dysfunction. The smaller the particle size the larger the potential health hazard. Another hazard with metal powders is their thermal instability in the presence of oxygen. Metal powders are pyrophoric (burn in air) and potentially explosive. A dust free environment must be maintained as metals like titanium and magnesium can ignite in air at concentrations on the order of 40 $g.m^{-3}$. The ignition can occur at relatively low temperatures ranging from 200°C to 700°C. Such dangers necessitate clean handling of metal powders. Measures to minimize pyrophoric reactions include venting, controlled oxidation, surface coatings and minimization of spark and heat sources. [14]

Powder de-agglomeration

Small particles pose special difficulties in powder metallurgy processing because of agglomeration. Agglomeration, which can be induced by a wetting liquid, makes packing, flow, mixing, compaction and sintering more difficult. De-agglomeration is achieved by milling or surface treatments. Agglomeration occurs because of high surface area and the action of weak forces. The common weak forces are van der Waal's attraction, electrostatic charges, chemical bonding, capillary liquid forces and magnetic forces. The van de Waal's force acts over a distance of ± 100 nm and is the most significant for particles below the 0.05µm in size. Agglomeration can also occur during mixing due to cold welding at particle contacts or during annealing at low temperature due to sinter bonding of small particles. An uncontrolled cause of agglomeration is atmospheric vapours mainly consisting of water, condensing on the powders surface. [14]

Small particles are the main cause of agglomeration. In powders with a wide particle size distribution, the smallest particles exert a strong effect on the large particles. Alternatively, agglomeration can be used selectively to minimize size segregation in a powder.

A simple technique to de-agglomerate a coarse powder is to lightly mill it in a dry atmosphere. The impact breaks apart otherwise stable agglomerates.

Jar mills with balls, cylinders or rods are appropriate for many powders. Sufficient shear forces are created to break apart agglomerates without necessarily fracturing, working or deforming the powder. The de-agglomeration rate varies with the number of ball collisions per unit time. For smaller particles it is more effective to use surface active agents to induce repulsive forces. Some common additives are polyvinyl alcohol, steric acid, sodium oleate, glycerine and oleic acid. These additives reduce interparticle friction by lubricating surfaces via short-range repulsive forces. Generally, particle flow and packing are improved by the presence of the appropriate surface active agent. [14]

Particle size and shape

Interparticle friction can arise from irregularities on the particle surface. The greater the surface roughness or the more irregular the particle shape the lower the packing density, the higher the angle of repose and the slower the powder flow. The highest density is associated with smooth spherical particles with hard surfaces. The use of vibration or lubricants can help attain high packing density but problems may arise with agglomeration or size segregation. A tumbling action proves effective in smoothing surface asperities on rough powder and for distributing a coating on the powder. The tumbling action minimises particle attritioning but is effective in de-agglomerating. This results in an increase in packing density. Larger balls in the mill collide with greater energy and alter the particle shape. The stored energy from this milling treatment decreases the temperature needed for sintering. [14]

Particle packing

Particle packing is important in most forming processes. The packing density dictates the die fill, binder content and shrinkage in sintering. Random packing structures are typical of powder metallurgy processing. While fractional density is between 0.6 and 0.64 for monosized spheres, the actual density depends on the powder characteristics, namely the size, shape and other factors that include the adsorbed moisture.

For common metal powders the packing density ranges from 30 to 65% of the theoretical; the lower value is representative of irregular and sponge powders. The greater the surface roughness or the more irregular the particle shape, the lower the packing density. For particles with the same size but different particle shapes, the packing density will decrease as the shape departs from the equiaxed. As the particle shape becomes more rounded the packing density increases. [14]

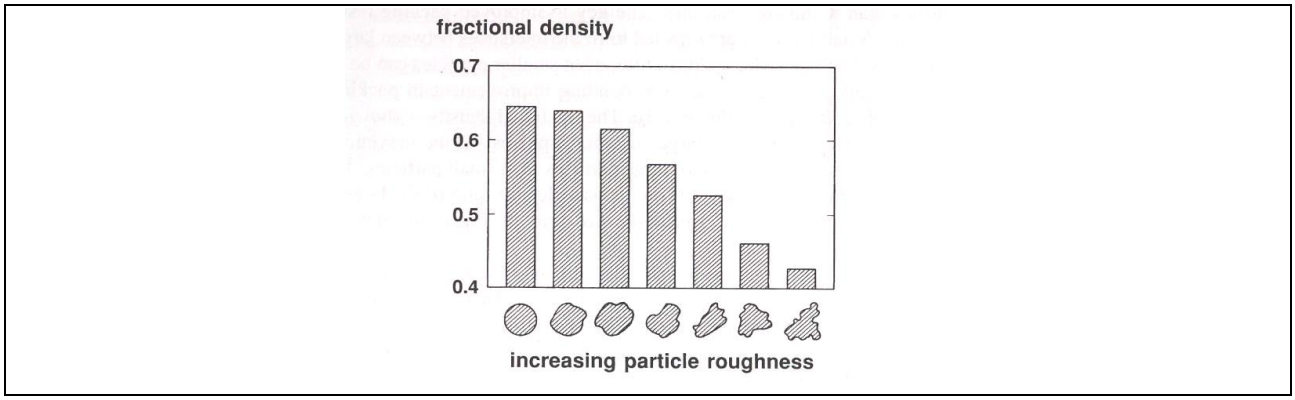

Figure 2.6: A plot of fractional density for monosized powders versus the roughness as expressed by a typical particle profile. The packing density depends on the particle roughness and irregularity. [14]

Improved packing techniques

To overcome the inherent packing limits of a powder, it is possible to tailor the particle size distribution for a higher packing density. Bimodal particle blends can pack to higher densities than monosized particles. The key to improved packing lies in the particle size ratio. Small particles are selected to fit into the interstices between larger particles without forcing the large particles apart. In turn even smaller particles can be selected to fit into the remaining pores, giving a corresponding improvement in packing density. The fractional packing density is shown as a function of the composition for a mixture of large and small spheres. At maximum packing density the powder composition has a greater volume of large particles than small particles .The relative improvement in packing density depends on the particle size ratio of small and large particles. Within a limited range the greater the size ratio the higher the maximum packing ratio. [14]

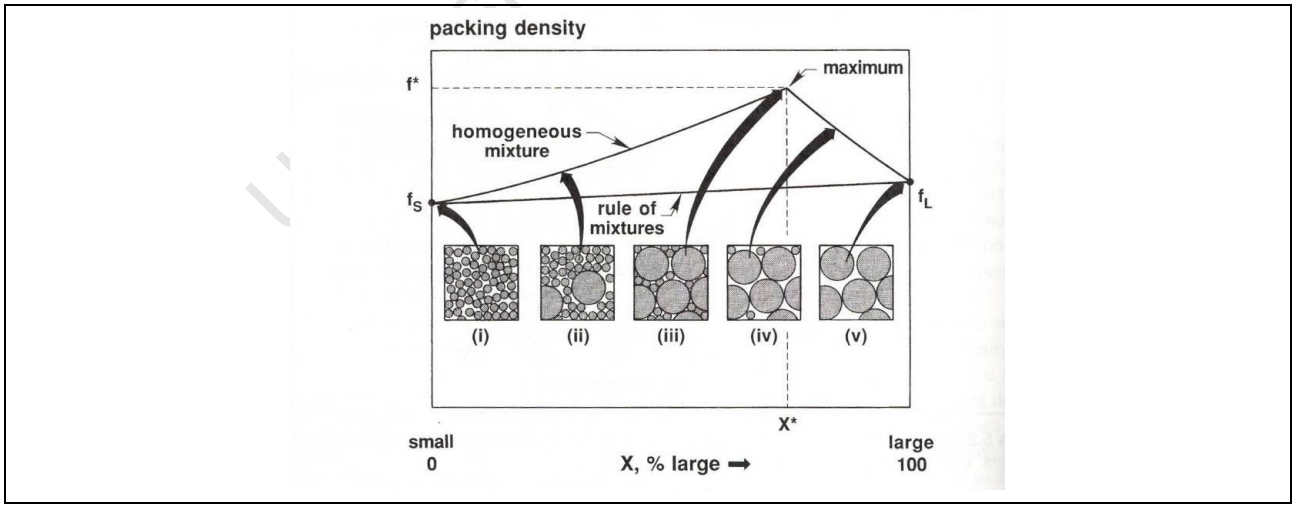

Figure 2.7: A plot of the fractional packing density versus composition for bimodal mixtures of large and small spheres. The sketches show how the density improves up to the critical point where the large particles are closely packed and the small particles fill the interstitial voids. [14]

Beginning with large particles the packing density initially increases as small particles are added to fill the voids between the large particles. Eventually the small particles fill all of the spaces between the large particles. Further additions force large particles apart and no longer improve packing density. If our starting powder consists of small particles, clusters of small particles and their associated voids can be removed or replaced by large particles. Large particles are considered fully dense as the same area occupied by small particles would have spaces between the particles, a porous region is replaced with a full density region everywhere a large particle is added. The packing benefit of replacing small particles with large particles continues until a concentration where the large particles come in contact with one another.

The point of maximum packing density corresponds to the intersection of those two curves. At this point the large particles are in point contact with one another and all the interstitial voids are filled with small particles. The optimal composition in terms of weight fraction of large particles X^* depends on the amount of space between large particles, which equals $1\text{-}f_L$, where f_L is the fractional packing density of large particles,

$$X^* = f_L / f^* \quad [11]$$

With the packing density at the optimal composition f^* given as,

$$f^* = f_L + f_S(1 - f_L) \quad [11]$$

And the fractional packing density for small particles is f_S.

In non spherical particles as with spheres, the density increase is associated with blending different particle sizes of similar shapes. However a major difference between the spherical and non spherical particles is that the initial packing is generally higher for spheres. The greater the surface roughness, shape irregularity or particle aspect ratio then the lower the inherent packing density. The relative density gain is similar for spherical and non-spherical particles when combining different particle sizes although the starting density for the non-spherical particles is lower. [14] Wide particle size distributions give higher packing densities up to a limiting value estimated to range between 0.82 and 0.96. Those values are comparable with fractional densities attainable with bimodal and trimodal mixtures with large particle size ratios. Optimal packing occurs when the particle size distribution can be described by the Andreasen equation:

$$W = AD^q \quad [10]$$

Where W is the weight fraction of particles less than size D, A and q are empirical constants used to fit particle size distribution. The observed maximum density occurs for q values between 0.5 and 0.67. A high proportion of small particles help fill the voids between the nearly continuous matrix of large particles. For every mixture involving unequal sizes there is a composition that will optimize the packing density. For optimal packing the largest particles form a fixed skeleton so that successively smaller particles fill the remaining voids.

Inhomogeneities in the structure degrade the packing density, thus it is very difficult in practice to obtain the model packing densities. [14]

Powder lubrication

Friction between the die wall and the powder during pressing is a fundamental problem. As compaction pressure is increased, ejection of the powder mass from the die becomes more difficult. Consequently, lubricants are used to minimise die wear and ease ejection. There are two means of lubricating a pressing die; die wall and powder lubrication. Die wall lubrication is preferred in theory but is not easy to incorporate into automatic compaction equipment. Therefore lubricants are usual mixed with the metal powder as a final step before pressing. Typical concentrations are between 0.5 and 1.5 wt. %. For metal powders stearate powders based on Al, Zn, Li, Mg, or Ca are in common use. The molecular chains contain 12 to 22 carbon atoms. The chains are surface active and melt at relatively low temperatures.

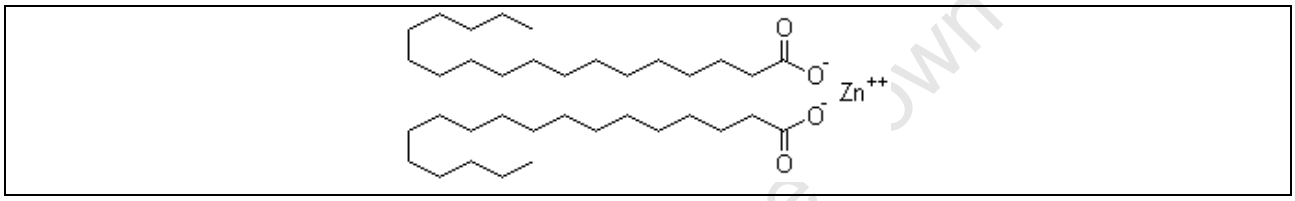

Figure 2.8: Molecular formula of Zinc Stearate [15]

The stearate is added to the metal powder in small spherical form with a mean size of 10 to 30 μm. Other lubricants include waxes and cellulose additives. During formation of the compact the lubricant forms a fluid that lowers friction by creating a thick film of high viscosity polymer. Low viscosity fluids are not effective since they will be forced away from the friction points by the high pressures used in powder compaction. [14]

2.2.4 Compaction

Most applications for powder metallurgy dictate that higher densities need to be attained in the final product. Powder densification can be achieved through one of three methods: i) sinter a low density perform to increase density, ii) press to a high density followed by sintering or iii) simultaneously press and sinter using a full density technique. Powders that exhibit good sintering densification can be shaped using low pressures, often with the aid of an organic binder. Injection molding is an example of that process. Compaction relies on an external source for deforming the powders into a high density component that approaches its final geometry.

The means of delivering that pressure to the powder, the mechanical constraints and the rate of pressurisation are the main process parameters which determine the resulting density. Densification by compaction processes involves particle deformation. [14]

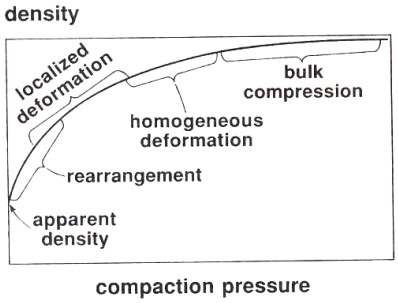

Figure 2.9: A sketch of the density versus compaction pressure during metal powder compaction, showing key stages and declining compressibility as the density increases [14]

At the beginning of a compaction cycle the powder has a density approximately equal to the apparent density. Voids exist between the particles, and even with vibration the highest obtainable density is only the tap density. For loose powder there is an excess of void space, no strength and low coordination number (number of touching particles). As rapid pressure is applied, the first response is the rearrangement of particles filling large pores, giving a higher packing coordination. This is analogous with vibrating the powder. Rearrangement is aided by hard, smooth particle surfaces. [14]

Increasing the pressure provides better packing and leads to a decreasing porosity with the formation of new particle contacts. The point contact undergoes elastic deformation and at all points in the compaction cycle a residual elastic energy is stored in the compact. High pressures increase density by contact enlargement through plastic deformation. The pressure causes localised deformation at the contacts giving work/strain hardening and allowing new contacts to form as gaps between the particles collapse. [14]

The interparticle contact zone takes a flattened appearance with a circular profile. The green density ρ and the diameter of the circular profile X are related as follows:

$$X = D[1-(\rho_0/\rho)^{2/3}]^{1/2} \quad [11]$$

Where D *is* the particle diameter and $\boldsymbol{\rho_0}$ is the initial density corresponding to $X = 0$. The subsequent bond strength depends on the amount of shear at particle contacts. The maximum shear stress occurs at the centre of the contact and is highest when the contact is small. During deformation cold welding at the interparticle contacts contributes to the development of strength in the compact. The strength after pressing but before sintering is termed the green strength. [14]

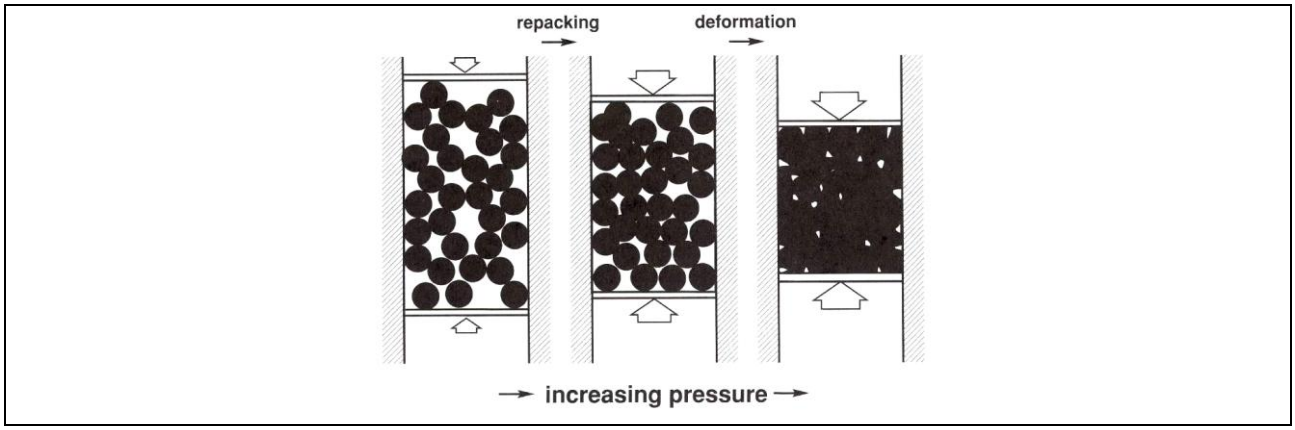

Figure 2.10: A simplified view of the stages of metal powder compaction. Initially repacking occurs with the elimination of particle bridges. With higher compaction pressures particle deformation is the dominant mode of densification. [14]

In the figure above we can see that as the compaction pressure increases, relative volume of each particle undergoing plastic deformation increases. [14]

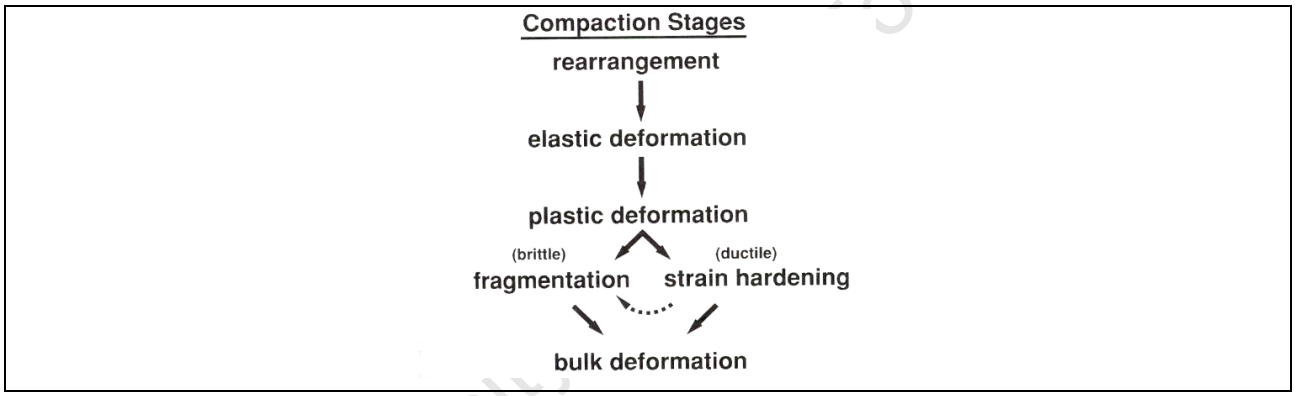

Figure 2.11: A flow chart of the compaction process, giving the key differences in the behaviour of ductile and brittle powders [14]

At low pressures plastic flow is localised to particle contacts. As the pressure increases homogeneous plastic flow spreads from the contacts and the entire particle becomes work hardened. The large pores are eliminated first and the particle coordination number increases to further distribute the load. Consequently, further gains in pressed density (green density) require even greater expenditures of energy from an external pressure source.

With considerable work hardening or brittle materials, densification can occur by fragmentation. The compact surface area increases due to fragmentation; however the strength shows little improvement. The hardness and the work hardening behaviour both influence compaction. Likewise a small particle size hinders compaction because of high interparticle friction and higher particle work hardening rate. At very high compaction pressures, in excess of 1GPa, massive deformation occurs leaving only small pores. Continual pressurisation beyond that level is of little benefit.

The material response is similar to that of a dense solid. In all cases relief of the pressure results in relaxation of the material with a release of the stored elastic energy noted by dimensional spring back. The elastic relaxation is shown by the compacts failure to fit back into the die cavity after ejection. The level of spring back increases with approximately the square of the compaction pressure. [14]

2.2.5 Sintering

Introduction

Sintering is the bonding together of particles at high temperatures. It can occur at temperatures below the melting point by solid-state atomic transport events, but in many instances involves the formation of a liquid phase. On a microstructural scale the bonding occurs as cohesive necks grow at the particle contacts. Such neck growth causes the property changes. [14]

Particles sinter by atomic motions that eliminate the high energy surface associated with powder. The surface energy per unit volume depends on the inverse of the particle diameter. Typically the surface energy is assessed by the surface area. Thus, smaller particles with high specific surface areas have more energy and sinter faster. However, not all surface energy is available for sintering. For a crystalline solid, nearly every particle contact will evolve a grain boundary with associated grain boundary energy. The grain boundaries, important to atomic motion, are defective regions with high atomic mobility. The sintering mechanism describes the path of atomic motion which produces the mass flow. For metal powders, the mechanisms are usually diffusion processes over the surfaces, along the grain boundaries, or through the crystal lattice. The stages of sintering follow a geometric progression. They relate to the driving force and kinetics and are used to mathematically describe the process. [14]

Sintering theory

Consider two spherical particles in contact with each other. In powder compacts there are many such contacts on each particle. The bonds between contacting particles enlarge and merge as sintering progresses.

At each contact, a grain boundary grows to replace the solid-vapour interface. Prolonged sintering causes the two particles to coalesce into a single sphere with a final diameter equal to 1.26 times the original diameter. See figure 2.12.

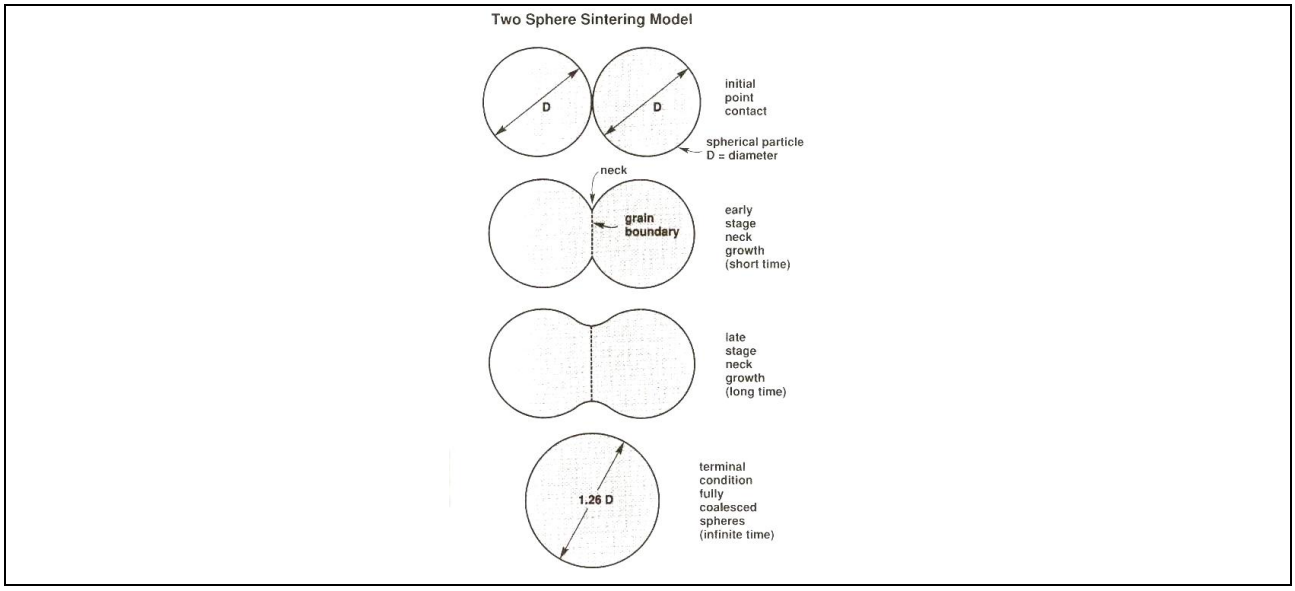

Figure 2.12: The two sphere sintering model with the development of the interparticle bond during sintering, starting with a point contact. Neck growth creates new grain boundary at the particle contact and with sufficient time the particles will eventually coalesce into a single larger particle. [14]

The initial stage of sintering is characterized by rapid growth of the interparticle neck. In the intermediate stage the pore structure becomes smoother and has interconnected cylindrical nature as the compact properties are developed. It is common for grain growth to occur in the latter portion of the intermediate stage of sintering, giving a larger average grain size with fewer grains. That is accompanied by possible pore isolation and a slower sintering rate. The open pore network becomes geometrically unstable when the porosity has shrunk by approximately 8% (92% of theoretical density). At which point the cylindrical pores collapse into spherical pores, which are not as effective at slowing grain growth. The appearance of isolated pores indicates the final stage of sintering and slow densification. Gas in the pores will limit the end point density, accordingly vacuum sintering can produce high final densities as long as the metal does not evaporate. [14]

2.2.6 Categories of Titanium Powder metallurgy

Direct Powder Rolling

The Direct Powder Rolling method entails using either blended elemental powder or prealloyed powder as a feedstock for a powder rolling mill. The mill consolidates the powder into a green-compact strip which has some ductility.

The strips are saw cut to fit inside the vacuum furnace where they are placed between Molybdenum plates and sintered. The sintered plate is then re-rolled to the desired thickness and then annealed to relieve stresses developed by re-rolling. [16]

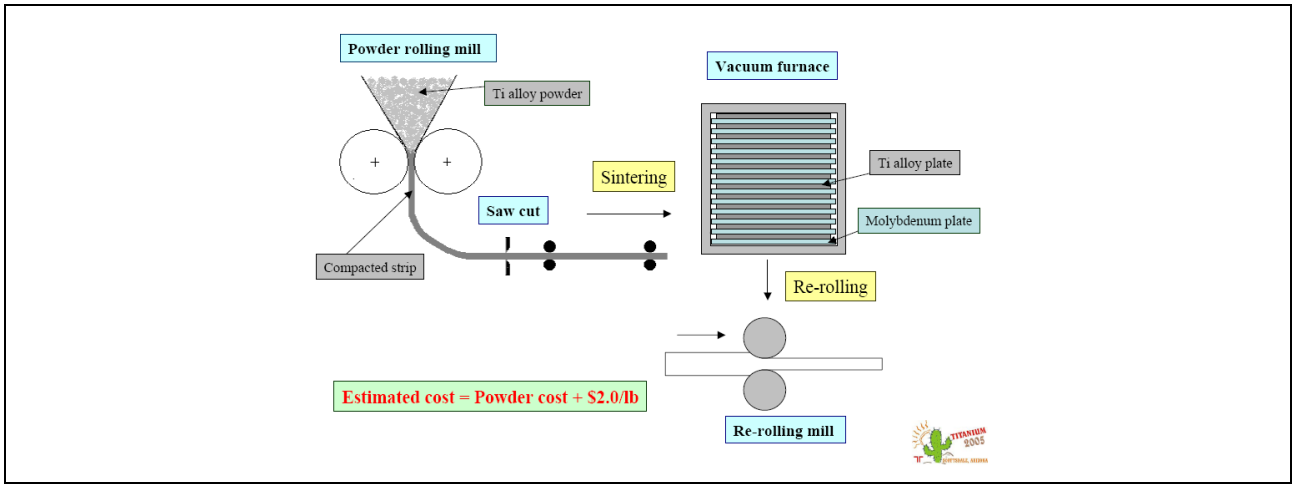

Figure 2.13: Schematic of the Direct Powder Rolling method of titanium powder metallurgy [16]

Advantages of Direct Powder Rolling

Direct powder rolling has a low capital cost when compared with traditional melting and forging. It has fewer operational steps than the traditional manufacture method. Raw materials are available at a low cost. Composition of the product is precisely controlled as high purity metals are commonly used in this method. The process is also applicable to composite type mixtures or immiscible components which cannot be produced by conventional methods. The resulting product has an absence of texture and has uniformity of microstructures and properties in transverse and longitudinal directions. Direct powder rolling is an adaptable and versatile consolidation method and can also be used to produce multi-layer strips. [18]

Blended Elemental Near Net Shaping

The most cost-effective PM processes are based on the use of low-cost Blended Elemental (BE) technology where alloying elements are added to titanium as elemental powders or master alloy powders. Traditionally this method includes the preparation of powder blends, their consolidation at room temperature and sintering in vacuum for transformation of initial heterogeneous powder compacts into massive homogeneous alloys. Consolidation at room temperature may be performed by low-cost conventional powder metallurgy processes such as die pressing, cold isostatic pressing (CIP), or by direct powder rolling. Cold isostatic pressing (CIP) is performed in practice either by the so called “wet bag” or “dry bag” method. With wet bag tooling, the flexible bag of the mould is filled outside the pressure vessel, sealed and finally placed within the vessel. The bag is completely surrounded by the pressure-exerting fluid. With dry bag tooling the bag is permanently sealed within the pressure vessel and powder filling occurs without removing it from the vessel. Wet bag tooling is therefore more versatile but requires mostly manual handling of the filled bag. Dry bag tooling is more suitable for mass production, but is more limited in shape flexibility. [17]

In order to achieve desired levels of mechanical properties (strength, ductility and fatigue strength) sintered materials should not only have a homogeneous chemical composition and microstructure, but also relative densities of greater than 98% of the theoretical value. The relative densities of titanium alloys produced by a blended elemental approach normally do not exceed 95%.In order to increase density, a sintered material can be subjected to hot isostatic pressing (HIP) or other hot deformation processes. However, this increases the number of production steps, which increases part cost and negates the advantages of the PM approach. [17]

Hot isostatic pressing (HIP) is a hot compaction process under isostatic pressure conditions. Near-isostatic conditions can be realised in axial hot pressing by embedding the compact into a suitable pressure transducing medium. Fully isostatic conditions require a fluid for ideal hydrostatic pressure transmittance. The external pressure can only become effective if the pressure medium cannot penetrate the open pore channels of the compact. This makes sealing the pores necessary. The pores can be sealed by flexible bag tooling as in cold isostatic pressing. At elevated temperatures, the flexible bag tooling becomes one of the limiting and cost controlling factors. Another method is the elimination of the open porosity by pressureless sintering and the application of gas pressure only in the final reduction of the residual closed porosity. [9]

Prealloyed Near Net Shaping

The prealloyed (PA) approach involves prealloyed powder and hot isostatic pressing (HIPing). The HIPing is done at a temperature below the beta transus temperature, for Ti-6Al-4V alloy, until full density is achieved. It is normally higher in cost but has enhanced mechanical properties when compared to the blended elemental approach. [17] The mechanical properties of PA compacts are between cast and wrought (ingot metallurgy) levels, including fatigue behaviour. [8]

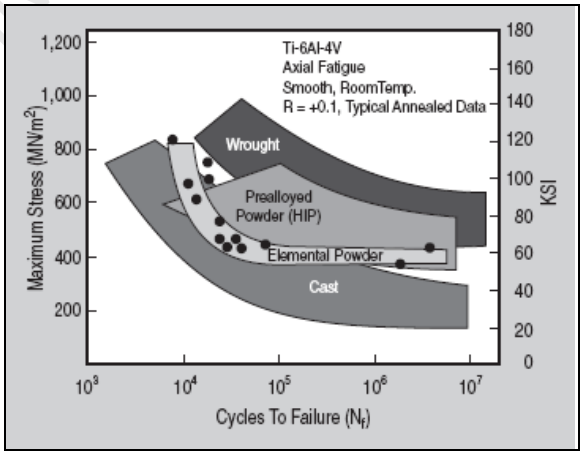

Figure 2.14: The fatigue behaviour of > 99% dense material compared to cast and wrought (ingot), cast and prealloyed PM material. [18]

The effect of porosity on mechanical properties

The strength and ductility of PM products improves significantly as the porosity decreases. Porosity has an even greater effect on the initiation–related properties such as S-N fatigue. Careful control of the size of the titanium powder and master alloy leads to a significant density enhancement and concurrent ductility improvement. The ductility can be increased even further by limiting beta grain growth with dispersion of second phase particles such as Y_2O_3 or B_4C. Another factor is the shape of the porosity. It has been evident in work done on steels that as the notch factor increases the endurance limit in degraded. [18]

Component Manufacture by Uniaxial Pressing

Compaction of the titanium powders is carried out under extremely high pressures exerted by either an automatic, hydraulic or mechanical presses.

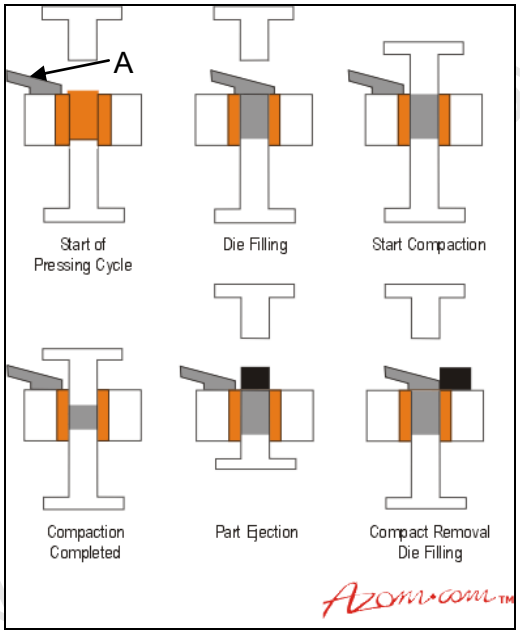

Figure 2.15: A typical compaction cycle, A: Powder shoe. [19]

The powder shoe initially moves over the die with the lower punch in such a position that the correct weight of powder is introduced. After the shoe has withdrawn the top and bottom punches move relative to the die to compress the powder at pressures between 400 MPa and 800 MPa. After compaction the top punch is withdrawn and the bottom punch moves relative to the die to eject the compacted powder. The filling shoe then moves again across the top surface of the die where it refills the die with powder and pushes the green compact away onto a moving belt which takes it to the sintering furnace. Generally compaction tools are produced from hardened and tempered die steels, but for longer life carbide insets are often added to the die. [19]

2.2.7 Direct Powder Rolling of Titanium

Direct powder rolling of titanium had been used to produce cost effective porous titanium plates that are used as a mechanical support for electrolyte membranes in water electrolysis cell technology and similar applications. The structures of the sintered metal powders are ideal for this application as they provide a unique combination of fine pores to allow the water to set the electrode and, within the same structure, larger pores to carry the product gas away from the electrodes. Porous plates of 5-10mm thickness and porous foils of 2.5-25μm thickness have been produced by rolling a compacted powder billet. The fabrication process includes direct powder rolling, sintering, re-rolling and annealing. SEM microscopy shows that the powder particles are welded to each other during fabrication, forming a honeycomb like structure with continuous pores. The irregular shape of the particles allows the synthesis of a monolithic skeleton with good strength properties. [20]

Direct powder rolling has also been used for the production of low cost titanium components for armour and structural applications. CP-Ti powder; blended elemental Ti-6Al-4V and blended TiAl powders are used to produce sheets of various thicknesses (0.5-2.5mm) and with various densities (50-99% of full density). Single layer CP-Ti, Ti-6Al-4V, TiAl as well as multilayer composites such as Ti/Ti-6Al-4V/Ti and Ti-6Al-4V/TiAl/Ti-6Al-4V strips were produced by first direct powder rolling into green compact strips and then sintering. It was concluded that foils, sheets and plates produced from single layer and/or multiple layers of material produced by the direct powder rolling followed by sintering process reached near full theoretical densities (±99% of theoretical value).[3]

2.3 Hot compression of metals

2.3.1 Introduction

The processes involved in the hot working of metals such as hot rolling, hot forging and isothermal forging have great industrial importance.

This is because at higher temperatures (above half the melting temperature) most metals exhibit a lower resistance to deformation and a higher ductility. A high rate of working is often necessary to improve the strength of the material but leads to an increase in the resistance to deformation and also to a decrease in ductility.

When conducting hot compression testing the sensitivity of the material to the rate of straining and the deformation temperature need to be taken into consideration. These conditions should be carefully controlled especially when the test results are intended to be used to define industrial processing parameters. [21]

2.3.2 Barrelling of Cylindrical Specimens

When a cylindrical sample is compressed Poisson expansion occurs. [18] Unless lubrication at the ends of the specimen is very good, friction between the compression platen and the sample occurs. The friction acts as a restraint retarding the outward motion of the end faces during compression. As seen in the diagram below, the end faces which are in contact with the compression platen are actually created by the folding over of the sides that make up the original cylinder. The barrelling that results from the frictional restraint introduces a complex state of stress and strain in the entire specimen. [21]

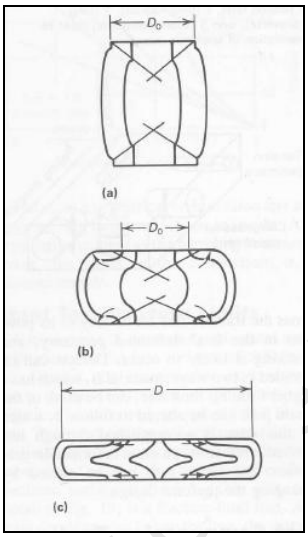

Figure 2.16: Deformation patterns in non-lubricated, non-isothermal hot forging a) initial barrelling. b) Barrelling and folding over. c) Beginning of end face expansion [21]

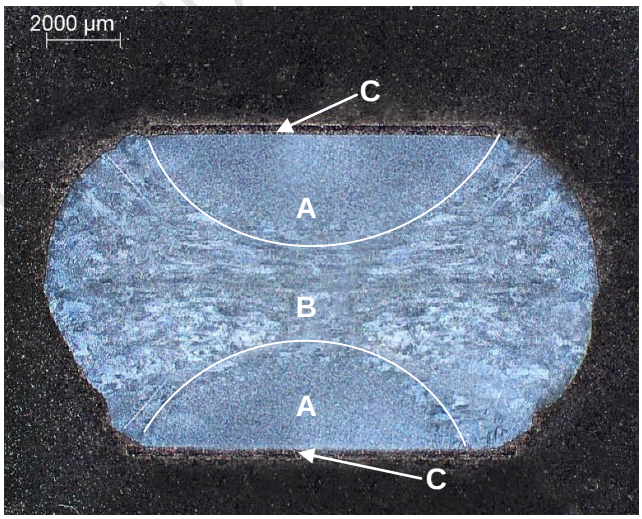

Figure 2.17: Deformation in a cylindrical wrought titanium sample which has been hot compressed. A: dead zones, B: maximum deformation zone and C: end faces

Low deformation zones develop adjacent to the compression platens, whereas severely deformed zones are concentrated more or less diagonally to the platens between the opposing

edges the specimen. In the figure 2.16, hot upsetting of a cylinder under poor lubrication, and where the platens are cooler than the specimen is shown schematically. The cooling that occurs on the faces that are in contact with the platens restricts the flow of the material resulting in the concentration of deformation being located in a central zone with dead-metal zones forming adjacent to the surface of the platens. As further deformation occurs severe inhomogeneity develops and the growth of the end faces is almost entirely due the folding over of the sides. The initial diameter of the specimen before compression is known as D_0 and the initial height of the specimen before compression is known as h_0. The final diameter of the specimen after compression is known as D and the final height of the specimen is known as h. When the value of D/h exceeds 3 expansion of the faces occurs and this should be avoided during hot compression testing. [21]

2.3.3 Reduction of friction

The use of lubrication could never improve the stress-strain condition to a point of homogeneous deformation but could significantly reduce barrelling. High pressure lubricant applied to the loading surface of the compression platen and the specimen reduces friction. A common lubricant used in high pressure environments is 0.1mm thick Teflon sheet. The action of the lubricant may be enhanced if the platen surfaces are hard and highly polished. [21]

2.3.4 Flow stress in compression

The determination of flow stress in hot compression must ideally be carried out under isothermal conditions (i.e. with the platens at the same temperature as the specimen), at constant strain rate and with a minimum amount of friction to minimize barrelling. For a predominately homogeneous upsetting test, a cylinder of diameter D_0 and initial height h_0 will be compressed to height h and spread out to diameter D, in accordance with the law of constancy of volume:

$$D_0^2 h_0 = D^2 h \quad [21]$$

If friction can be neglected, the flow stress corresponding to a deformation force P is:

$$\sigma_0 = \frac{P}{A} = \frac{4P}{\pi D^2} = \frac{4Ph}{\pi D_0^2 h_0} \quad [21]$$

If substantial friction is present, the average pressure $\bar{p}$ required to deform the cylinder is greater than the flow stress of the material σ_0 where α is the radius of the cylinder and μ is the Coulomb coefficient of friction:

$$\frac{\bar{p}}{\sigma_0} = \left(\frac{h}{4\mu a}\right)^2 \left(e^{2\mu a/h} - \frac{2\mu a}{h} - 1\right) \quad [21]$$

The true compressive strain is therefore given as:

$$\varepsilon = \ln\left(\frac{h_0}{h}\right) \quad [21]$$

The effect of friction can be minimized by using long thin specimens. This would result in most of the specimen volume being unaffected by the dead metal zones at the platens. This approach is restricted because the specimens will buckle if *h/D* exceeds approximately 2. [21] In our testing facility friction is present and results in the barrelling of the specimen. We attempt to reduce the friction but do not eliminate it completely. Due to the limitations of our testing facility we are not able to determine the frictional co-efficient while at compression temperature. Therefore the true compressive strain formula was used to calculate the nominal strain during hot compression.

2.4 Recrystallization caused by hot deformation

2.4.1 Introduction

The softening process of recovery and recrystallization may occur during deformation at high temperatures. These phenomena are called dynamic recovery and dynamic recrystallization in order to distinguish them from static annealing processes which occur during post-deformation heat treatments. The static and dynamic processes have many processes in common, although the simultaneous operation of deformation and softening mechanisms lead to some important differences. [23]

Dynamic recovery and dynamic recrystallization occur during metal working operations such as hot rolling, extrusion or forging. They are important because they lower the flow stress of the material thus enabling it to be deformed more easily and they also influence the texture and grain size of the worked material. Dynamic recrystallization may also occur during creep deformation with the main difference between hot working and creep being the strain rate. Hot working is generally carried out at a strain rate range of 1-100 s^{-1} whereas typical creep rates are below 10^{-5} s^{-1}. In many cases similar atomistic mechanisms occur during both types of deformation. Dynamic recrystallization also occurs during the natural deformation of minerals in the earth's crust and mantle. [23]

2.4.2 Dynamic recovery

In metals of high stacking fault energy, such as aluminium and its alloys, dislocation climb and cross slip occur readily. Dynamic recovery is therefore rapid and extensive at high temperatures and is usually the only form of dynamic restoration which occurs. The stress strain curve in this case is typically characterized by a rise to a plateau followed by constant or steady state flow stress. During the initial stages of deformation there is an increase in the flow stress as dislocations interact and multiply. However, as the dislocation density rises, so does the driving force and hence the rate of recovery increases. During this period a microstructure of low angle

boundaries and subgrains develops. At a certain strain the rates of work hardening and recovery reach a dynamic equilibrium. The dislocation density remains constant and a steady-state flow stress is obtained. During deformation at strain rates larger than ± 1 s^{-1}, the heat generated by the work of deformation cannot all be removed from the specimen and the temperature of the specimen rises during deformation. This may cause a reduction in the flow stress. [23]

2.4.3 Dynamic recrystallization

In a metal in which the recovery is slow such as those with a low or medium stacking energy, dynamic recrystallization may occur when a critical deformation condition is reached. A simplified description of the phenomenon of dynamic recrystallization may take place as follows. New grains originate at old grain boundaries but as the material continues to be deformed the dislocation density of the new grains increases. This reduces the driving force for further grain growth and the recrystallizing grains eventually cease to grow. Another factor which may limit the growth of the new grains is the nucleation of further grains at the migrating grain boundaries. [23]

The Zener-Hollomon Parameter (Z)

At temperatures where thermally activated deformation and restoration processes occur, the microstructural evolution will be dependent on the deformation temperature (t) and the strain rate ($\dot{\varepsilon}$) in addition to the strain (ε). The strain rate and the deformation temperature are often incorporated into a single parameter – the Zener-Hollomon parameter (Z), which is defined as:

$$Z = \dot{\varepsilon} \exp\left(\frac{Q}{RT}\right) \text{ [23]}$$

Q is the activation energy for deformation. If the flow stress follows a mechanical equation of state, i.e. it is dependent only on the instantaneous values of T, $\dot{\varepsilon}$, ε and not their history, then the relationship between these parameters may be expressed by relatively simple empirical equations.

It is found that during hot work such a mechanical equation of state is closely followed and during steady-state deformation, the relationship between the flow stress (σ) and Zener-Hollomon parameter is often found to be:

$$Z = c_1 \sinh(c_2\sigma)^n \text{ [23]}$$

C_1, C_2 and n are constants. Thus Z is seen to be closely related to the flow stress and hence to the dislocation density. The Zener-Hollomon parameter is particularly convenient for discussions of hot working processes in which temperature and strain rate are generally known, whereas the flow stress may not always be measurable. [23]

During our testing the Zener-Hollomon parameter is not the same throughout sample due to the presence of a temperature gradient within the sample. The end faces are far cooler than the centre of the sample due to the heat sink effect of the ceramic platens.

Characteristics of dynamic recrystallization

The general characteristics of dynamic recrystallization are as follows:

1. The stress-strain curve of a material which undergoes dynamic recrystallization generally exhibits a broad peak that is different to the plateau, which is characteristic of a material which undergoes only dynamic recovery.

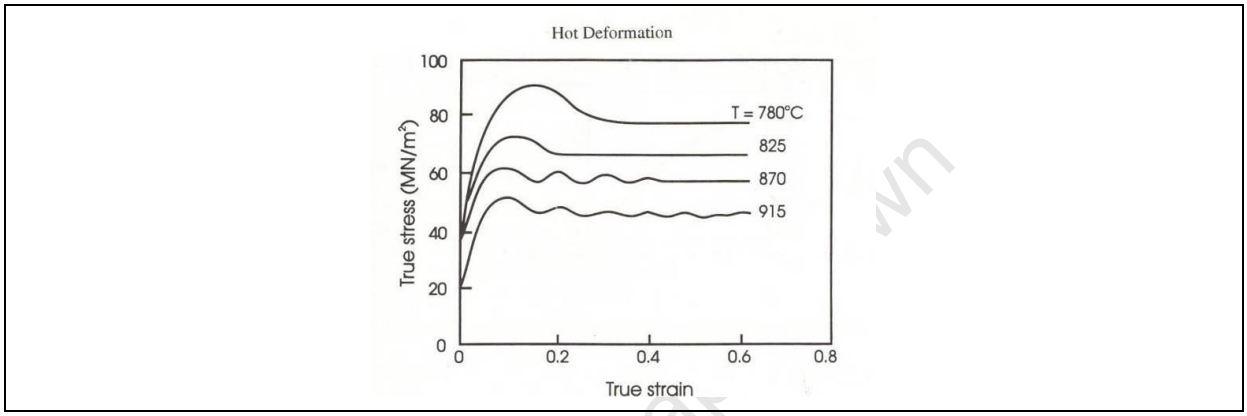

Figure 2.18 The effect of temperature on the stress strain curves for 0.68% C steel, deformation in axisymmetric compression, $\dot{\varepsilon} = 1.3 \times 10^{-3}\ s^{-1}$ [23]

2. A critical deformation (ε_c) is necessary in order to initiate dynamic recrystallization. This is somewhat before the peak (σ_{max}) of the stress-strain curve.

3. The ε_c decreases steadily with decreasing strain rate.

4. The size of dynamically recrystallized grains (D_R) increases monotonically with decreasing stress. Grain growth does not occur and the grain size remains constant during the deformation.

5. The flow stress (σ) and D_R are almost independent of the initial grain size (D_o), although the kinetics of dynamic recrystallization is accelerated in specimens with smaller initial grain sizes.

6. Dynamic recrystallization is usually initiated at pre-existing grain boundaries although for very low strain rates and large initial grain sizes, intragranular nucleation becomes important. [23]

The curves produced during our hot compression testing do not resemble the curves in figure 2.18 as our Stress vs. Compressive strain curves as we did not use true stress and true strain when plotting the curves.

The shape of the sample changes during hot compression but we are not able to measure that information using our testing facility, therefore engineering stress is used. Another important factor is the effect of the co-efficient of friction on the graphs. The graphs that were created using our testing equipment do not correct for friction which is another reason why our curves do not follow the expected pattern.

Nucleation of dynamic recrystallization

Dynamic recrystallization originates at high angle boundaries. These may be the original grain boundaries, boundaries of dynamically recrystallized grains or boundaries created while straining (e.g. those associated with deformation bands). Bulging of grain boundaries is frequently observed as a prelude to dynamic recrystallization and it is usually assumed that a mechanism closely related to strain induced grain boundary migration operates.

Microstructural evolution

Dynamic recrystallization generally starts at the old grain boundaries. New grains are subsequently nucleated at the boundaries of the growing grains and in this way thickening the band of recrystallized grains formed. (See figure 2.19) If there is a large difference between initial grain size (D_0) and the crystallised grain size (D_R), then a necklace structure of grains maybe formed and eventually the material will become fully recrystallized.

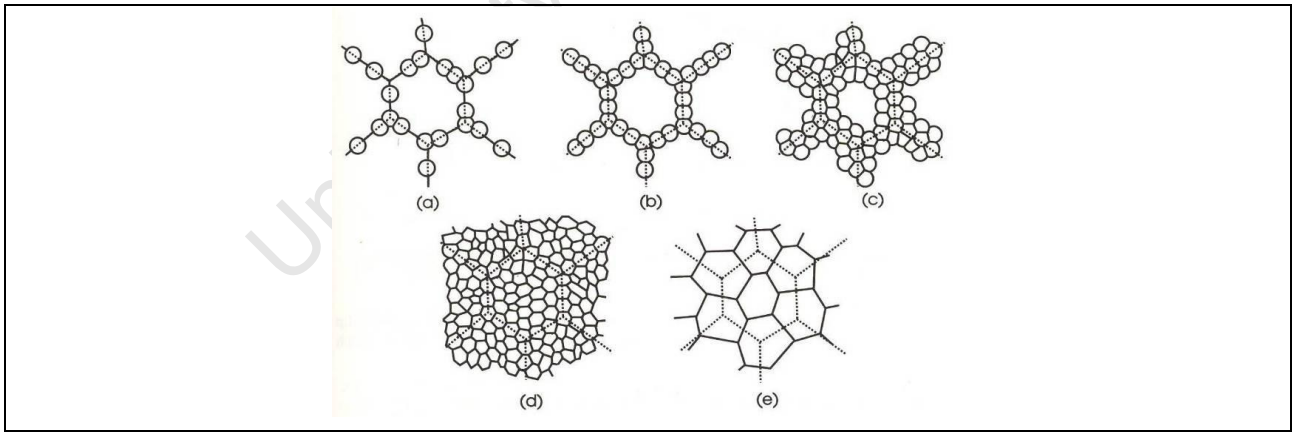

Figure 2.19 the development of microstructure during dynamic recrystallization. (a-d) Large initial grain size, (e) small initial grain size [23]

Unlike static recrystallization, the mean size of dynamically recrystallized grains does not change as the recrystallization process proceeds.

Flow stress during dynamic recrystallization

The stress strain curves of a dynamically recrystallizing material may be characterized by a single peak or several oscillations.

At low stresses the material recrystallizes completely before a second cycle of recrystallization begins and this process is then repeated. The flow stress which depends on the dislocation density therefore oscillates with strain. At high stresses subsequent cycles of recrystallization begin before the previous ones are finished. The material is therefore always in a partially recrystallized state after the first peak and the stress strain curve is smoothed out, which results in a single broad peak. [23] It has been suggested that the shape of the stress strain curve depends primarily on the ratio of recrystallized and starting grain sizes (D_0/D_R). If (D_0/D_R) >2 then the microstructure develops as shown in figure 2.19(a)-(d). The material is only partly recrystallized except at very high strains, resulting in a smooth single peak curve. However if $D_0/D_R < 2$ then the new grains all develop at about the same time because there are enough sites (i.e. grain boundaries) for recrystallization to be complete in one cycle as seen in figure 2.19 (e).

This fully recrystallized and softened material then undergoes further deformation, hardens and recrystallizes again. As this cycle is repeated an oscillatory stress strain curve results. The shape of the stress strain curve therefore depends on the deformation conditions (Z) and on the initial grain size. The figure bellow illustrates schematically the relationship between stress-strain behaviour and these parameters.

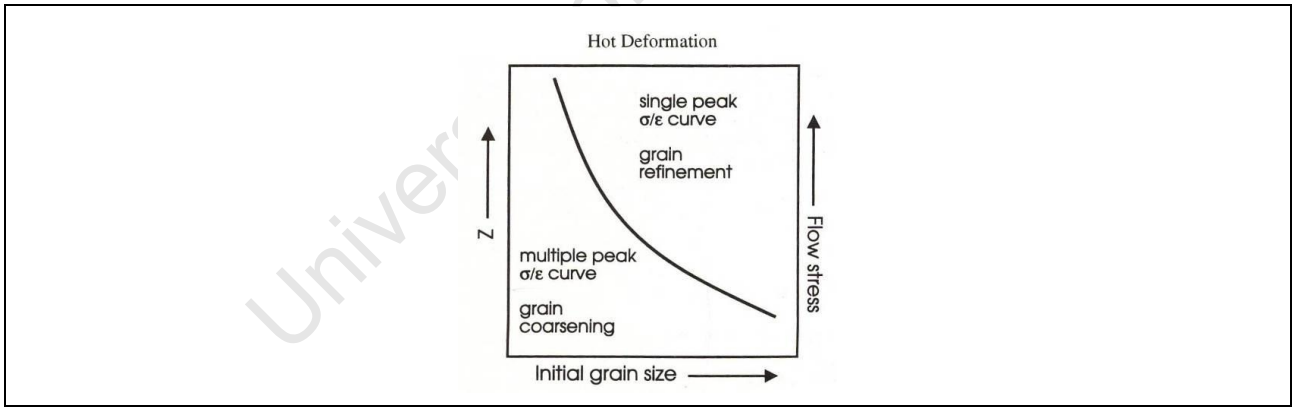

Figure 2.20 The conditions for multiple and single peak dynamic recrystallization [23]

2.4.4 Metadynamic recrystallization

Whenever the critical strain for dynamic recrystallization (ε_c) is exceeded, recrystallization nuclei will be present in the material. If the straining is stopped but the annealing is continued, then these nuclei will grow with no incubation period into a heterogeneous, partially dynamically recrystallized matrix. This phenomenon is known as metadynamic recrystallization. [23]

The microstructure of the material which has undergone some dynamic recrystallization is very heterogeneous and may contain:

A. Small dynamically recrystallized grains which are almost dislocation free.

B. Large dynamically recrystallized grains with moderate dislocation density.

C. Unrecrystallized material with high dislocation density (ρ_m)

Each of these kinetic regions will have a different static annealing behaviour and the overall annealing kinetics and grain size distributions maybe extremely complex. [19]

Region A may continue to grow during the early stages of post deformation annealing by the mechanism of metadynamic recrystallization. Region B will, if their dislocation density (ρ) is below the critical value (ρ_{RX}), recover, and this has been termed metadynamic recrystallization. If $\rho>\rho_{RX}$ then these regions may subsequently recrystallize statically. Region C will undergo static recovery, followed by static recrystallization. Once the material is fully recrystallized then further grain growth may occur. [23]

2.4.5 Grain growth after primary recrystallization

The process of primary recrystallization is generally considered to be complete when the boundaries of the expanding, recrystallized regions have migrated through the metal to such an extent that they have impinged on each other; thereby replacing the original deformed structure with a new strain free polycrystalline microstructure. At this stage of annealing the metal has a new grain size which is the minimum that can be attained for that particular combination of metal composition, amount of prior deformation and annealing temperature and time. Although the relatively high initial energy of the deformed stated has been removed by the primary recrystallization, the resulting structure is still considered theoretically metastable and a further reduction in overall internal energy can be achieved with a reduction in total grain boundary area within the metal. A continuation of the annealing process leads to a further migration of grain boundaries through the recrystallized structure, thereby producing a structure containing a smaller number of enlarged grains. [24]

Despite the basic mechanistic similarities of the two processes of the growth of primary recrystallization nuclei (to form strain-free grains within the initially deformed metal) and the subsequent growth of recrystallized grains (to form larger grains within an initially strain-free structure) they should be regarded a separate processes, within the overall response of a metal to annealing because of the differences in the driving forces. The driving force for the growth of new grains (from viable nuclei to boundary impingement) during primary recrystallization is provided by the removal of the stored energy associated with the deformed state. Whereas the driving force for the growth of strain-free grains after primary recrystallization is provided by the reduction of the total grain boundary area in the strain-free structure. This difference leads to the characteristic differences in both the kinetic and topological aspects of the two processes.

The growth rate during the formation of new grains during primary recrystallization is more rapid than the growth rate during the expansion of strain-free grains during grain growth after primary recrystallization. Also grain boundaries migrate away from their centre of curvature during primary recrystallization but they migrate towards their centre of curvature during grain growth [24]

2.5 Recrystallization of titanium under hot deformation

While there has been much written about texture and deformation twins related to plastic anisotropy of titanium and on the general microstructure of titanium, relatively few studies have been made about the metallurgical importance of the recrystallization behaviour of titanium during hot deformation. [25] Thus this chapter summarizes 3 key papers/journal articles which have formed the bases for outlining the parameters and expected outcomes from which comparisons can be made to the hot compression of sintered CP-Ti compacts.

2.5.1 Recrystallization behaviour of CP-Ti during hot rolling

CP-Ti is manufactured generally by hot deformation processes such a forging and hot rolling. Problems however arise due to the reactivity and anisotropy of plasticity in titanium. These problems are most conspicuous during hot rolling. Therefore it becomes necessary to experimentally investigate the restoration processes i.e. recovery and recrystallization that occur during the hot rolling of ingots into slabs and then from slabs into sheets. CP-Ti ingots (as cast condition) were heated to between 400°C and 1200°C. The specimens were then hot rolled in a single pass on a two-high mill. As soon as the slab was hot rolled the specimen was water quenched for 2-3 seconds. [25] The study concluded that when the hot rolling temperature was high (800°C), hardness scarcely changes with increasing reduction. When the hot rolling temperature is low (600°C-700°C), hardness slightly increases with increasing reduction. As for structural change during hot rolling, a recrystallization nose exists at the high temperature side (near 800°C) of the α-region. When the CP-Ti slab is rolled in this temperature region, a recrystallized structure gradually emerges from the deformed structure containing lamellar deformation twins as the reduction rate is increased. At the lower temperature side (600°C), a recovered structure appears where deformation bands containing lenticular deformation twins are formed. The recovery and recrystallization processes do not readily proceed when the microstructure of the titanium material is coarse grained. The recrystallized structure observed in this study is considered to have resulted from static recrystallization immediately after hot rolling, and is influenced by strain, temperature and strain rate. [25]

2.5.2 Microstructure evolution of CP-Ti during high temperature deformation

Superplastic forming (SPF) is a cost effective process for the manufacturing of complex shaped structural components and SPF of CP-Ti is very attractive in many areas due to the inert nature of this alloy. Investigations of its potential for superplasticity, mechanisms, related phenomena and microstructural evolution are important for achieving the desired mechanical properties. [4]

CP-Ti sheets were used to create tensile specimens with a gauge of 11mm length, 4mm wide and 1.5mm in thickness. The specimens were machined with the tensile axis orientated parallel to the final rolling direction. The specimens were deformed at 600°C, 750°C and 800°C with different initial strain rates. After testing the deformed specimens were cooled rapidly to room temperature by forced cooling in order to preserve the microstructure. Specimens were sectioned along the gauge and grip part of the deformed sample. The volume fraction of fine grains ratio was measured using an optical microscope. SEM and EBSD are used to produce grain maps based on the orientation measurements. [4] This study concluded that CP-Ti alloy does not show good superplasticity at 600°C-800°C due to rapid grain growth. The maximum elongation to failure value that can be obtained is 188% at 600°C with an initial strain rate of 0.001/s. Dynamic recrystallization happens when the alloy deformed between 600°C and 800°C. The optimum DRX conditions are found to be at 600°Cwith an initial strain rate of 0.001/s, attaining the highest volume fraction of fine grains whose average grain size is ± 9.7μm at a strain of 80%. The distribution of fine grains is not homogeneous. These processes not only decrease the average grain size of the alloy, but also increase the misorientation angle. [4]

2.5.3 Dynamic recovery and recrystallization in Ti alloys by hot deformation

In (α + β) alloys and metastable β titanium alloys, hot deformation by rolling or forging is conventionally performed in β single-phase and (α + β) two-phase regions. During hot deformation dynamic recovery and dynamic recrystallization takes place. It is known that the refinement of β grain size is beneficial for the improvement of strength-ductility balance. Dynamic recrystallization is quite effective in grain refinement when deformation is performed at high strain rate and lower temperature (i.e. a higher Z (Zener-Holloman parameter)) condition. This study examined hot deformed microstructures of β titanium alloys in β single-phase and (α + β) two-phase regions by means of using a SEM and transmission electron microscopy (TEM). [26] A variety of alloys are solution treated so that equiaxed β structures were obtained. Solution treatment was followed by furnace cooling or air cooling to produce a lamellar (α + β) structures and by water quenching to obtain a martensite structure. After β solution treatment was performed the specimens were isothermally held at various temperature in the β phase region or the (α +β) two-phase region and subsequently compressed at the same temperature at initial strain rates of between 4.2×10^{-1} and 4.2×10^{-5} s^{-1} up to 55% to 75% reduction. [26] This study concluded that when local orientation measurement techniques in SEM and TEM were applied to study the dynamic restoration mechanisms in hot deformation of titanium alloys, DRC was found to be the most dominating restoration process in β single-phase alloys. However, DRX also occurred partly along the β grain boundaries. When the (α + β) two-phase alloys with larger volume fractions of the 2nd phase are deformed, continuous DRX occurs and the (α + β) microduplex structures containing high angle boundaries were formed after certain amounts of deformation. Such application of DRX and manipulation of the grain boundary structures are important and useful in titanium alloys as well as other duplex alloys for lowering flow stresses, improving superplasticity and obtaining ultra-fine grained structures. [26]

3 DESIGN AND SET-UP OF TESTING FACILITY

3.1 Testing facility requirements

In order to simulate hot deformation on a laboratory scale it is necessary to simulate the high strain rate and high temperature conditions present during the deformation cycle. The facility has to be able to heat a sample up to 1000°C under a vacuum of 10^{-4} Torr; this is a safety precaution as titanium has a tendency to burn at temperatures above 400°C. Our testing facility would utilize an existing mechanical testing frame and would have to be compact and portable. The sample would have to undergo compression at high temperature according to following the following sequence:

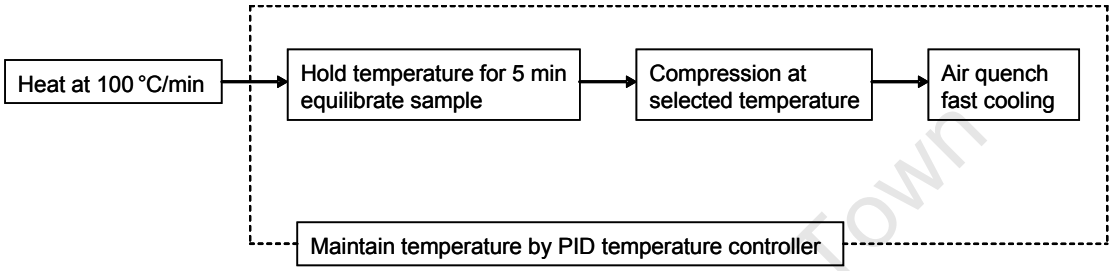

Figure 3.1.1 Flow diagram of general testing procedure

To achieve this effectively certain design and operating requirements have to be fulfilled

- Rapid heating to required temperature
- Hold the temperature stable within ±5°C of the test temperature
- Maintain a high vacuum (10^{-4} Torr)
- Minimize friction between the sample and the compression platens

3.1.1 The Mechanical Testing Frame

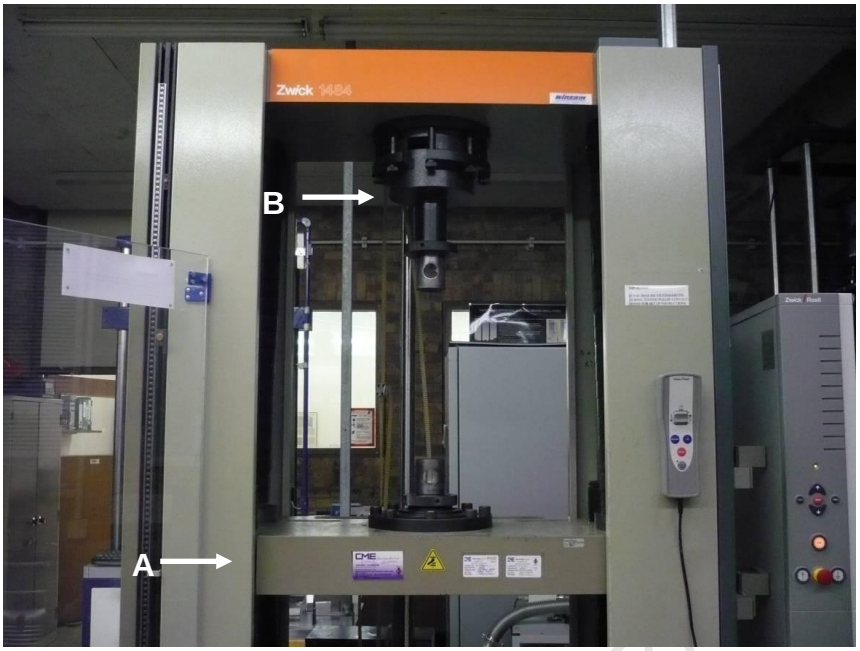

Figure 3.1.2 Picture of mechanical testing frame: A-crosshead and B- 200 kN load cell

Constraints and limitations of the testing frame:

The vacuum vessel, heating and compression setup must fit within the testing frame and not interfere with the functioning of the testing frame. The mechanical testing frame is used for other types of testing and therefore the entire testing setup has to be movable and compact, to allow for removal after testing

3.2 Design of the Heating System

Due to the space restriction the best option for a heating system would be an induction heating system. The system that was selected is the EasyHeat 2.4kW induction heating system manufactured by Ambrell and supplied by L H Power Electronics (Johannesburg, Gauteng).

Figure 3.2.1 EasyHeat remote heating system and power controller

The Easy Heat is a water-cooled system, connected to a heat exchanger for dissipating heat. The controller for the Easy heat induction system controls the power output of the Easy Heat's RF generator. The dimensions of the coil were specially designed to heat a titanium sample of our dimensions and to accommodate the compression platens that have to fit within the coils. The dimensions of the specimens are indicated in Fig.3.2.2.

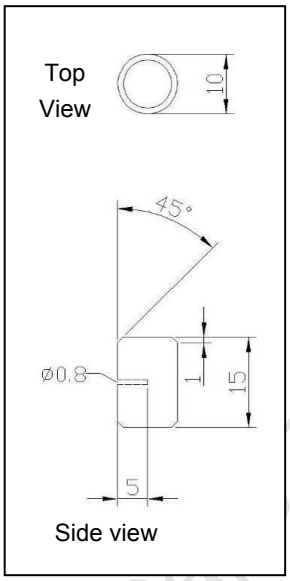

Figure 3.2.2 Dimensions of the samples (mm)

The temperature control system comprises of a K-type single strand thermocouple wire which connects the sample to the Gefran 800P programmable temperature controller. The temperature controller is connected to the power controller.

The temperature controller adjusts the amount of power output to the coil based on the amount needed to hold the test temperature. The thermocouple is welded at the tip and attached to the sample by securing it in a small hole with heat sink paste.

The hole in the sample is made midway along the length of the sample and midway through the sample, (see Fig 3.2.2). The wire is stabilized by an L shaped clamp which is bolted to the upper side of the base plate. The purpose of the clamp is to reduce the movement of the wire and the sample during assembly of the setup and during testing.

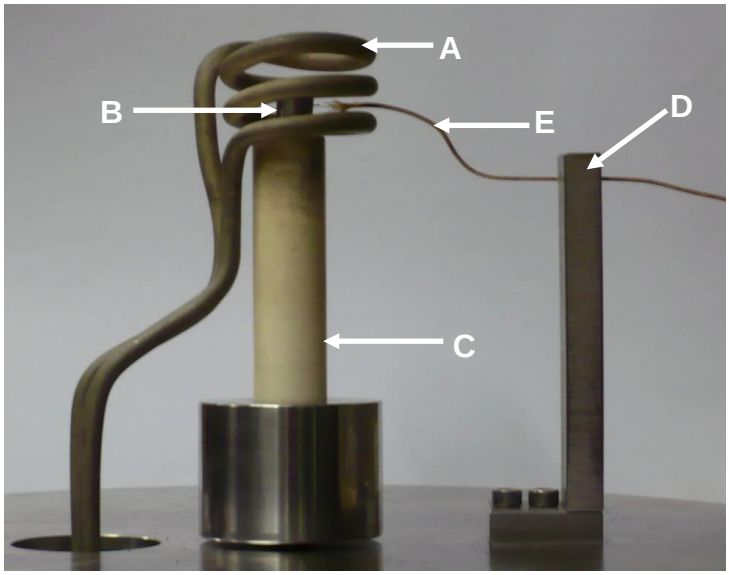

Figure 3.2.3 Internal components of the heating system A – heating coil, B – sample, C – compression platen in lower platen support, D – thermocouple clamp and E – thermocouple

3.3 Design of the Compression System

The compression system comprises of the compression platens, the upper push rod, lower platen support, the base plate and cover plate. The dimensions of the compression system are restricted by the glass vacuum vessel on the outside and the induction heating coil on the inside.

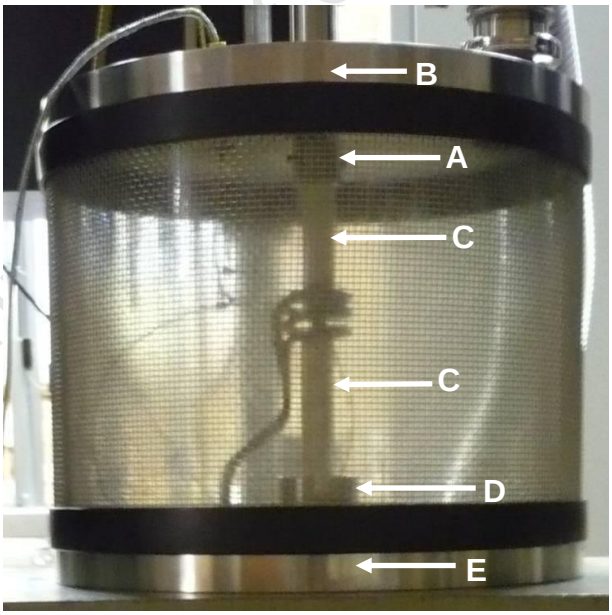

Figure 3.3 Compression system A – Upper push rod, B – Cover plate, C – Ceramic platens, D – Lower platen support and E – Base plate

3.3.1 Compression Platen Design

The material selection for the platens and sample geometry are very important to the success of the compression setup. The use of an induction heating system restricts the space for the compression platen to the inner diameter of the coil. The compression of the sample will occur within the internal space of the coil. Metallic compression platens cannot be used because of the platens proximity to the coil which would result in the platens being heated by the induction coil. Since the sample is being heated up to 1000°C it will cause the metallic platens to lose their strength during compression. Furthermore, too much power would be consumed from the induction system.

To negate this effect the platens have to be made of a high strength, non-conducting material which can withstand temperatures of up to 1000°C and forces up to 13 kN. Consequently, the focus was directed towards the use of ceramic materials. The compression platen was manufactured from 99.95% Alumina ceramic (LINE-OX® 99, manufactured by CERadvance). It was densely sintered and diamond ground for the reduction of friction between the sample and the platens. The mechanical and physical properties for the alumina ceramic are listed in the table below.

Table 3.3 Mechanical and physical properties of the alumina ceramic

Properties	
Compressive strength	2200-2600 MPa
Tensile strength	260-300 MPa
Hardness (Vickers)	1500-1650 kg f mm^{-2}
Density	3.9 $g.cm^{-3}$
Thermal conductivity @ 20°C	26-35 $W.m^{-}1.K^{-1}$
Co-efficient of thermal expansion @ 20-1000°C	8.0 x 10^{-6} K^{-1}
Upper continuous use temperature	1700°C

The ceramic compression platens will be sensitive to extreme thermal fluctuations therefore radical thermal shocks should be avoided. This necessitated the use of a multistep programmable temperature controller so that the platens could be heated and cooled at a steady rate. The platens are solid cylinders with a diameter of 20 mm and a length of 100mm.

3.3.2 Upper push-rod and lower stainless steel platen support

The push-rod and platen support that hold the ceramic platens were specially designed to hold and stabilize the ceramic compression platens during the compression of the sample. The lower platen support is a solid cylindrical rod with a recess on one end to accommodate the ceramic compression platen.

As the ceramic compression platen is held in place by gravity, additional fasteners are required for the upper push-rod. Two small bolts are used to secure the upper platen inside the recess of the upper push rod. The push rod and platen support are made from AISI 304 Stainless Steel to avoid oxidation as they would experience some of the residual heat from the sample being heated by the induction heating coils.

3.3.3 Stainless steel base and cover plates

The base and cover plates are made of the same AISI 304 Stainless Steel as the upper and lower grips. The base plate is 20 mm thick in order to provide a stable platform for the lower half of the compression setup. It has an opening for the power leads of the induction coil to be fitted using a high density polymer plug. The cover plate has three openings, one for the upper stainless steel push-rod so that it can be attached to the mechanical testing frame, one for the thermocouple feedthrough which connects the thermocouple wire inside the vacuum cylinder with the thermocouple lead from the temperature controller and lastly, a flanged opening for the vacuum pipe.

3.4 Vacuum system

Commercially pure titanium is prone to oxidation and even burning in an environment where oxygen is present at temperatures above 400°C. Since the titanium alloy will be tested at temperatures ranging from 800°C to 1000°C, it is imperative to maintain an oxygen free environment by keeping the samples in a very high vacuum for the duration of the test. The vacuum vessel is a quartz glass tube with a stainless steel base plate and cover plate. The vacuum is achieved by a Varian SH-110 Dry scroll and turbomolecular pump.

3.4.1 Seals and O-rings

The glass vacuum cylinder is covered by a steel wire mesh which is tightly wrapped around the vessel. This is a safety precaution to prevent shrapnel should the vessel fail during testing. It also has two larger rubber seals on either end which provide a vacuum tight seal under the weight of the stainless steel cover plate and the vacuum inside the vessel.

Figure 3.4.1 Glass vacuum vessel covered by steel wire mesh with large rubber seals on the top and bottom

During compression testing the load cell remains stationary as the mechanical testing frame moves upward during compression. This results in movement up and down along the upper stainless steel grip of the ceramic platen. This movement requires a special type of seal to prevent the quartz glass vacuum vessel from leaking. A dynamic gland – reciprocating seal is used to seal whilst allowing the free movement of the mechanical frame. An important component of the reciprocating seal is the use of several o-rings. The o-rings used in the compression setup need to be able to withstand the ambient temperature in the quartz glass vacuum vessel, especially the o-rings in contact with the push rod. For this reason, Viton® o-rings were selected which have very good high temperature performance.

3.4.2 Power Lead feedthrough

The induction coil used to heat the specimens during testing has power leads which connect the coil to the RF generator. These leads have to pass through the stainless steel base plate. This presented a challenge as the metal immediately surrounding the power leads could also be affected by the induced magnetic field and consequently the base plate would heat up thereby consuming too much power, which will hamper the effective and precise control of the heating and cooling rate.

This challenge was solved by designing a polymer plug to act as a feedthrough for the power leads. The plug is designed with recessed o-ring grooves which maintain the high vacuum environment and is indicated in Fig. 3.4.2.1.

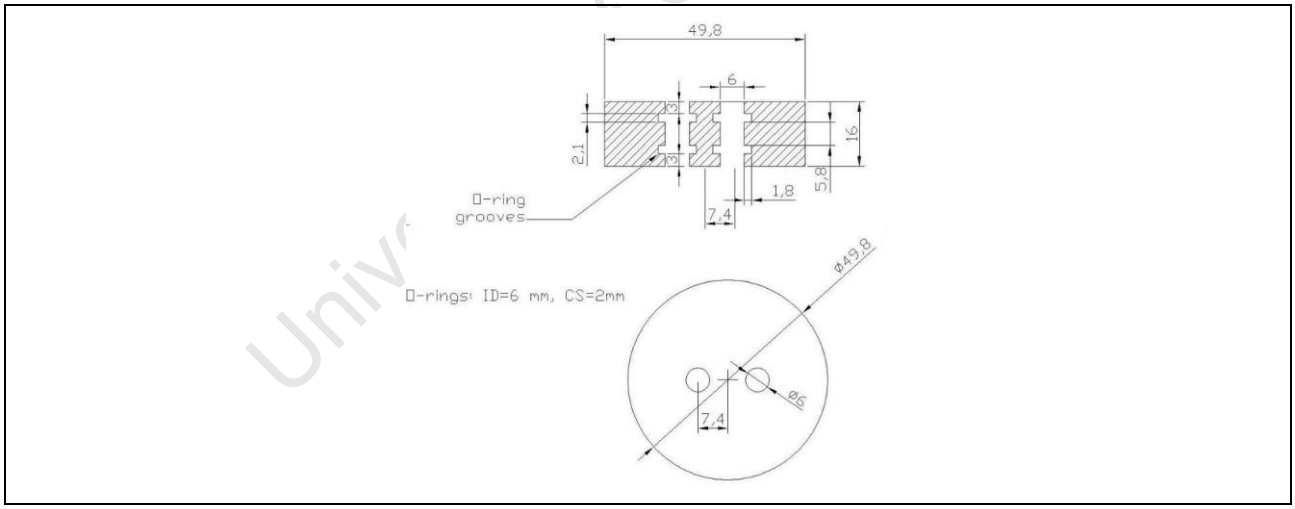

Figure 3.4.2 Design of the polymer plug to be used as the Powder Lead Feedthrough

The plug fits into a stepped hole in the base plate and is sealed with an o-ring and held in place with a stainless steel ring which also screws into the base plate.

3.5 Modifications to the testing facility

3.5.1 Design changes to the stainless steel cover plate

The initial design of the cover plate consisted of a solid circular Stainless steel plate which was 15 mm thick. This design resulted in the cover plate being very heavy. The weight of the cover plate made moving and placing the cover extremely cumbersome. In order to make the assembly of the testing facility more manageable, the bulk of the material was removed leaving an outer rim of 15 mm thickness and an inner area of 5 mm thickness. The area around the opening for the upper stainless steel push-rod and the flanged neck for the attachment of the vacuum fittings has been left at the original thickness. This is particularly necessary for the push-rod since the cover plate contains up to three o-rings to ensure good vacuum. The thermocouple feedthrough has been removed and the hole welded closed. The outer rim of the underside has had a groove cut into it to ensure that the modified cover plate does not shift during compression as it no longer has the extra weight to stabilise it.

Figure 3.5.1 Modified stainless steel cover plate

3.5.2 Design changes to the stainless steel base plate

The base plate was modified to accommodate the relocation of the thermocouple feedthrough from the cover plate to the base plate. A small stepped hole was cut into the base plate adjacent to the lower grip and the thermocouple feedthrough was welded into place. The initial design was difficult to work with as positioning the cover plate caused too much movement of the thermocouple wire inside the sample and affected the ease with which the sample was positioned between the platens.

There was also the danger of damaging the fragile spade type connections on the inner side of the cover plate when lowering the cover plate. These problems were eliminated by the relocation of the thermocouple feedthrough.

Figure 3.5.2 Modified stainless steel base plate

3.5.3 Redesign of the upper steel push-rod

The original design for the upper steel push-rod had a length of 200 mm excluding the fixture for securing the push-rod. This length was found to cause misalignment of the upper and lower platens. The extra length also acted as a heat sink when meant that more power was required to heat the sample and the sample cooled at a faster rate. In the new design the length of the upper steel push-rod was reduced to 150 mm; this resulted in a better alignment of the platens and lowered the amount of power required for heating the sample.

3.5.4 Redesign of the stainless steel lower platen support

The original design for the lower platen support did not provide sufficient stability for the ceramic platen which caused bending forces on the ceramic leading to failure. Also the lower platen support did not raise the sample on the ceramic platen to the optimum height for efficient heating by the coil. The new design for the lower support encloses a larger portion of the ceramic platen and therefore offers more stability to the compression system.

The upper portion of the neck of the lower support is reduced to make sure that it does not get too close to the induction heating coil.

Figure 3.5.4 Modified stainless steel lower platen support (compared with Fig.3.2.3)

3.6 Problems experienced with new designs

Having a shorter upper push-rod and a longer lower platen support results in the sample taking longer to cool than before which increased the waiting time before the tested sample could be removed and the next sample could be inserted. The shortening of the upper push-rod also meant that the entire rig was now positioned higher off the ground than before; this resulted in us needing to add an extension to the stainless steel vacuum hose.

3.7 Temperature control

3.7.1 Tuning a PID controller

If the temperature inside the vacuum cylinder was observed over a period of time, it would be unusual for the temperature to remain exactly at the set point temperature. The temperature would vary above and below the set point most of the time. To control is the variation of the temperature around the set point temperature a temperature controller is needed. [27]

The temperature controller used was a Gefran 800 P PID controller. To understand how the PID (Proportional-Integral-Differential) controller works there are a few definitions that must first be understood:

Derivative – which is also known as the rate, senses the rate of rise and fall of the system temperature and automatically adjusts the proportional band to minimize overshoot or undershoot. [28]

Cycle time – is also known as the duty cycle. It is the total length of time for the controller to complete one on/off cycle. E.g. with a 20 seconds cycle time, an on time of 10 seconds and an off time of 10 seconds represents a 50% power output. The controller will cycle on and off while within the proportional band. [30]

Integral – which is also known as the reset, is a function which adjusts the proportional bandwidth with respect to the set point temperature to compensate for the offset (droop) from the set point. It adjusts the controlled temperature to set point after the system stabilizes. [28]

Proportional – means a value varying relative to another value. The output of a proportional controller is relative to or a function of the difference between the temperature being controlled and the set point. The controller will be full on at some temperature which is well below the set point. It will be full off at some point well above the set point. [28]

Proportional Band (PB) of a controller is the difference in degrees between the highest full on point and the lowest full off point. It is the band of temperature, or the range of temperature over which the output of the controller is proportional. The width and the centre point temperature on this band can be varied using adjustments on the controller. [27]

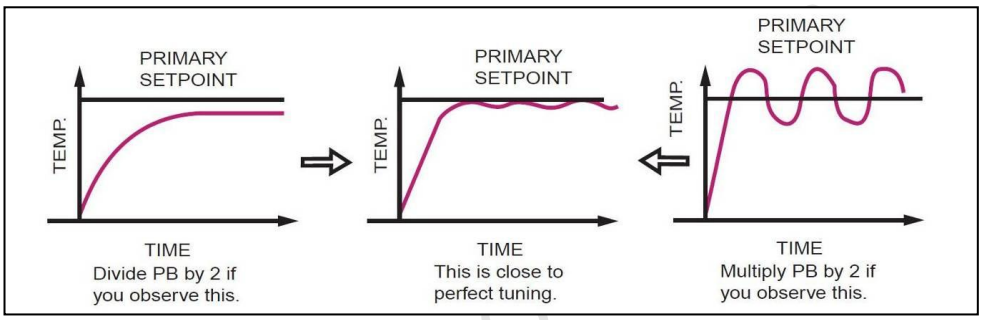

Figure 3.7.1 Temperature Oscillations [27]

3.7.2 Transformer tap adjustment on the Remote Heat Station (RHS)

The Ambrell EasyHeat Induction system has a power rating of 2.4 kW. The power is produced by the power supply and directed through the transformer. The transformer has taps that adjust the maximum amount of power which the controller puts out. The higher tap setting allows more power through and is needed to heat larger and denser samples to higher temperatures. The lower tap settings are used to heat samples to lower set point temperature as well as less dense samples more effectively. When the tap settings are too high the temperature controller has greater difficulty in controlling the oscillations around the set point temperature. Frequent overshooting makes the average temperature much higher than required. A tap setting that is too low will result in the sample being unable to reach the set point temperature. This causes excessive stress on the transformer as the remote heat station strains to heat the sample to set point temperature.

3.7.3 Calibrating the temperature controller and RHS

Wrought Ti samples

The auto-tuning settings were used as a starting point for the manual fine tuning of the PID settings. The PID setting had to be recalibrated for each set point temperature required due to the nature of titanium and the change in required transformer tap settings. The heating became erratic during the phase transformation from HCP α-titanium to BCC β-titanium around the Beta-transus temperature which increased the volume of the sample. To remedy this problem the heating rate was slowed down between 900°C and 1000°C to give the controller more time to stabilize the temperature oscillations. The initial transformer tap settings came preset from the factory when it had been set to heat a Ti slug of the same dimensions as our sample. The setting did not take into account the external factors which would affect the efficiency of the heating.

The ceramic compression platens have to pass through the induction heating coil in order to compress the sample while it's being heated. To accommodate the platens which have a larger diameter than the samples and still have some clearance to ensure smooth uniaxial compression the coils had to have a substantially larger diameter than would be used for optimum heating. This leads to a reduction in the efficiency of the heating coil meaning that more power is required to heat the sample to the set point temperature than was originally expected.

The ceramic platens, the upper push-rod and lower platen support also act as heat sinks during the induction heating of the sample. The ceramic platens are not affected by the induction heating coil and are therefore substantially cooler than the sample. When the ceramic platens are in contact with the sample they channel the heat away making it harder for the induction heater to maintain the temperature. This also increases the demand for sufficient power to maintain a constant temperature especially during the holding periods.

The trial and error method was use to determine the exact combination of PID setting and transformer tap settings. Once a combination had been selected and a set point chosen, the induction heater was allowed to run a specific heating program. At every increase of 100°C the power was measured and at each hold the time that the temperature took to stabilize at the set point was measured. Analysing this data the best combinations were selected.

Table 3.7.3.1 Transformer tap and PID settings for temperature control during the heating of Wrought Ti samples

Temperature Range	Transformer tap setting	P - Proportional	I - Integral	D - Derivative
600°C - 900°C	9	12	2	0.1
950°C -1000°C	11	12	1	0.05

Sintered Ti samples

The sintered samples are smaller and less dense than the wrought titanium samples. It was found that the PID and tap setting selected for the wrought Ti samples were not adequate to control the temperature of the sintered samples and therefore new settings had to be determined using the trial and error method described above.

Table 3.7.3.2 Transformer tap and PID settings for temperature control during the heating of Sintered Ti samples

Temperature Range	Transformer tap setting	P - Proportional	I - Integral	D - Derivative
900°C -950°C	9	12	1	0.1

4 METHODOLOGY

4.1 Material selection

As mentioned in the introduction and the literature review, there is a great interest in expanding the use of titanium in the aerospace and automobile manufacturing industries. A crucial step in the expansion of use lies in finding methods of reducing the cost of titanium products made via powder metallurgy.

4.1.1 Direct reduction CP titanium powder

Powder analysis was done by the powder metallurgy research group at the University of Stellenbosch. The titanium powder used for the project was supplied from Alpha Aesar, Germany and comprised grade 99.5 % purity titanium sponge fines with a particle size of -200 mesh. Particle size was checked using laser diffraction powder size analysis. According to the statistical data from the laser diffraction, the mean particle size of 32.27μm was obtained. Approximately 85% of the particles are less than 50μm indicating a fine powder distribution.

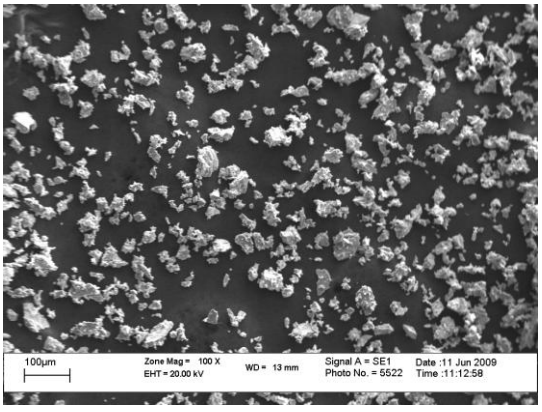

Figure 4.1.1.1 SEM images of the CP-titanium powder (low mag.)

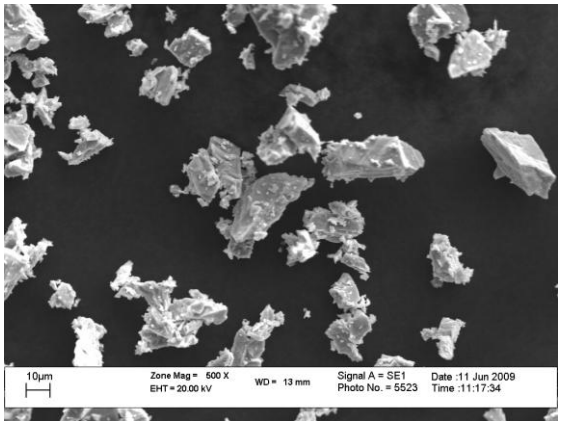

Figure 4.1.1.2 SEM images of the CP-titanium powder (high mag.)

The SEM images of the powder shown in figures 4.1.1.1 and 4.1.1.2 shows that the powders were irregular with fine microstructure and flaky. The particles average particle size is approximately less than 100µm which agrees with the laser diffraction data.

4.1.2 Wrought CP titanium

The wrought titanium was purchased from Goodfellow Metals in the form of 10 mm diameter rods which were the machined to the sample dimensions. The metal is 99.6% pure and was supplied in the annealed state.

4.1.3 Sintered CP titanium

The titanium green compacts were made from direct reduction titanium powder and compacted by the powder metallurgy research group at the University of Stellenbosch. The powder size was -200 mesh which should have been ± 74µm but laser diffraction particle analysis showed that the mean particle size of the powder was smaller at ± 32.27µm. The compaction pressures ranged from 325 – 405 MPa which resulted in a green density of between 3.01 and 3.6g.cm^{-3}, which is approximately 70% of the full density of CP-Ti. The green compacts were sintered at the Centre for Material Engineering at the University of Cape Town. The sintering process results in a decrease of volume and an increase in density.

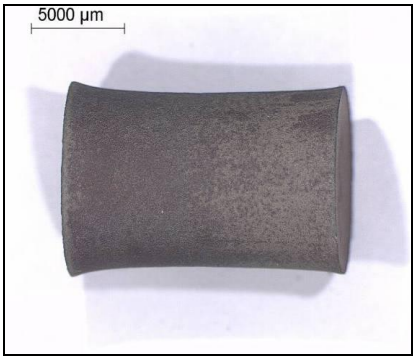

Figure 4.1.3 Photograph of Sintered CP-Ti compact

4.2 Sintering Methodology

4.2.1 Sintering trials

Sintering was done in a vacuum furnace which has a maximum operating temperature of 1200°C. The various parameters were tested in order to determine which is best for sintering. Based on the testing done by Heaney and Randall [29], a graphite lined crucible and a fused silica crucible were selected as possible options for the sintering vessels.

The atmosphere was also varied between a high purity Argon atmosphere and a high vacuum (10^{-4} mbar) atmosphere. Three sintering trials were run to establish optimum sintering parameters.

Trial 1:

Sintering parameters:

Temperature: 1200°C, Atmosphere: Argon

Soak Time: 2 hours, heating rate: 300°C/hr

Cooling: Furnace cool, Crucible: Graphite lined – Alumina

Table 4.2.1.1 Results of sintering trial 1

Sample	**Before Sintering**	**After Sintering**
Mass	2.5 g	3.2 g
Diameter	10.0 mm	10.8 mm
Height	10.2 mm	10.7 mm

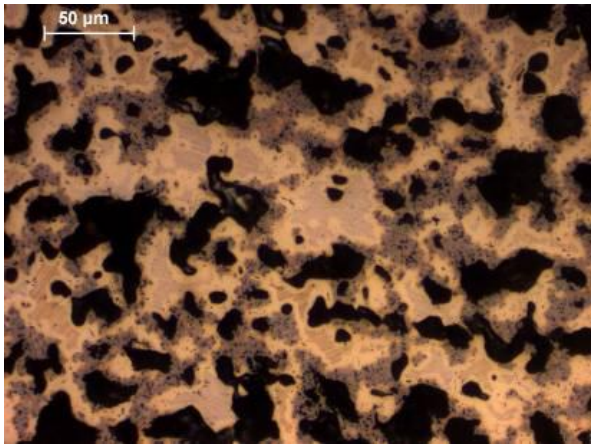

Figure 4.2.1.1 Microstructure of the sintered CP-Ti from Trial1. The microstructure shows large, irregular shaped pores throughout the sample. This indicates that the sample has been poorly sintered and is still very porous.

This trial resulted in high levels of oxidation and poor sintering. The increase in mass is as a result of the absorption of oxygen and possibly also carbon during sintering. Therefore the graphite-lined alumina crucible was deemed unsuitable for sintering the CP-Ti compacts

Trial 2:

Sintering parameters:

Temperature: 1200°C, Atmosphere: Argon

Soak Time: 2 hours, heating rate: 300°C/hr

Cooling: Furnace cool, Crucible: Translucent fused Silica

Table 4.2.1.2 Results of sintering trial 2

Sample	**Before Sintering**	**After Sintering**
Mass	3.79g	3.84g
Diameter	10.0 mm	Max: 10.2 ,Min: 9.2 mm
Height	15.4 mm	14.8 mm

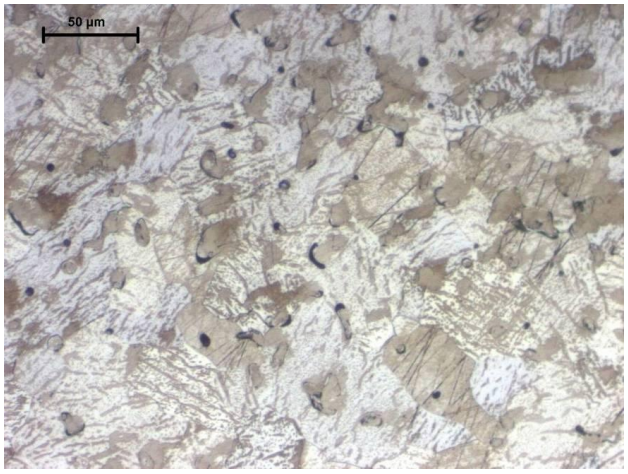

Figure 4.2.1.2 Microstructure of the sintered CP-Ti from Trial 2. This microstructure shows significantly less porosity than that of Fig. 4.2.1.2. The pores are small and circular; also the grain structure of the sintered metal can clearly be seen thus indicating an advanced degree of sintering within the sample.

The trial resulted in good sintering when compared to sintering trial 1. We can therefore deduce that a fused silica crucible is better for sintering CP-Ti compacts.

There is a slight increase in the weight of the sample but this can be attributed to oxidation from the Argon atmosphere.

Trial 3:

Sintering parameters:

Temperature: 1200°C, Atmosphere: High Vacuum (10^{-4} mbar)

Soak Time: 2 hours, heating rate: 300°C/hr

Cooling: Furnace cool, Crucible: Translucent fused Silica

Table 4.2.1.3 Results of sintering trial 3

Sample	**Before Sintering**	**After Sintering**
Mass	3.76g	3.78g
Diameter	10.0 mm	Max: 9.8 ,Min: 9.4 mm
Height	15.9 mm	14.6 mm

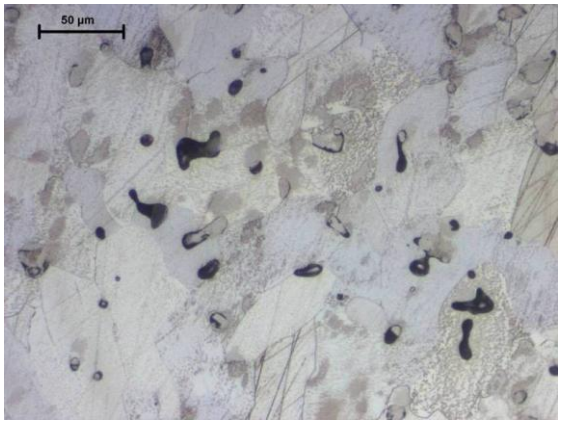

Figure 4.2.1.3 Microstructure of the sintered CP-Ti from Trial 3. The microstructure is similar to that of Fig. 4.2.1.2 and has many of the same features.

The sample shows very good sintering and the microstructure shows clearly defined grains. The difference in weight is negligible as almost no oxidation has occurred in this sample.

Therefore we can deduce that the high vacuum atmosphere is better for sintering than the Argon atmosphere. On the basis of these trials our samples will be sintered using the same parameters as Trial 3.

4.3 Determining the volume fraction of porosity in the sintered samples

4.3.1 Point counting method

The point counting method (ASTM Specification E562) for volume fraction estimation was used to determine the volume fraction of porosity in the sintered samples before and after hot compression. The technique uses a 2-dimensional point grid. The point grid is placed as a plastic overlay on a printed version of the micrograph of the sample in question. The magnification used was high enough so that the location of the test points with respect to the structural elements can clearly be discerned. [30]

The point grid was applied to a field selected at random at the optimum magnification and the number of points lying in the phase of interest P_α i.e. porosity is counted. Points lying on the porosity or the edge of a pore are counted as one half. Most point counting grids use crosses rather than points as the points are harder to see on the micrographs. When crosses are used, the intersection of the two crossed lines is the point and the intersection must lie in the phase to be considered a hit. The arms of the crosses are ignored. Generally, one measures 10 or more fields in this manner and computes the point fraction P_p as follows:

$$P_p = \frac{\Sigma P_\alpha}{P_T} = \frac{\sum P_\alpha}{nP_0} \quad [30]$$

Where n is the number of fields and P_0 is the number of grid points. Thus P_T is equal to nP_0, the total number of test points. Grid overlays usually employ a 16, 25, 49, 64 or 100 points in a systematic pattern although grids with more than 100 points are seldom used. The magnification and point density should be chosen so that no more than one grid point falls on a given particle of interest. In most work the volume fraction is expressed as a percentage by multiplying P_p by 100. [30] In our testing a 40X objective lens was used in conjunction with 100 point grid. Ten fields were analysed per sample.

4.3.2 Water displacement method

The Water Displacement Method is used to determine the density of the sample which has an irregular shape. Volume of an irregular shaped object can be difficult to calculate as well as the density of the object. The volume of the irregular shaped sample is determined by placing the sample inside a measuring cylinder filled with water. The volume increase when the sample is inserted is deemed to be the volume of the sample. To determine the density the mass of the sample is measured and then divided by the volume of the sample.

4.4 Hot compression testing procedure

Initial testing was performed on the wrought CP titanium samples. The testing was performed at 800°C, 900°C and 1000°C. The force was applied at a cross-head speed of 100 mm/min. All samples were strained to a nominal strain of 0, 0.2 and 0.5 to determine the influence of strain on recrystallization and subsequent grain size reduction. The microstructures were analysed and grain size differences compared. The 0 nominal strain samples were used as a control to differentiate between temperature effects and the effect of the strain on the samples. Micro-hardness testing was also performed to see if there had been an improvement in the hardness of the CP titanium. From this data the optimum amount of strain and temperature for the initiation of recrystallization was determined. The optimum deformation conditions which were selected from the wrought metal analysis were employed to determine the microstructure evolution in the sintered sample. All samples are then mounted and polished for light microscopy. Void size, shape and quantity were studied.

4.4.1 Heating conditions for compression testing

The samples were heated by an induction coil inside the vacuum vessel (see Section 3). The samples were heated at a rate of 100°C/min. This rate is fast enough to heat the entire sample quickly but not too rapid to cause thermal shock in the Alumina ceramic platens. The samples were then held for 10 minutes at the selected temperature to ensure that the entire sample is at the selected temperature and that there are almost no temperature gradients within the sample. Another effect to consider is the heat sink effect that is caused by the ceramic compression platens in the respective push-rod and platen support.

It was noted that when the upper platen was not in contact with the sample during the ε=0 condition the induction heating coil required substantially less power to heat the sample to the selected temperature. This proves that there is a significant heat sink effect due to the ceramic platens. This was overcome by increasing the power output of the induction unit to compensate for the heat loss when the platen is in contact with the sample.

Heating rates

Heating rates were programmed into the temperature controller for each testing temperature according to the parameters listed in Table 4.4.1.1:

Table 4.4.1.1 Heating rate schedules for the respective deformation temperatures

Temperature	**Step number**	**Heating from**	**Heating time**	**Hold time**
800°C	0	25°C - 600°C	6 min	10 min
	1	600°C - 800°C	2 min	10 min
	2	800°C - 25°C	Air quench	---
Temperature	**Step number**	**Heating from**	**Heating time**	**Hold time**
900°C	0	25°C - 700°C	7 min	10 min
	1	700°C - 900°C	2 min	10 min
	2	900°C - 25°C	Air quench	---
Temperature	**Step number**	**Heating from**	**Heating time**	**Hold time**
1000°C	0	25°C - 900°C	9 min	10 min
	1	900°C -1000°C	2 min	10 min
	2	1000°C - 25°C	Air quench	---

Table 4.4.1.1 can also be represented as a set of graphs which outline the temperature profile for each heating rate schedule (see Fig. 4.4.1.1-4.4.1.3).

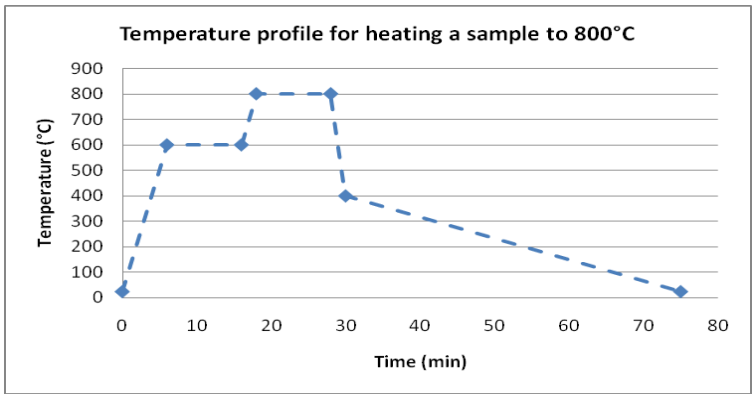

Figure 4.4.1.1 Heating profile for heating a sample to 800°C (based on Table 4.4.1.1)

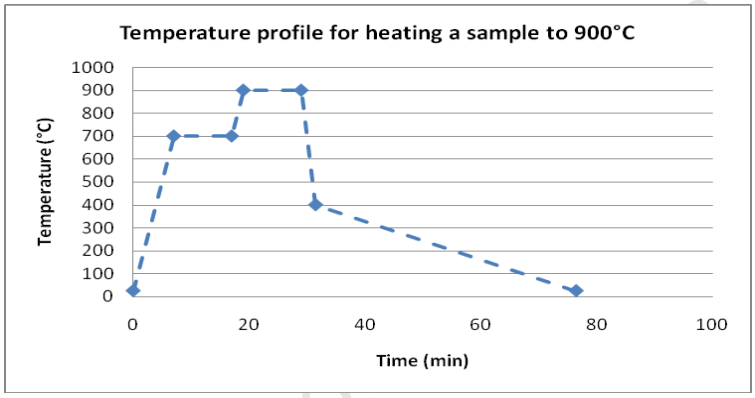

Figure 4.4.1.2 Heating profile for heating a sample to 900°C (based on Table 4.4.1.1)

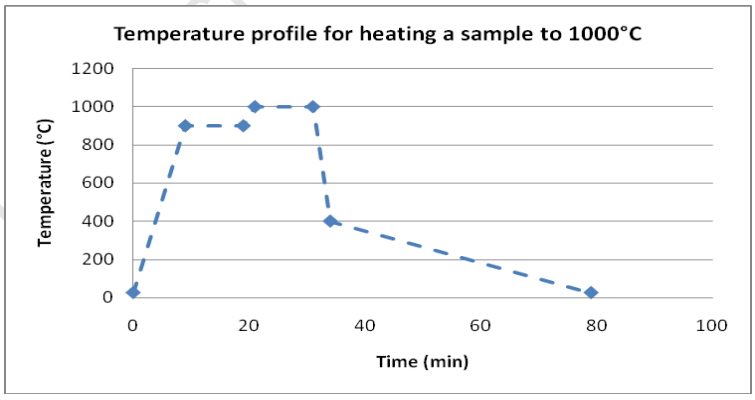

Figure 4.4.1.3 Heating profile for heating a sample to 1000°C (based on Table 4.4.1.1)

Samples were air quenched by turning off the induction furnace and allowing the samples to cool in the vacuum. The sample initially cooled down rapidly at approximately 200°C/min to a temperature of around 400°C, after which it cooled more slowly to room temperature.

Between 900°C and 1000°C a phase change occurs from α to β titanium and this phase transition affects the heating rate due to the change in crystal structure resulting in an increase in volume. Therefore a slower heating rate is used to prevent power surges and overheating.

4.4.2 Lubrication

Lubrication between the samples and the platens is extremely important when trying to ensure uniform deformation by decreasing friction. The most common lubricant used for hot compression is Graphite lubricant which consists of finely milled graphite powder dispersed with engine oil. However, Li, Peng *et al* [29] found that the graphite lubricant was only effective at temperatures under 800°C which is too low for the testing parameters used. Rao and Hawbolt [31] used tantalum foil between the specimen and dies to avoid welding between the sample and the platen during hot compression in a Gleeble 1500 hot compression testing machine. The tantalum foil was effective between 750°C and 1000°C. As the testing would occur within this temperature range the tantalum foils were chosen as the lubricant. The tantalum foil was purchased from Goodfellow R & D Products and the properties are listed in Table 4.4.2. The dimensions of the tantalum foils are 15 mm in diameter and 0.100 mm in thickness. Two foils are used for each test.

Table 4.4.2 Properties of Tantalum

Properties	**Values**
Density	16.6 $g.cm^{-3}$
Melting point	2996°C
Yield Strength	310-380 MPa
Thermal conductivity	57.5 $W.m^{-1}.K^{-1}$

4.4.3 Compression

The samples are compressed using a constant cross-head speed of 100mm/min to yield an initial strain rate of $0.1s^{-1}$. The amount of displacement is entered into a compression programme before the start of the test. The machine gauges strain as the displacement of the cross-head. The resistance to displacement was then measured by the load cell. Once the selected deformation has been achieved the load is removed from the sample and the test is completed.

4.5 Microscopy

4.5.1 Specimen preparation

The specimens were sectioned through the centre parallel to the axis of compression on a diamond cutting wheel in the Buehler Isomet Low Speed saw at a medium speed (speed 7) to prevent microstructural damage. Each sample is set with the axial face down in black acrylic hot mounting resin, using a Struers LaboPress 3 Hot mounting machine (see Fig 4.4.1).

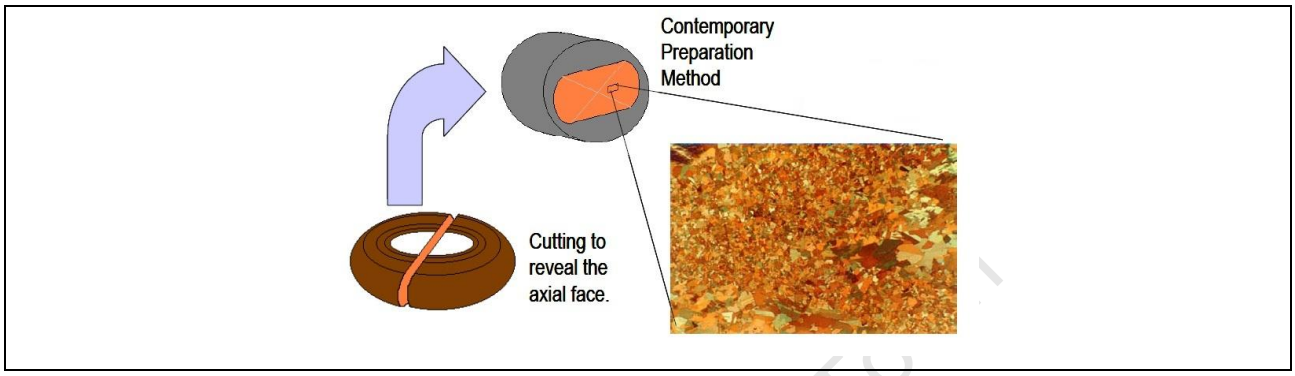

Figure 4.5.1 Schematic diagram for the sample preparation of a hot compressed sample. [32]

The black resin is Struers Polyfast acrylic resin, the black colour is an effect of the carbon content of the resin. It has good edge retention and is conductive. The specimens are then ground and polished using a Struers RotoPol-22 Automatic polisher according to the polishing recipe in Table 4.5.1.The polishing step takes place using an Attack solution with a higher concentration of hydrogen peroxide than a regular Attack solution. The “extra-strength” Attack solution consists of 20 ml of 30 vol. % hydrogen peroxide and 40 ml of Colloidal Silica suspension.

Table 4.5.1 Polishing recipe for polishing CP-Titanium

Grit / Pad	Speed	Force	Time	Lubricant	Repeats
500 SiC	150 Rpm	15 N	3:00	Water	2
800 SiC	150 Rpm	15 N	3:00	Water	2
1200 SiC	150 Rpm	15 N	3:00	Water	2
MD Nap	150 Rpm	30 N	10:00	“extra-strength” Attack solution	1
MD Nap	150 Rpm	30 N	10:00	Water	1

The samples were prepared for light microscopy examination by etching in Keller's reagent. Keller's Reagent is made up of 190 ml of Water, 5 ml of HNO_3, 3 ml of HCl and 2 ml of HF. The sample is immersed for 30 seconds or until a light haze is observed on the polished surface of the sample.

Following etching, the sample is washed with distilled water and then forced-air dried. The usual etchant for titanium alloys is the Kroll's Reagent but it was found to produce too much staining to clearly see the grain boundaries in the CP-Ti.

4.5.2 Strain distribution in the deformed sample

The flow of material between the ceramic platens during hot compression results in the uneven distribution of strain within the deformed sample. The specimen undergoes barrelling during the compression which forms an area of high strain through the centre of the sample adjacent to the direction in which the strain is applied and an unstrained dead zone in the faces which make contact with the ceramic compression platens (see Fig.2.17) This is discussed in more detail in Chapter 2.3. The strain is inhomogeneous across the axial plane. The area which exhibits the highest amount of retained strain is therefore the area of interest. Micrographs and Microhardness testing will be focussed in this area.

4.5.3 Light optical microscopy

The post deformation microstructures were examined using the Nikon Optiphot light microscope. The micrographs of the surfaces were taken under low and high magnification. The light microscope was used to identify the strain distribution within the sample. It was also used to determine the pore size and shape in the sintered CP-Ti before hot compression testing. The higher magnification micrographs were captured using Leica Reichert MeF3 light microscope fitted with a 100X objective lens.

4.5.4 Scanning Electron Microscopy (SEM)

The post deformation microstructures were also examined using the Leica Stereoscan 440 scanning electron microscope. The SEM was used to determine grain size and shape as well as the size, shape and frequency of the porosity.

4.6 Hardness testing

Micro-hardness testing was conducted on all samples that were sintered and compressed at high temperature. The hardness values are taken through the centre of the sample along the homogenous region with the highest amount of strain.

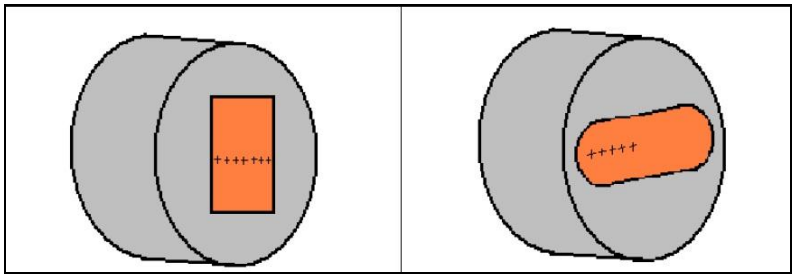

Figure 4.6 Schematic diagrams of the samples showing where the hardness indentations were made. [32]

The Vickers hardness values for each of the hot compressed samples were determined using the Matsuzawa MXT α7 digital microhardness tester fitted with a Vickers diamond indenter. The load used was 200g force for the wrought titanium samples and 1000g force for the hot compressed sintered samples. Each sample had 5 indentations made and 10 samples were tested for each strain condition. Thus the resultant hardness value is the average hardness determined from the measurement of 50 indentations.

4.7 Post deformation heat treatment

4.7.1 Post deformation annealing (PDA)

After the wrought and sintered Ti samples have been hot compressed, the deformed samples were then annealed at 870°C for 1hr. The post deformation annealing was done to continue the recrystallization process of grains that was started during the hot deformation via static recrystallization.

The annealing cycle was as follows:

The samples were heated at 5°C/min to 870°C. It was then held at 870°C for 1 hr. Following the holding period the samples were cooled from 870°C to 600°C at a rate of 3°C/min. At 600°C the samples were allowed to furnace cool to room temperature (± 25°C) at rate is > 5°C/min. Samples were prepared for light optical microscopy by the method described in section 4.4.1.

5 RESULTS AND DISCUSSION

The following section contains the presentation and the discussion of those results that were obtained from the experimental procedure described in Chapter 4. The results follow the same format as the sections in the Methodology.

5.1 Initial testing of the wrought CP-Titanium

5.1.1 Hot Compression testing of wrought Ti samples

Determining the required machine cross-head displacement

The actual input (ΔH) is the calculated change in height + 0.5 mm to account for the initial slackness and the elastic deformation of the machine set up. Although great effort has been made to be as accurate as possible with the strain calculations, the actual strain experienced by the sample might differ from the expected strain if the elastic region is greater than expected and there is more slackness in the compression setup than was initially anticipated. The expected strain will henceforth be referred to as the nominal strain. In the calculations negative strain represents compressive strain. The strain is calculated using the formula for true strain (log. strain), $\varepsilon = \ln\left(h_1/h_0\right)$, where h_0 = the initial height and h_1 = the final height. For the wrought samples the initial height is 15mm and the diameter is 10mm. Therefore the calculated height change to achieve the nominal strain level (Δh) and the actual required machine cross-head displacement (ΔH) are determined as follows:

ε = -0.2 $-0.2 = \ln\left(h_1/15\right)$

$$e^{-0.2} = h_1/15$$

$$15\, e^{-0.2} = h_1$$

$$12.3 = h_1$$

Δh = 15 - 12.3 = 2.7 and ΔH = 3.2mm

ε = -0.5 $-0.5 = \ln\left(h_1/15\right)$

$$e^{-0.5} = h_1/15$$

$$15\, e^{-0.5} = h_1$$

$$9.1 = h_1$$

Δh = 15 – 9.1 = 5.9 and ΔH = 6.4mm

The stress vs. strain curves for the various testing temperatures are shown in Figures 5.1.1.1 and 5.1.1.2. Each figure shows the stress required to achieve a preselected amount of compressive strain. As expected the highest stress is required to deform the samples at the lowest temperature and that the more deformation required the higher the stress needed. This relationship is independent of the temperature of the sample, but the work hardening rate is highest for the lowest deformation temperature.

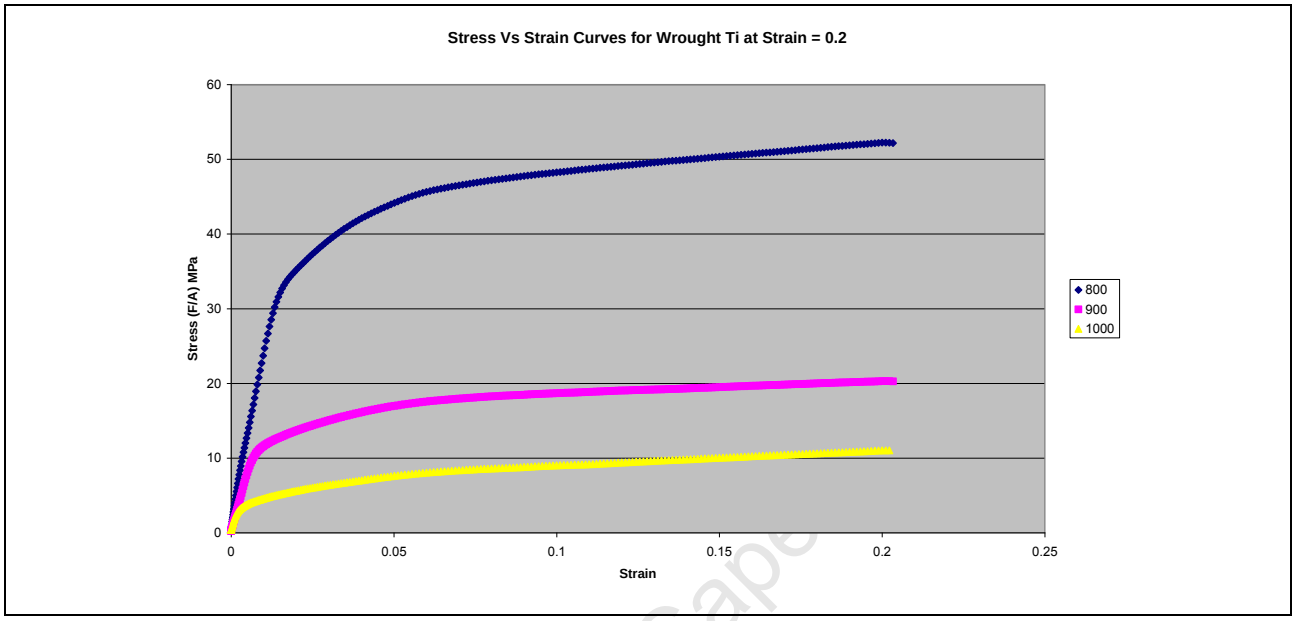

Figure 5.1.1.1 Stress Vs Strain curves for Wrought Ti at various test temperatures for a nominal strain of 0.2 (initial strain rate = $0.1s^{-1}$)

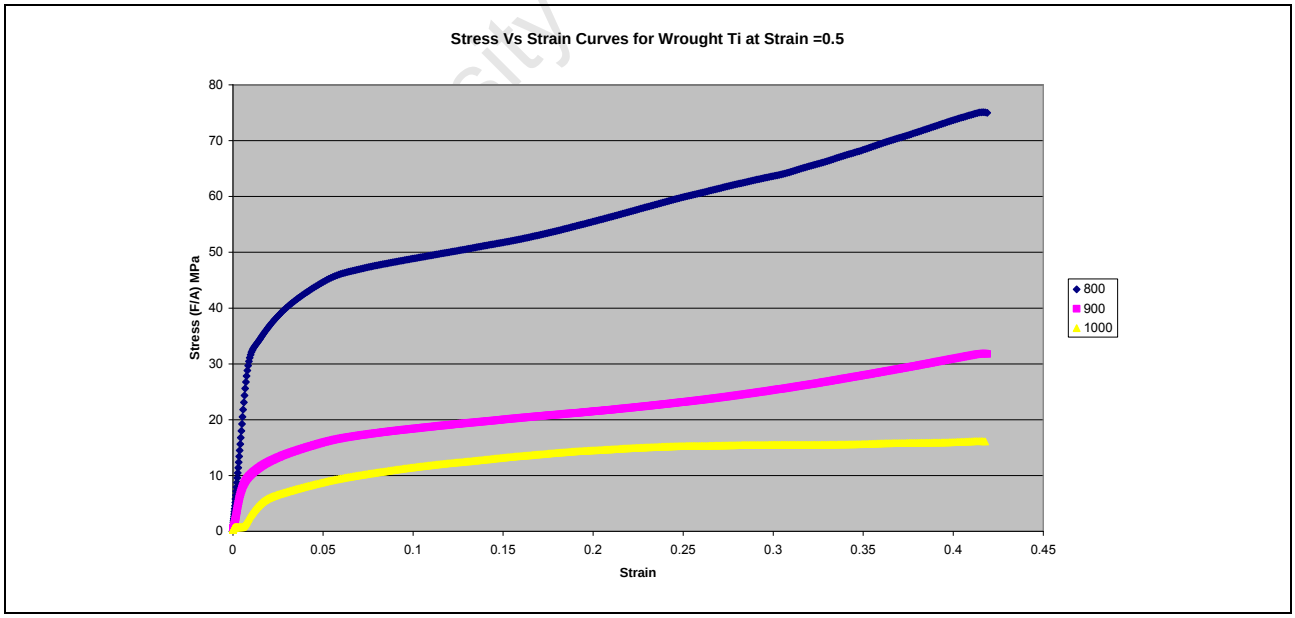

Figure 5.1.1.2 Stress Vs Strain curves for Wrought Ti at various test temperatures for a nominal strain of 0.5 (initial strain rate $0.1s^{-1}$)

From the graphs we can see that the actual strain experienced by the samples differs from the nominal value. For the nominal compressive strain of 0.2 the actual strain was found to be 0.21 and for the nominal strain of 0.5 the actual strain was found to be 0.43.

5.1.2 Microstructure of hot compressed wrought Ti samples

The microstructures of the samples are compared after hot compression at varying amounts of compressive strain namely 0, 0.2 and 0.5. The samples that have a compressive strain = 0 condition represents the same thermal cycle as the other samples but without the compression. The strain values include both elastic and plastic deformation as indicated on the stress-strain curves. The samples are compressed at 800, 900 and 1000°C. For each temperature and strain condition 3 tests were conducted. A comparison of the microstructures in Figure 5.1.2.1 shows the microstructural development at 800°C and strains of 0, 0.2 and 0.5. From the micrographs the extent of the barrelling of the sample with regards to the nominal strain can be seen. Also the position where the thermocouple was placed inside the sample is visible in some of the micrographs and this indicates the midsection of the sample. The microstructures of the three samples are very fine and the average grain size in the annealed sample before hot compression was approximately 30µm.

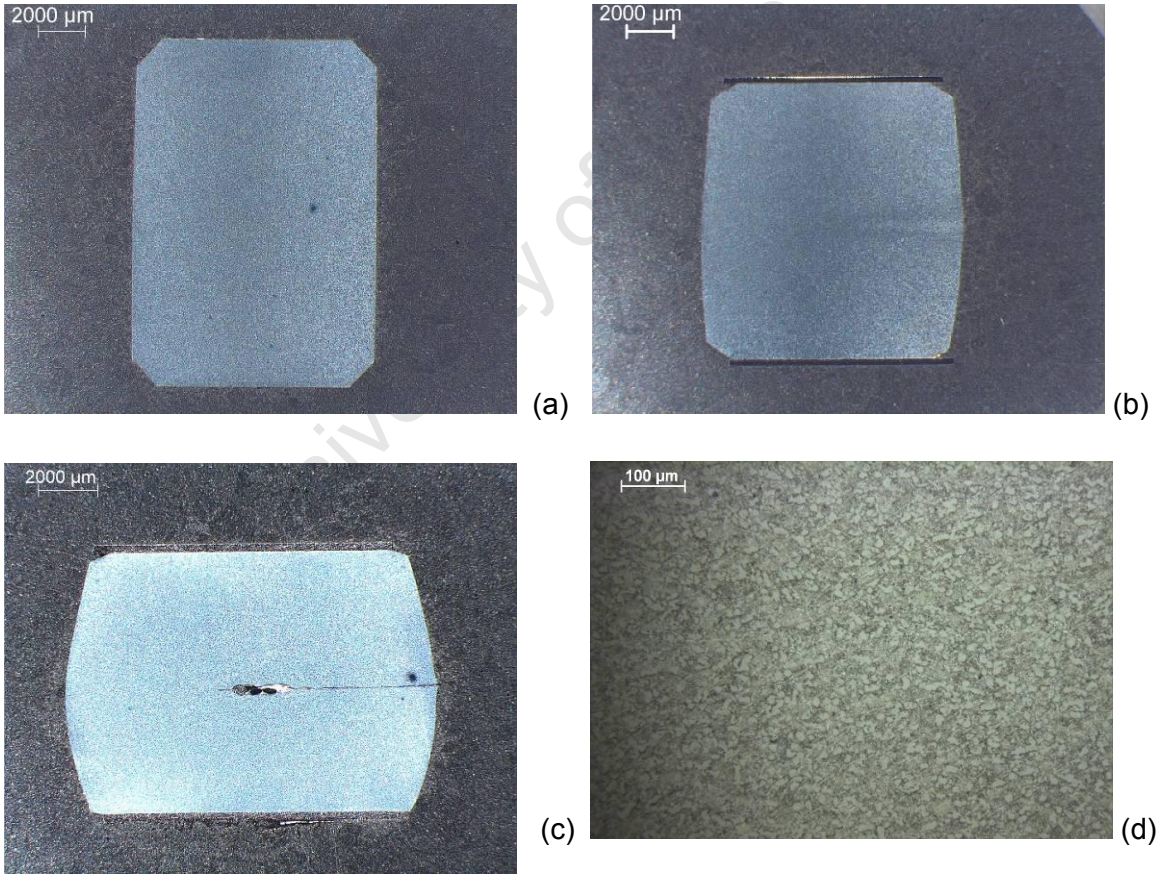

Figure 5.1.2.1 Microstructure of samples that have been hot compressed at 800°C and a compressive strain of (a) 0, (b) 0.2, (c) 0.5 and (d) close up of the high strain region of the 0.5 strain sample.

The next comparison is that of the microstructures in Figure 5.1.2.2. The micrographs show grain growth at 900°C when no strain is applied. When the nominal strain is increased to 0.2, it can be observed that the grains in the midsection of the sample have been noticeably deformed. In the sample that has undergone a strain of 0.5 it has a significantly larger region of deformed grains. It also appears that the grains in the midsection of the sample are more deformed than those of the 0.2 strain sample. It is difficult to measure the exact grain size of the hot compressed wrought titanium sample due to the deformed grain structure but grain size can be measured and compared after post deformation annealing when the grains have recrystallized further and their boundaries are more defined.

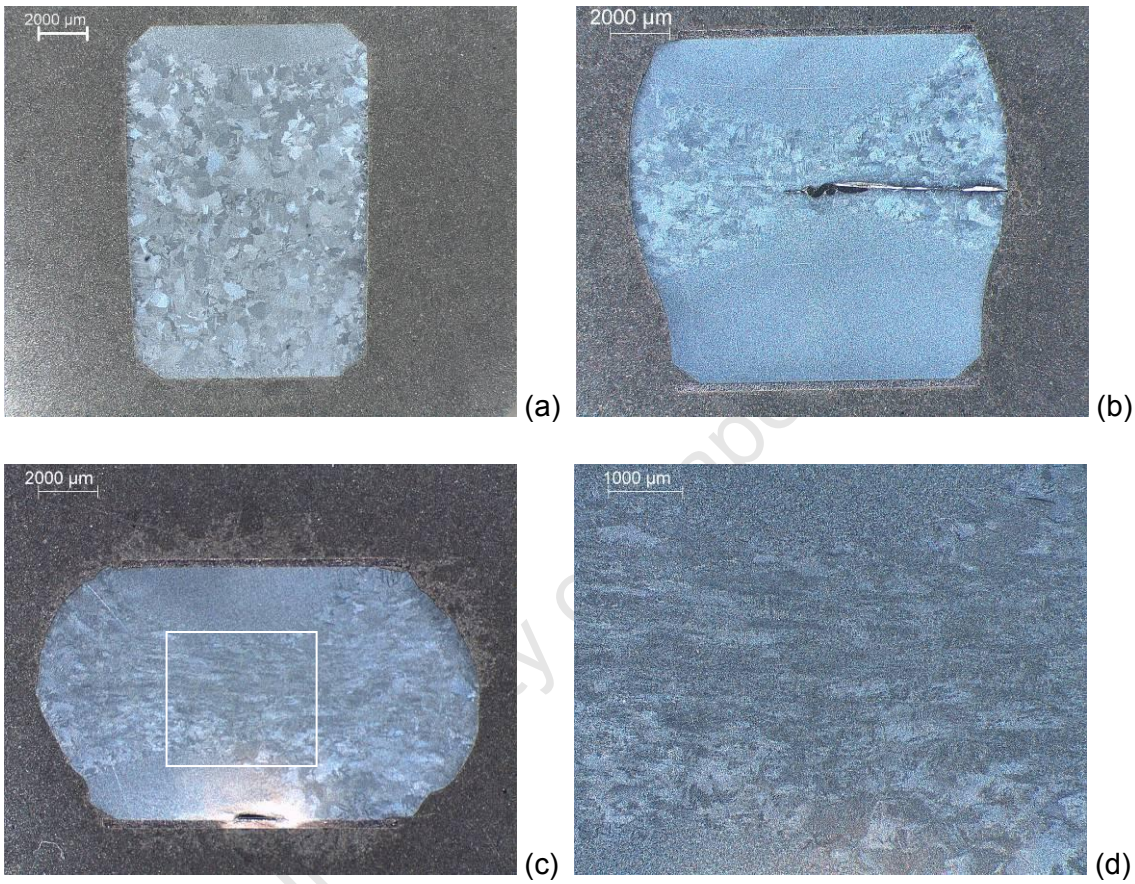

Figure 5.1.2.2 Microstructure of samples that have been hot compressed at 900°C and a compressive strain of (a) 0, (b) 0.2, (c) 0.5 and (d) close up of the high strain region o f the 0.5 strain sample.

In the microstructures of Figure 5.1.2.2(a)-(c) there is a noticeable region of fine grains where the sample would have been in direct contact with the ceramic platens. These features can be explained by the heat sink effect caused by the ceramic platens. The platens draw heat away from the sample thereby causing the contact faces of the sample to be cooler than the centre of the sample. It has been reported that 900°C is a critical temperature for rapid grain growth within the sample [25]. When the temperature is lower the grain growth is not as rapid which results in the grain size variation in the different regions observed.

The hot compression testing introduces retained strain into the samples which in turn creates nucleation sites for the initiation of recrystallization. At this point the grains are deformed and do not have an equiaxed shape as commonly seen in recrystallized grains.

These deformed grains require more energy and time in order to fully recrystallize which is why a post deformation annealing treatment is necessary.

A further comparison of the microstructures in Figure 5.1.2.3 show that at 1000°C and strain of 0, grain growth occurs and is more extensive than that of the 900°C sample. When the strain is increased to 0.2, an area of high retained strain can be seen through the midsection of the sample.

The grains in the midsection of the sample have been noticeably deformed. The sample that has undergone a strain of 0.5 has a significantly larger region of high retained strain. As expected the grains in the midsection of the sample are more deformed than those of the 0.2 strain sample.

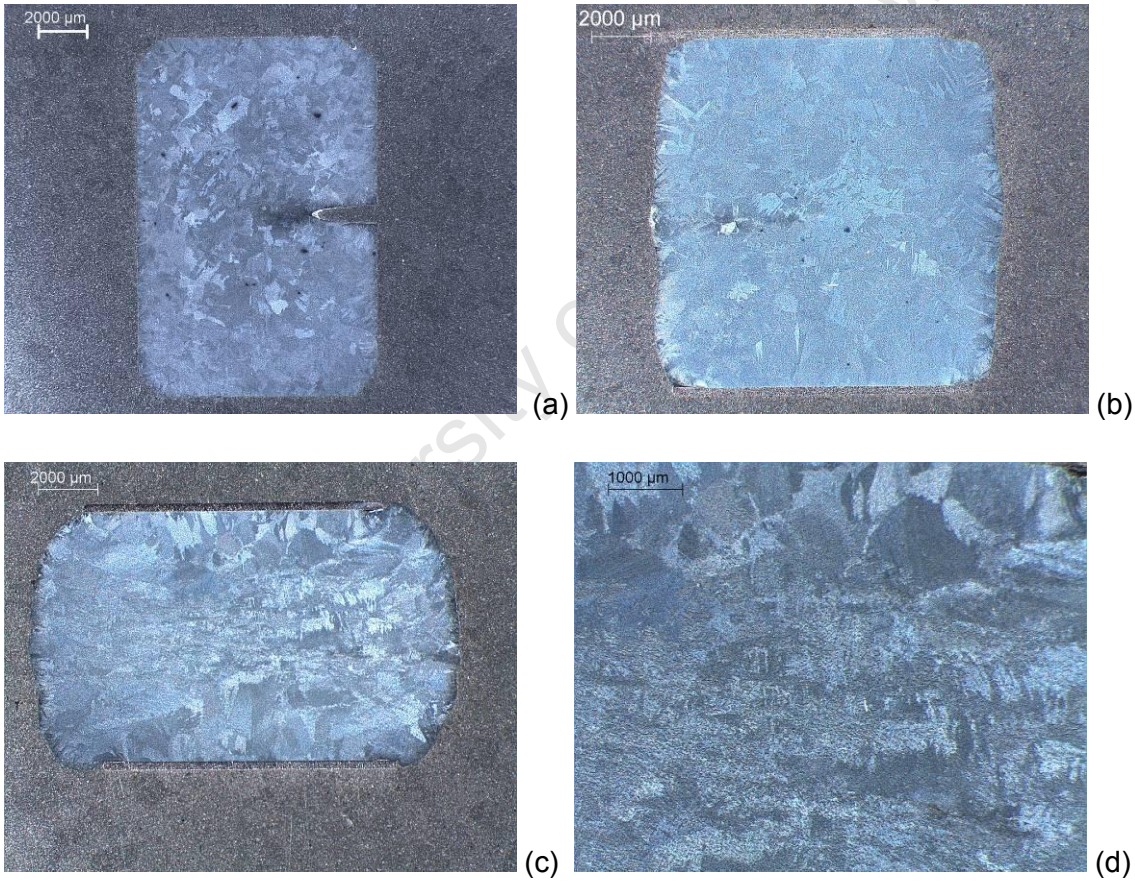

Figure 5.1.2.3 Microstructure of samples that have been hot compressed at 1000°C and a compressive strain of (a) 0, (b) 0.2, (c) 0.5 and (d) close up of the high strain region o f the 0.5 strain sample.

5.1.3 Post deformation annealing of wrought Ti samples

The annealing cycle is as follows: The sample is heated at 5°C/min to 870°C. It is then held at 870°C for 1hr. Following the holding period the sample is cooled from 870°C to 600°C at a rate of 3°C/min. At 600°C the sample is allowed to furnace cool to room temperature, whith a cooling rate of >5°C/min.

Hot compression Temperature = 800°C and nominal strain = 0.2

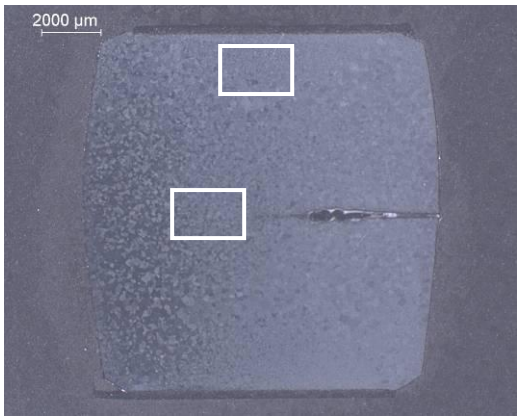

5.1.3.1(a) Overview low mag.

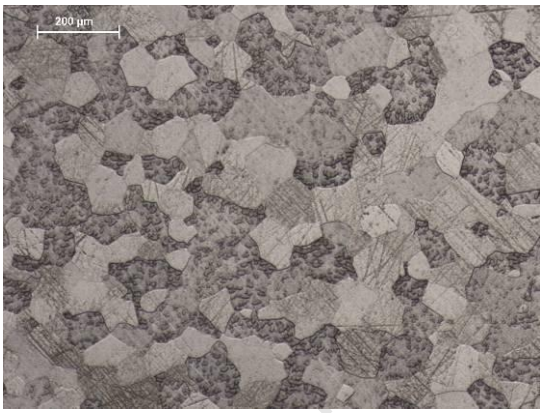

5.1.3.1(b) Centre low mag.

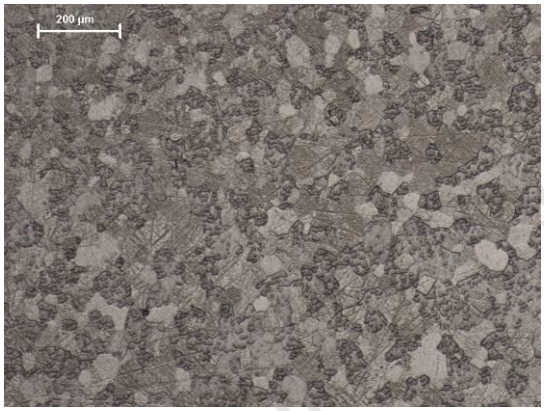

5.1.3.1(c) Edge low mag.

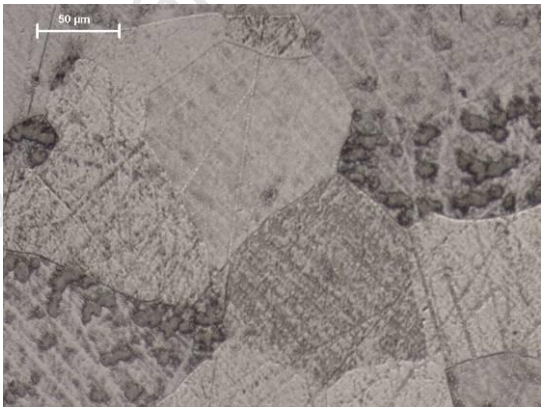

5.1.3.1 (d) Centre high mag.

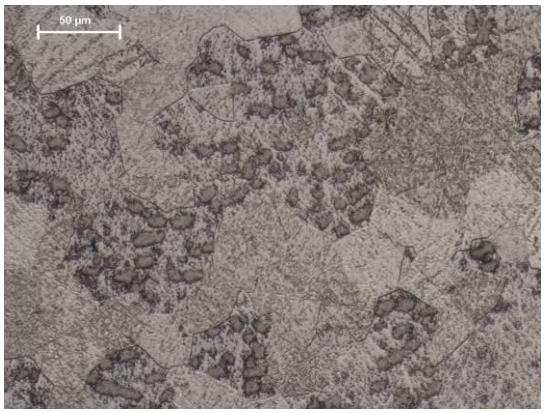

5.1.3.1 (e) Edge high mag.

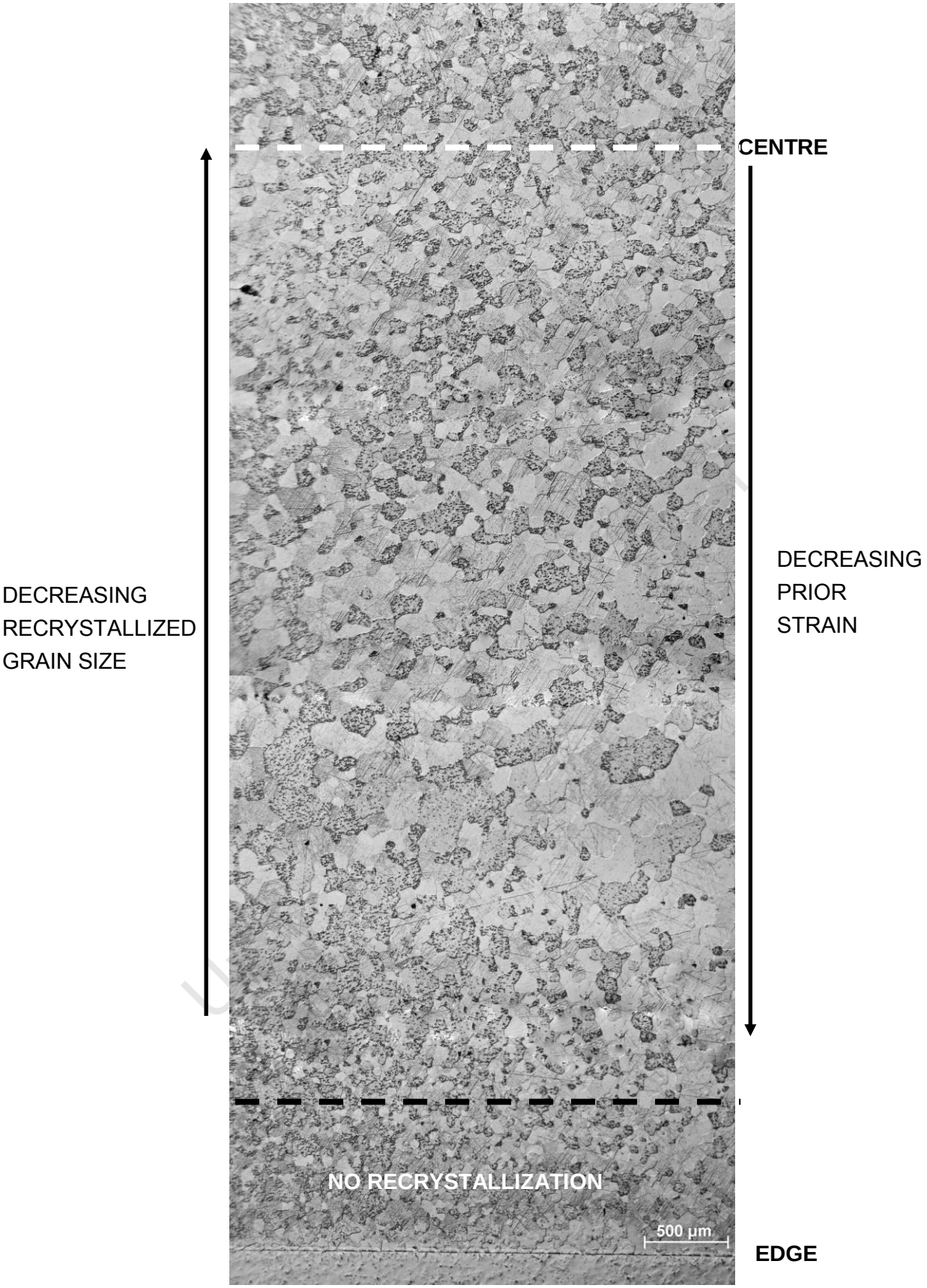

Figure 5.1.3.1 (f) Section from the centre of the sample to horizontal edge

Interpretation of microstructures 5.1.3.1(a)-(f)

It is observed in the micrographs above that there are regions with different microstructures within the sample itself. From the gradient in grain size it can be seen that the grain size increases from the centre towards the edge but at the region closest to the edge the grain size is smaller. The edges of the sample have a similar average grain size (28.2 ± 6.5μm) to that of the centre of the sample which has an average grain size of 50.1 ± 18.4μm. The grain size in the centre of the sample is the result of many nucleation sites being caused by the high retained strain during hot compression in this region. During recrystallization the many nucleation sites form newly recrystallized grains which are smaller than the original grains until grain growth occurs during post deformation annealing.

The region of grains between the centre and the edge of the sample that has the largest grain size is the result of only a few nucleation sites being developed during hot compression of the sample. This area has a lower amount of retained strain than the centre of the sample. During recrystallization these few nucleation sites recrystallize and absorb the surrounding grains producing grains which are larger than the original grain size and grow further during post deformation annealing. The region of grains closest to the edge of the sample has the smallest grain size.

This is because this region of the sample was in direct contact with the ceramic platens during hot compression, experienced a lower temperature during hot compression and also experiences the least amount of strain overall during hot compression. Thus the edges of the sample have not undergone recrystallization. The grain size is larger than the original grain size due to grain growth during the post deformation annealing treatment.

Hot compression Temperature = 800°C and nominal strain = 0.5

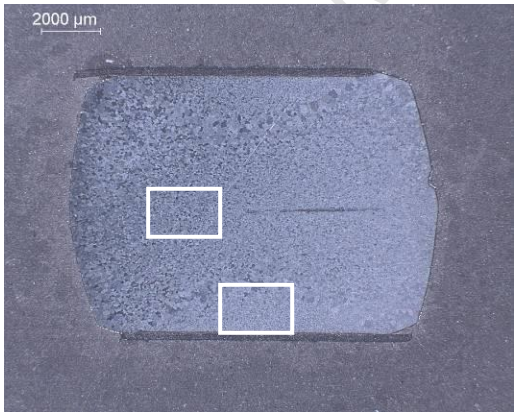

5.1.3.2(a) Overview low mag.

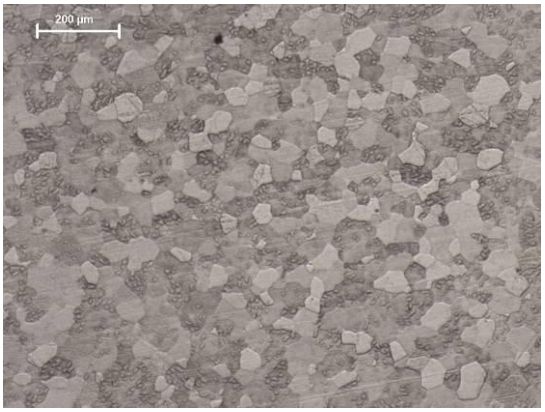

5.1.3.2(b) Centre low mag.

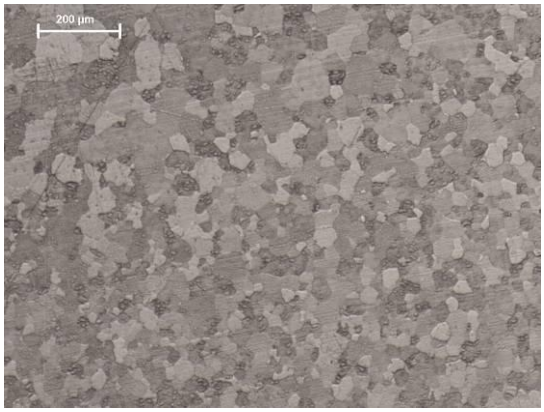

5.1.3.2(c) Edge low mag.

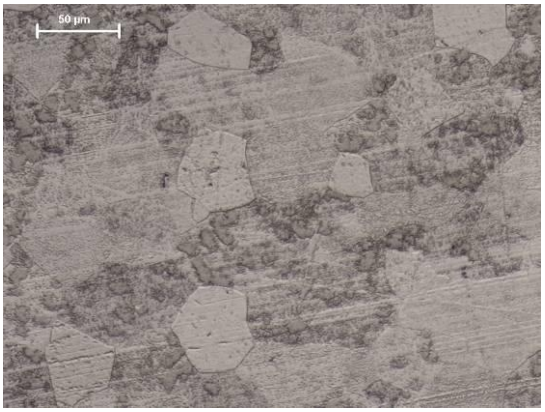

5.1.3.2 (d) Centre high mag.

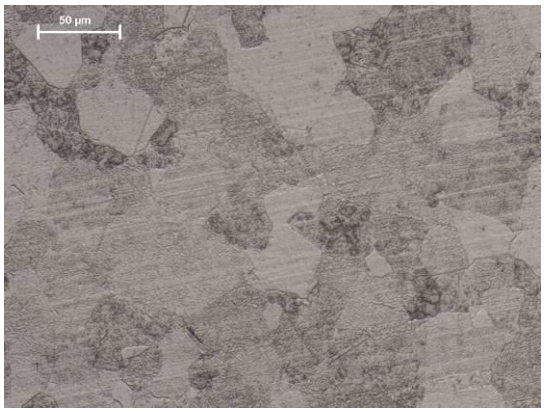

5.1.3.2 (e) Edge high mag.

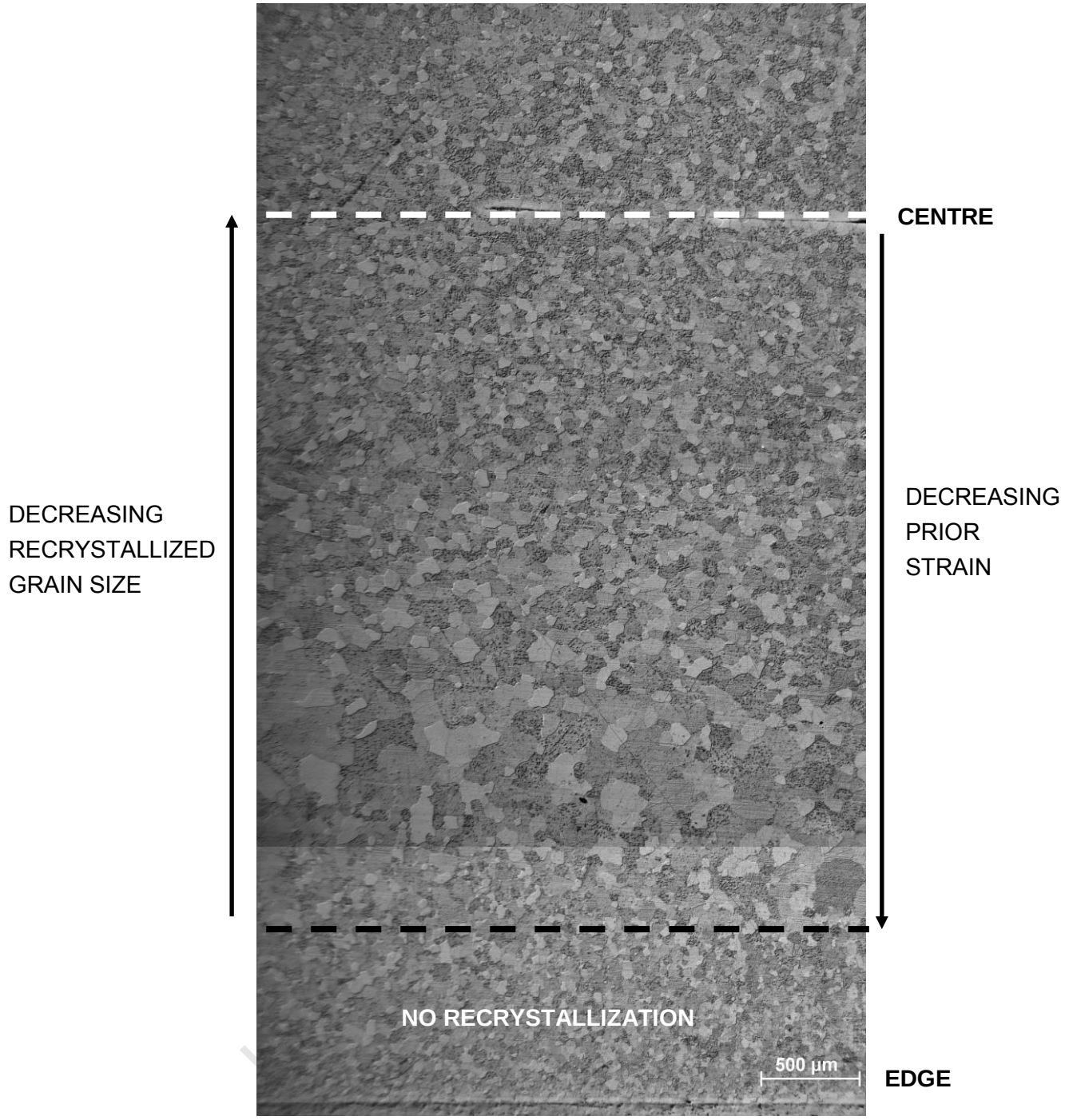

Figure 5.1.3.2 (f) Section from the centre of the sample to horizontal edge

Interpretation of the microstructures 5.1.3.2(a)-(f)

The micrographs clearly show individual regions with different microstructures within the sample. The grain size increases from the centre towards the edge but at the region closest to the edge the grain size is smaller. The edges of the sample have a similar average grain size (29.2 ± 8.8μm) to that of the centre of the sample which has an average grain size of 31.0 ± 11.6μm. The size of the grains in the centre of the sample is caused by the creation of multiple nucleation sites by the high retained strain during hot compression in this region. During recrystallization the multiple nucleation sites form newly recrystallized grains which are initially smaller than the original grains until grain growth occurs during post deformation annealing.

The region of grains between the centre and the edge of the sample has the largest grain size. This is the result of only a few nucleation sites developing during the hot compression of the sample. The amount of retained strain in this region is much lower than the centre of the sample. During the post deformation anneal these few nucleation sites initiate recrystallization and absorb the surrounding grains thus producing grains which are larger than the original grain size prior to hot compression. The recrystallized grains also undergo grain growth during the post deformation annealing process.

The region of grains nearest to the edge of the sample has does not follow the same grain size gradient as the other regions. The grains are smaller than the adjacent region's grains. This is because this region of the sample was in direct contact with the ceramic platens during hot compression, experienced a lower temperature and also experiences the least amount of strain overall during hot compression. Thus the edges of the sample have not undergone recrystallization. The grain size is larger than the original grain size due to grain growth during the post deformation annealing treatment.

The recrystallized grains in the centre of the sample are slightly larger than the original grain size and in agreement with the size of the recrystallized grains in the centre of the sample which had been hot compressed at 800°C to a nominal strain of 0.2.

Hot compression Temperature = 900°C and nominal strain = 0.2

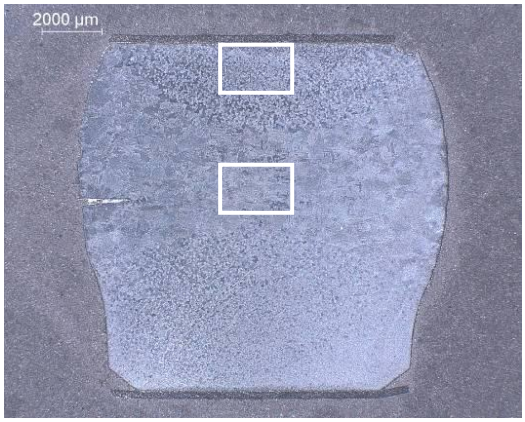

5.1.3.3(a) Overview low mag.

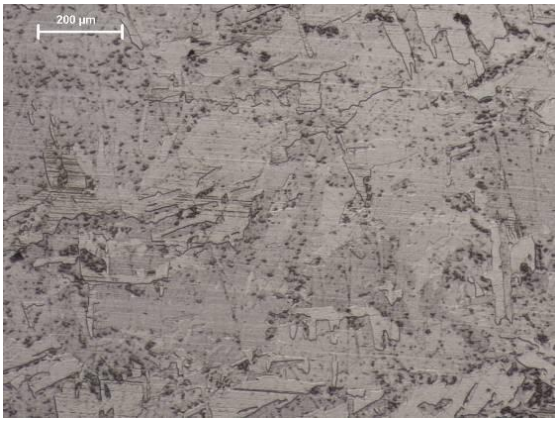

5.1.3.3(b) Centre low mag.

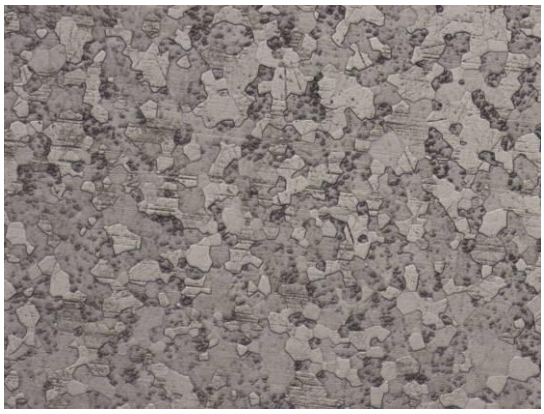

5.1.3.3(c) Edge low mag.

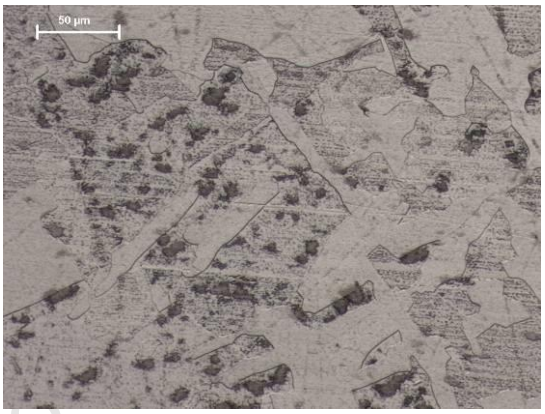

5.1.3.3 (d) Centre high mag.

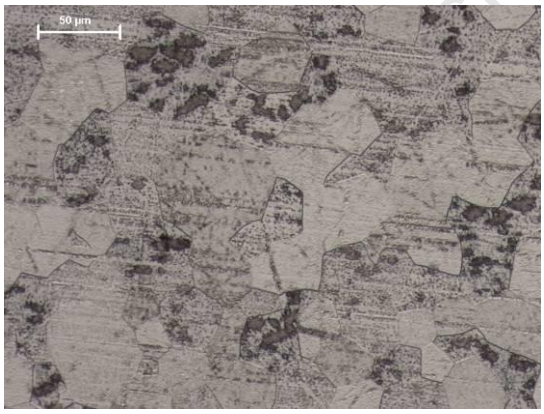

5.1.3.3 (e) Edge high mag.

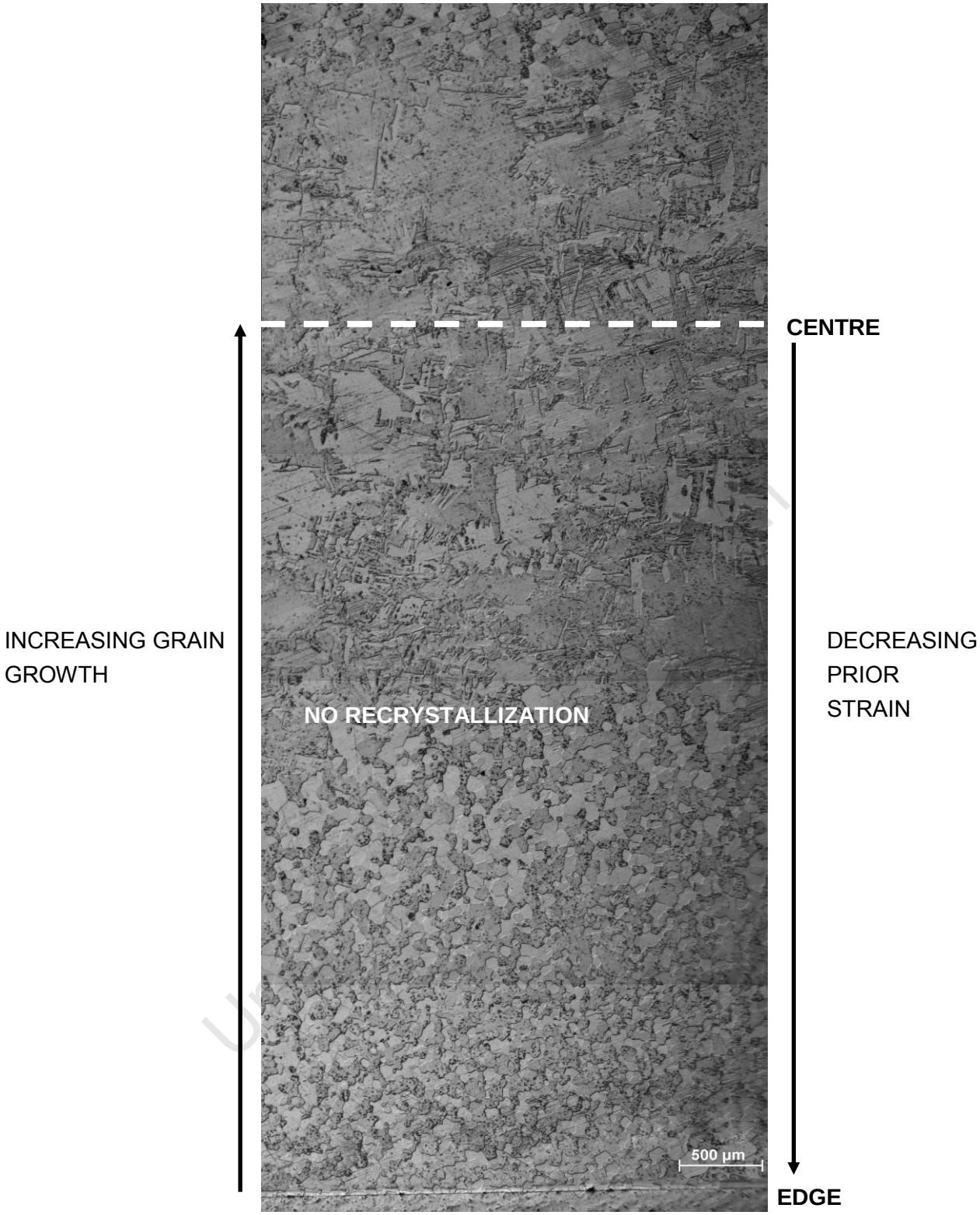

Figure 5.1.3.3 (f) Section from the centre of the sample to horizontal edge

Interpretation of the microstructures 5.1.3.3(a)-(f)

Analysis of the micrographs above shows that the sample has distinct regions with different microstructures. From the gradient in grain size it can be seen that the grain size decreases from the centre towards the edge. The grain size in the centre of the sample is very large and irregular in shape. In the Stress vs. Strain curves for wrought Ti at strain = 0.2 (see fig 5.1.1.1) the measured stress directly relates to the amount of retained strain in the samples. The sample which had been hot compressed at 800°C to a nominal strain of 0.2 reached a measured stress of just over 50 MPa whereas the sample which had been hot compressed at 900°C to a nominal strain of 0.2 had undergone a measured stress of ± 20MPa. From the comparison of the curves it can be seen that this sample has had a much lower measured stress and therefore a lower retained work hardening than that of the sample which has been hot compressed at 800°C to the same nominal strain (just above 50 MPa). At this temperature the retained strain was too low to form nucleation sites for the initiation of recrystallization and grain growth occurs at a high rate.

The grains in the region between the centre and the edge of the sample are larger than the grains at the edge and smaller than the grains at the centre because the rate of grain growth in this region was higher than that of the grains nearest to the edge but lower than that of the grains at the centre. This is because of the temperature gradient between the centre of the sample and the edge of the sample which affects the grain growth rate. The centre of the sample was the hottest region during hot compression and had the highest grain growth rate whereas the edge regions were cooler and had a slower grain growth rate during compression. The region of grains closest to the edge of the sample has the smallest grains. This is because this region of the sample that was in direct contact with the ceramic platens during hot compression experienced the lowest temperature during hot compression The unrecrystallized grains in the centre of the sample are significantly larger than the original grain size and are irregularly shaped in comparison to recrystallized grains in the centre of the samples which had been hot compressed at 800°C to nominal strains of 0.2 and 0.5, which are smaller and equiaxed in shape.

Hot compression Temperature = 900°C and nominal strain = 0.5

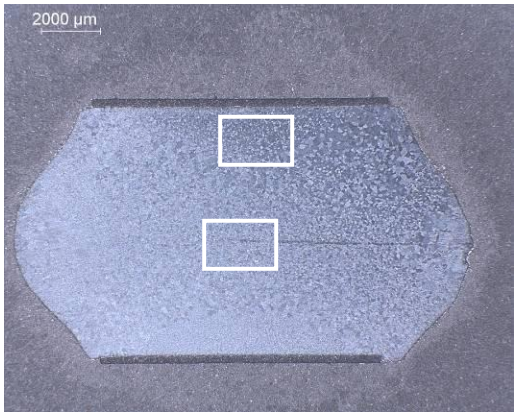

5.1.3.4(a) Overview low mag.

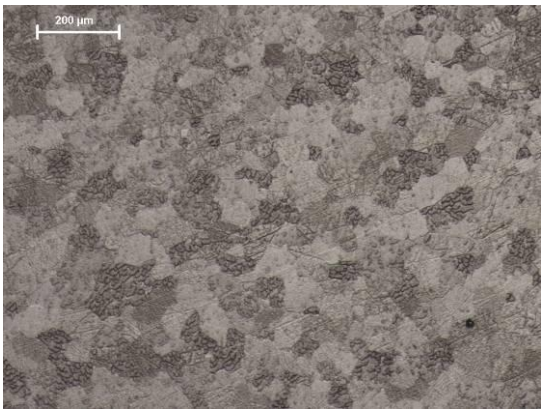

5.1.3.4(b) Centre low mag.

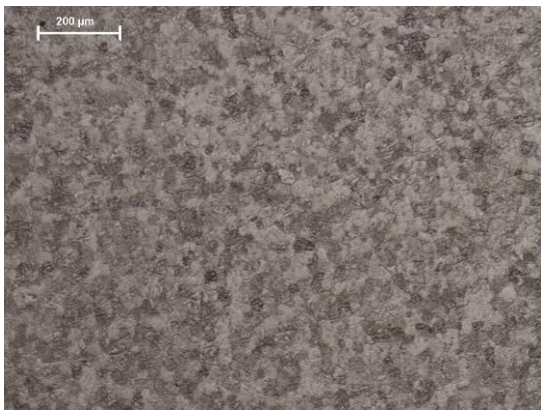

5.1.3.4(c) Edge low mag.

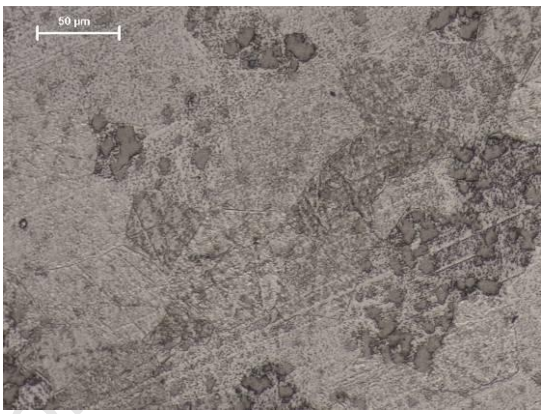

5.1.3.4(d) Centre high mag.

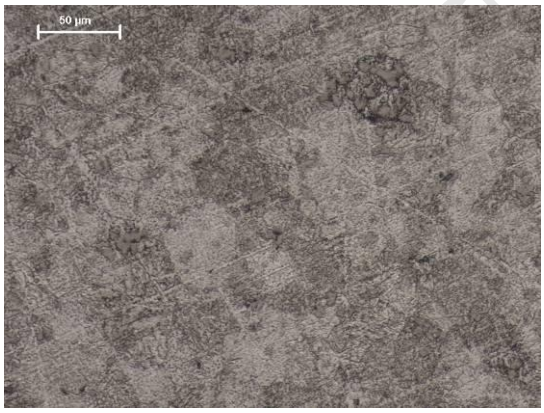

5.1.3.4(e) Edge high mag.

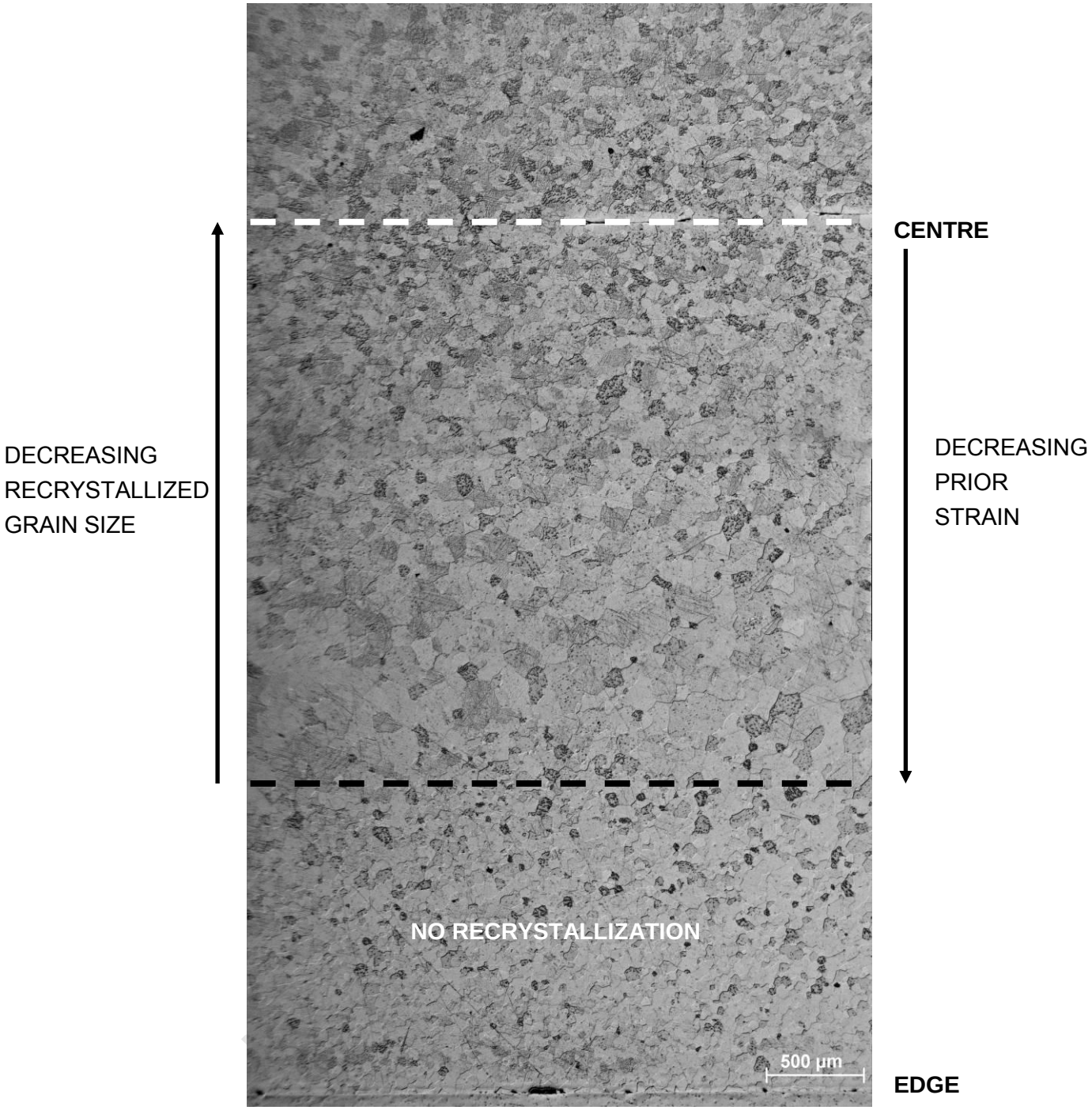

Figure 5.1.3.4 (f) Section from the centre of the sample to horizontal edge

Interpretation of the microstructures 5.1.3.4(a)-(f)

In the micrographs above it can be seen that there are varying regions of different microstructures within the sample itself. It is observed that there is a gradient with regard to grain size in the sample. The grain size increases from the centre towards the edge but at the region closest to the edge the grain size is smaller. The edges of the sample have a similar average grain size (24.2 ± 9.7μm) to that of the centre of the sample which has an average grain size of 34.3 ± 11.2μm. The grain size in the centre of the sample is the product of many nucleation sites being caused by the high retained strain during hot compression in this region. During recrystallization the many nucleation sites form newly recrystallized grains which are smaller than the original grains until grain growth occurs during post deformation annealing.

The region of grains between the centre and the edge of the sample has the largest grain size which is the result of only a few nucleation sites being developed during hot compression of the sample. This area has a lower amount of retained strain than the centre of the sample. During recrystallization these few nucleation sites recrystallize and incorporate the surrounding grains to produce grains which are larger than the original grain size and grow further during post deformation annealing. The region of grains closest to the edge of the sample has slightly smaller grains. This is because this region of the sample was in direct contact with the ceramic platens during hot compression, which acts as heats sinks during hot compression and also has the least amount of retained strain (almost zero) overall after hot compression. Thus the edges of the sample have not undergone recrystallization. The grain size is only slightly larger than the original grain size due to grain growth during the post deformation anneal.

The reason why recrystallization occurred in the centre of this sample and not in the centre of the sample which had been hot compressed at 900°C to a nominal strain of 0.2 is due to the increased amount of retained strain in the centre of the sample. The Stress vs. Strain curves for wrought Ti at strain = 0.2 and strain = 0.5 (see figures 5.1.1.1 and 5.1.1.2) show that the measured stress on the sample which had undergone hot compression at 900°C to a nominal strain = 0.2 is ± 20 MPa and the measured stress on the sample which had undergone hot compression at 900°C to a nominal strain = 0.5 is just over 30 MPa. As there is a direct relationship between the measured stress and retained work hardening we can deduce that the sample which had been hot compressed at 900ºC to a nominal strain = 0.5 has more retained strain and therefore has the necessary nucleation sites for the initiation of recrystallization during post deformation annealing.

Hot compression Temperature = 1000°C and nominal strain = 0.2

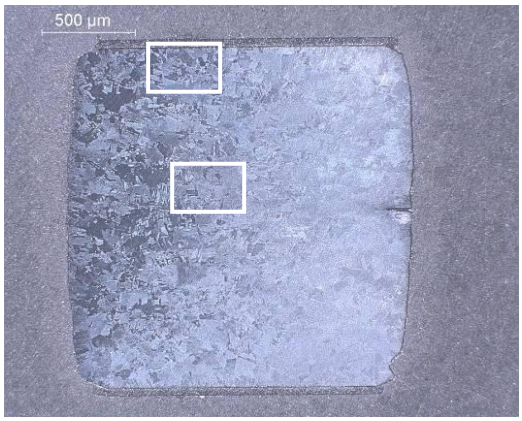

5.1.3.5(a) Overview low mag.

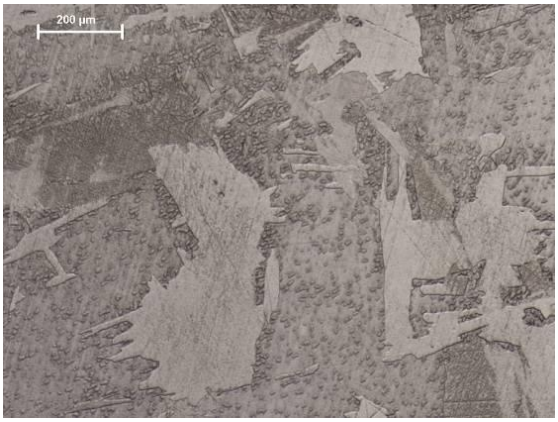

5.1.3.5(b) Centre low mag.

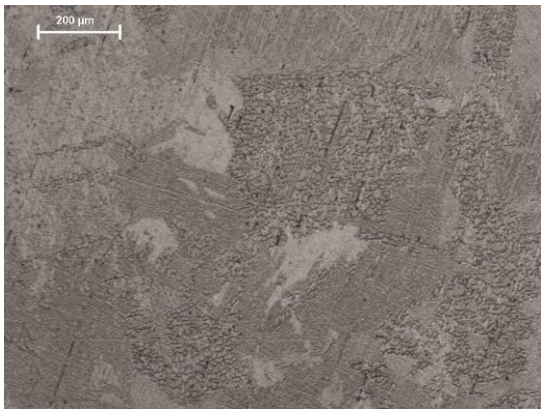

5.1.3.5(c) Edge low mag.

5.1.3.5(d) Centre high mag.

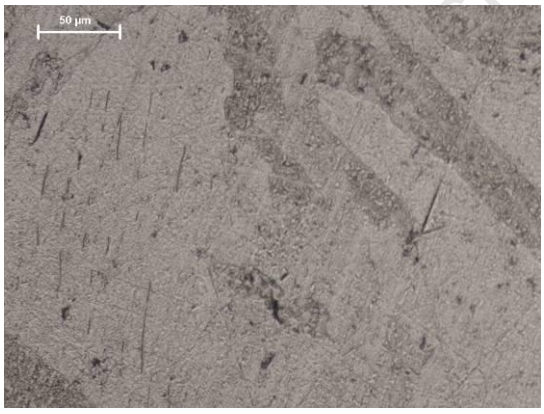

5.1.3.5(e) Edge high mag.

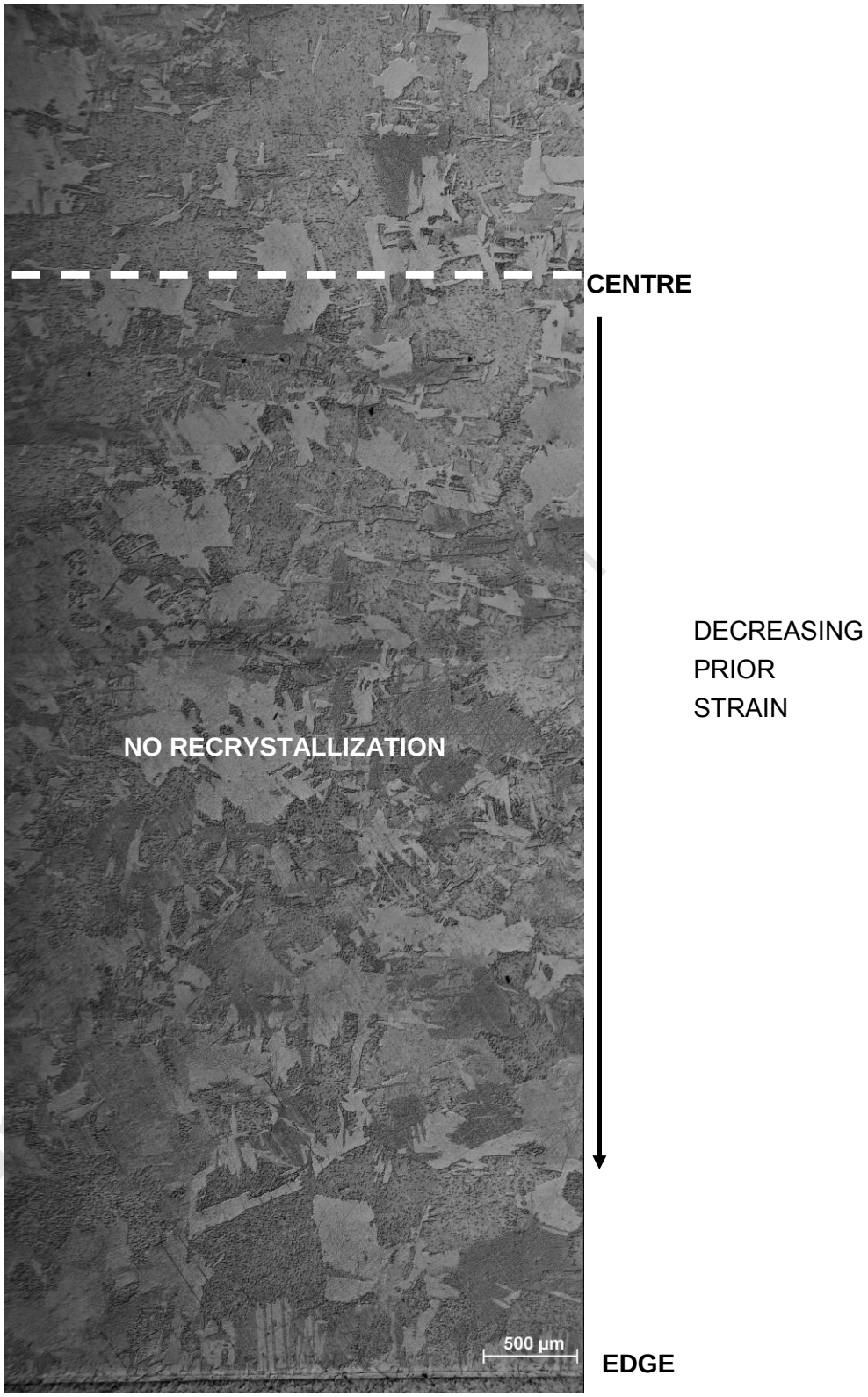

Figure 5.1.3.5 (f) Section from the centre of the sample to horizontal edge

Interpretation of the microstructures 5.1.3.5(a)-(f)

The micrographs above show that there are no distinct regions within the sample itself. The grains in the sample are very large and irregular in shape. There is no gradient in the grain size. The grain size and shape is due to the fact that no recrystallization occurred anywhere in the sample during post deformation annealing.

The Stress vs. Strain curve for wrought Ti at strain = 0.2 (see figure 5.1.1.1) shows that the measured stress on the sample which had undergone hot compression at 1000°C to a nominal strain = 0.2 is just above 10 MPa. This would mean that the sample had a very low amount of retained strain and therefore would not have sufficient retained strain to form the necessary nucleation sites for the initiation of recrystallization during post deformation annealing. Grain growth is the dominant mechanism in the microstructural evolution of this sample during both the deformation cycle and post deformation annealing.

Hot compression Temperature = 1000°C and nominal strain = 0.5

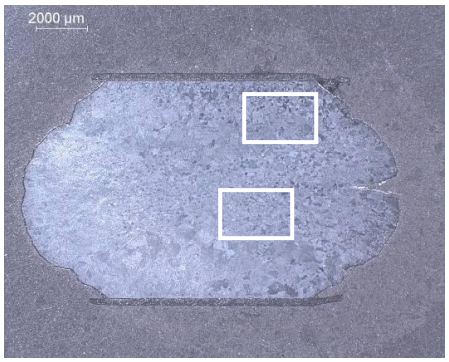

5.1.3.6(a) Overview low mag.

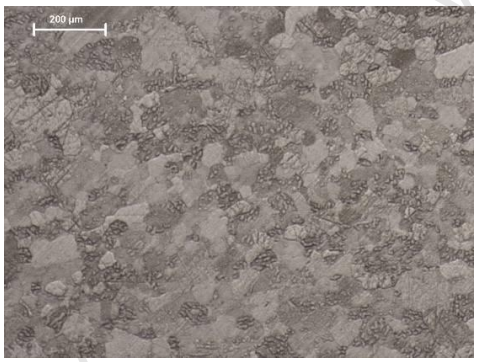

5.1.3.6(b) Centre low mag.

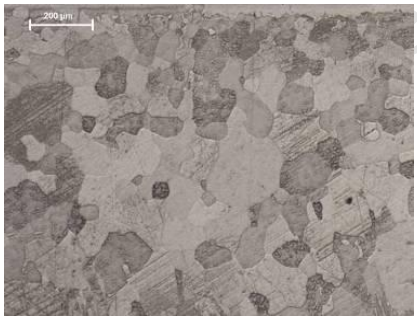

5.1.3.6(c) Edge low mag.

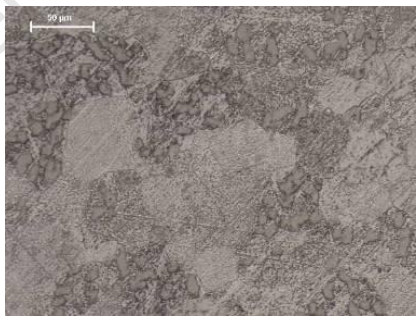

5.1.3.6(d) Centre high mag.

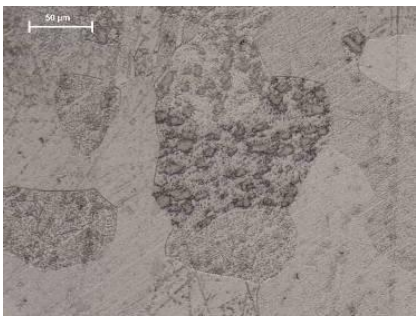

5.1.3.6(e) Edge high mag.

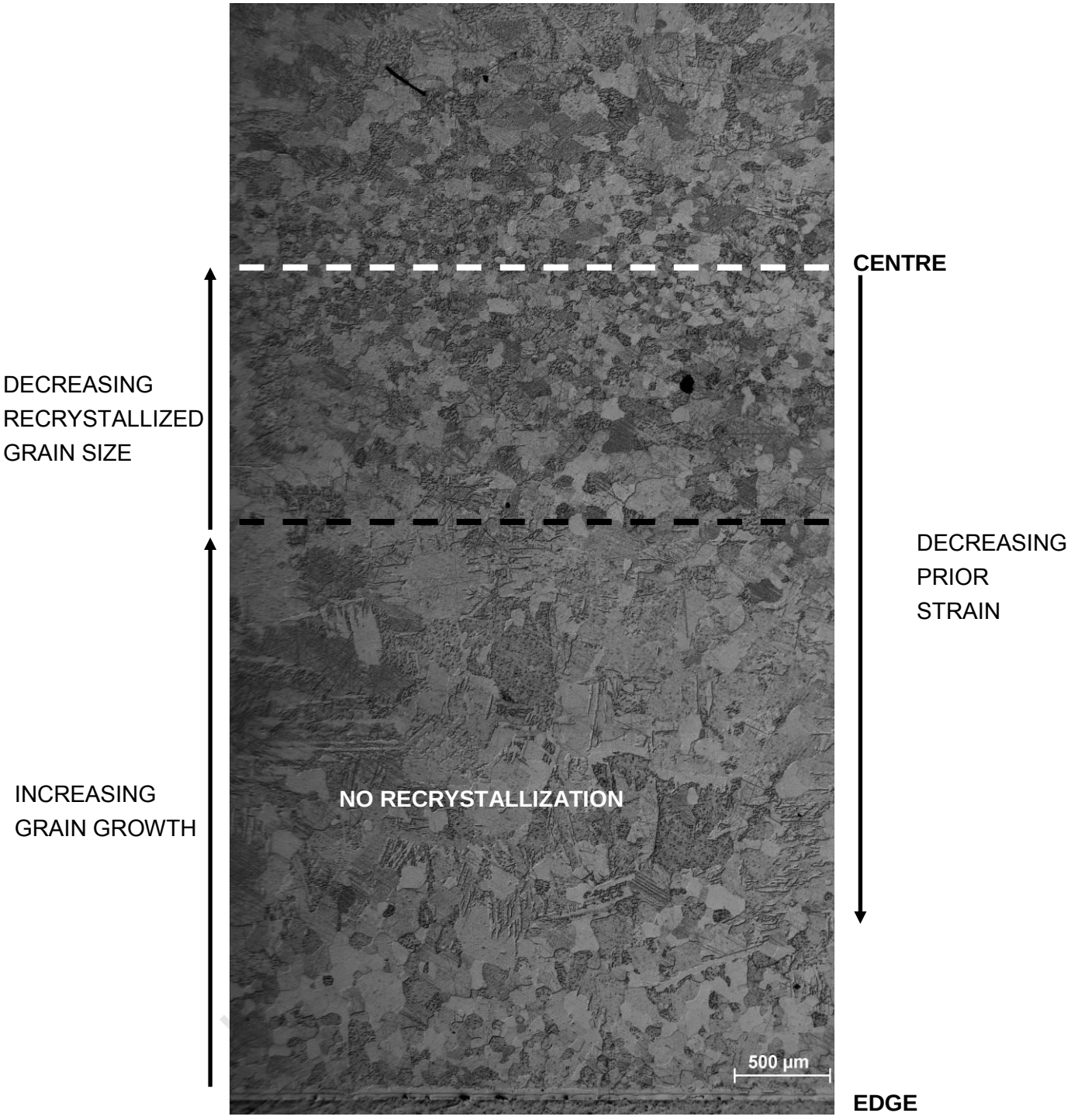

Figure 5.1.3.6 (f) Section from the centre of the sample to horizontal edge

Interpretation of the microstructures 5.1.3.6(a)-(f)

Upon analysing the micrographs above it can be seen that there are many regions with different microstructures within the sample itself. The edges of the sample have a similar average grain size (44.8 ± 14.9μm) to that of the centre of the sample which has an average grain size of 36.9 ± 8.1μm. The grain size in the centre of the sample is the result of many nucleation sites being caused by the high retained strain during hot compression in this region. The Stress vs. Strain Curves for Wrought Ti at strain = 0.5 (see fig. 5.1.1.2) shows that the measured stress on a sample that had been hot compressed at 1000°C to a nominal strain = 0.5 is just above 15 MPa. During recrystallization the many nucleation sites form newly recrystallized grains which are smaller than the original grains until grain growth occurs during post deformation annealing.

The grains in the region between the centre and the edge of the sample have a very large and irregular shape. This microstructure occurred because the amount of retained strain in this region was too low to form nucleation sites for the initiation of recrystallization during post deformation annealing. The grains in this region are very similar to those of the sample which had been hot compressed at 1000°C to a nominal strain = 0.2. In the Stress vs. Strain Curves for Wrought Ti at strain = 0.2 (see fig. 5.1.1.1) the measured stress is ± 10 MPa and the retained strain is also insufficient to form nucleation sites. The dominant process responsible for the microstructure of this region is grain growth during both the deformation cycle and post deformation annealing. The region of grains closest to the edge of the sample have also not undergone recrystallization but are smaller than the grains closer to the centre of the sample. This is because this region of the sample was in direct contact with the ceramic platens during hot compression, experienced a lower temperature during hot compression and thus a slower rate of grain growth. The grain size is larger than the original grain size due to the grain growth during both the deformation cycle and post deformation annealing treatment. The recrystallized grains in the centre of the sample are slightly larger than the original grain size and in agreement with the size of the recrystallized grains in the centre of the samples which had been hot compressed at 800°C to nominal strains of 0.2 and 0.5 and 900°C at a nominal strain of 0.5.

5.1.4 Microhardness Testing

The hardness measurements are taken through the centre of the sample at the region of highest strain. Figures 5.1.4.1 - 5.1.4.3 are based on the table below. The values are an average of 24 measurements taken from 3 separate samples for each temperature and strain condition.

Table 5.1.4.1 Average hardness of hot compressed wrought Ti samples:

	Average Hardness Values (Hv)		
Nominal Strain	**0**	**0.2**	**0.5**
Temp: 800°C	178.5 ± 6.0	183.1 ± 6.4	186.3 ± 12.7
900°C	176.5 ± 14.7	172.7 ± 12.3	179.6 ± 9.9
1000°C	172.7 ± 7.4	173.9 ± 14.5	179.7 ± 18.5

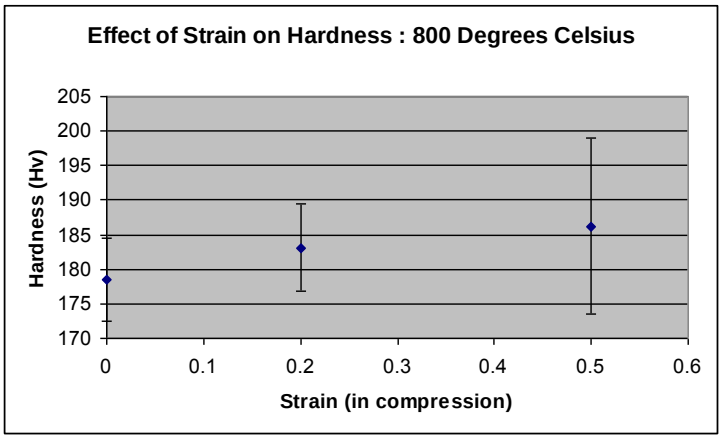

Figure 5.1.4.1 Comparison of average hardness values of wrought Ti samples that have been hot compressed at 800°C for varying strains

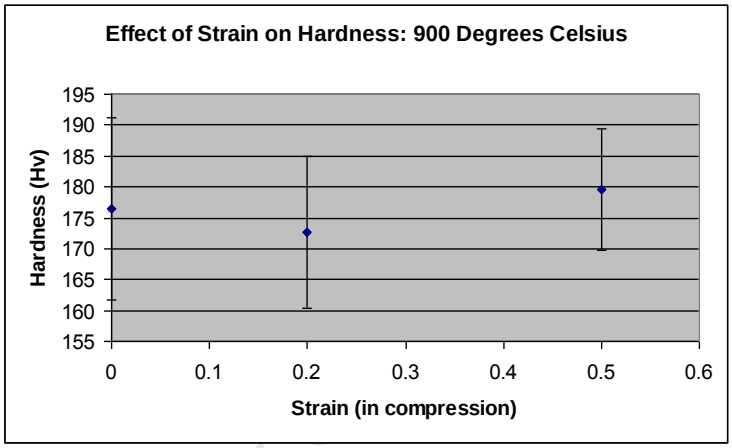

Figure 5.1.4.2 Comparison of average hardness values of wrought Ti samples that have been hot compressed at 900°C for varying strains

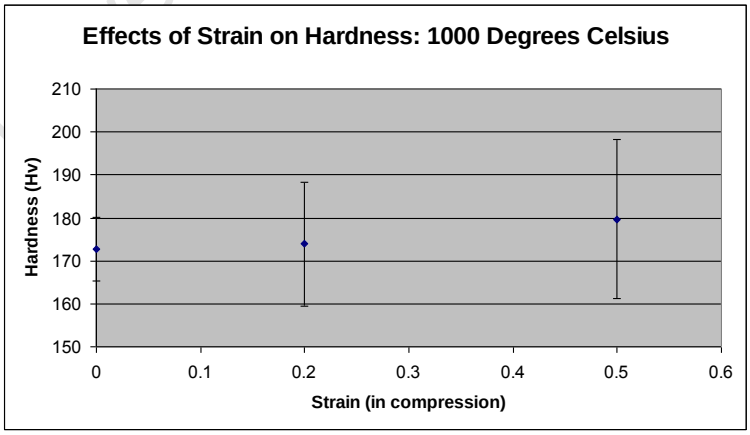

Figure 5.1.4.3 Comparison of average hardness values of wrought Ti samples that have been hot compressed at 1000°C for varying strains

The large range in the microhardness values are due to the nature of microhardness testing. During the testing, indentations are made on the surface of the samples. If the indentation was made inside the grain the hardness would be lower than if the indentation was made on a grain boundary. It is expected that the increase in strain during compression would cause an increase in hardness but as the temperature increases this is no longer the case. This is because post deformation softening occurs during the air cooling of the sample after hot compression. As there is no quenching, the sample is allowed to cool at a natural rate (± 17°C/min) in air which is much slower than water or oil quenching cooling rate.

From the analysis of the post deformation annealed wrought Ti (see figures 5.1.3.1- 5.1.3.2) it can be observed that at 800°C at a nominal strain = 0.2 and 0.5 there is a high amount of retained strain which causes the initiation of recrystallization during post deformation annealing. The retained strain results in an increase in hardness with an increase in applied strain which is due to work hardening occurring during the hot compression.

In the analysis of the post deformation annealed wrought Ti samples (see figures 5.1.3.3(a)-5.1.3.3 (f)) it was observed that for the 900°C and nominal strain = 0.2 sample, the amount of retained strain was insufficient for the nucleation and initiation of recrystallization. In the high strain region (centre of the sample) where no recrystallization occurs, grain growth is the dominant process. At 900°C and nominal strain = 0.5 (see Fig. 5.1.3.4(a)-5.1.3.4(f)) the retained strain is high enough to initiate recrystallization in the centre of this sample.

At 1000°C grain growth is the dominant factor at a nominal strain of 0.2 (see Fig. 5.1.3.5(a) and 5.1.3.5(f)) as the amount of retained strain is too low to initiate recrystallization within the sample.

At 1000°C and ε=0.5 recrystallization occurred in the centre of this sample due to the retained strain being high enough to initiate recrystallization i.e. the creation of nucleation sites. However, unlike the case for the 900°C ε=0.5 condition, in this case the recrystallization is confined to a small region in the centre of the sample.

The average hardness at ε=0.5 for 900°C and 1000°C are similar i.e. 900°C and ε=0.5: 179.6 ± 9.9 Hv; 1000°C and ε=0.5: 179.7 ± 18.5 Hv because the grains in the high retained strain region (the centre of the sample) have similar average grain sizes.

5.1.5 Conclusions based on the initial testing on the wrought Ti

Based on the analysis of the results of the initial testing the following conclusions can be made. The best temperature for the hot compression testing of the sintered Ti samples is 900°C for the following reasons:

- Hot compression at 900°C requires lower loads and therefore reduces the stress on the ceramic platens. Deformation at 800°C causes a higher incidence of platen failure.

- There is less rampant grain growth at 900°C than at 1000°C thereby eliminating the benefit gained from further stress reduction at 1000°C.

- At 900°C the interface between the regions with varying microstructure and grain size is more clearly defined than samples deformed at 800°C and 1000°C.

The best combination of temperature and strain that results in the highest amount of retained internal strain is a temperature of 900°C and a nominal strain=0.5. Furthermore, increasing the temperature to 1000°C at a nominal strain = 0.5 does not lead to an increase in the retained internal strain of the sample nor does it increase the hardness of the sample significantly.

Based on these conclusions, parameters were set for the hot compression testing on the sintered samples. The temperature for all the tests will be set at 900°C and the samples will be deformed to a nominal strain of 0.2, 0.5 and 0.65. By keeping the temperature constant the effects of the strain can be isolated and analysed. The nominal strain of 0.5 has shown the highest amount of microstructural deformation in the high retained strain region and therefore this strain will be analysed as well as the lower strain of 0.2 and a slightly higher strain 0.65.

It must be kept in mind that the diameter of the platen restricts the amount of strain that can be allowed as the sample is more likely to slip over the edges of the platen at higher strains due to the increase in diameter of the sample associated with the decrease in height during compression.

5.1.6 Comparison of testing results to other research done on the recrystallization of hot deformed wrought CP-Ti

When the results of our hot compression testing was compared to those of a study [25] conducted on the hot rolling of as cast CP-Ti ingots from temperatures between 600°C and 1200°C (see Section 2.5.1) the following observations were made:

- The previous study found that there was very little change in hardness with increasing reduction of the thickness of the samples that were hot rolled at 800°C. In comparison our testing found that there is a slight increase in hardness over the samples hot compressed at 800°C with increasing nominal strain. The difference could be caused by difference in testing conditions such as cooling rates.

- The previous study also found that recrystallization occurs in the α-region near 800°C which agrees with the results of the present study.

- The previous study concluded that a majority of the recrystallization observed in the microstructure occurred after the deformation event. When our sample underwent post-deformation annealing the results were in agreement with those of the previous study.

5.2 Sintering of the CP-Ti green compacts

5.2.1 Results of the sintering

Green compacts were pressed and delivered in batches and each batch was sintered under the same conditions. Due to the nature of the green compacts there are small differences in their dimensions. The increase in mass after sintering is due to oxidation during sintering. The sintering occurs under high vacuum but a negligible amount of oxygen can still be present in oxide form on the basket which lowers the samples into the furnace and indeed within the furnace atmosphere since the vacuum is not perfect. The mass increase is not considered significant in comparison with the mass of the sample.

Table 5.2.1.1 Results of sintering Ti green compacts

Batch	Height Before (mm)	Height After (mm)	Mass Before (g)	Mass After (g)	Minimum diameter before (mm)	Minimum diameter after (mm)
1-15	15.11 ± 0.17	13.91 ± 0.17	3.61 ± 0.02	3.63 ± 0.02	10.09 ± 0.03	8.90 ± 0.05
16-31	15.05 ± 0.08	13.74 ± 0.06	3.60 ± 0.01	3.61 ± 0.01	10.1 ± 1.83E -15	8.88 ± 0.04
32-35	15.05 ± 0.05	13.75 ± 0.05	3.60 ± 0.004	3.61 ± 0.01	10.1 ± 0	8.92 ± 0.04

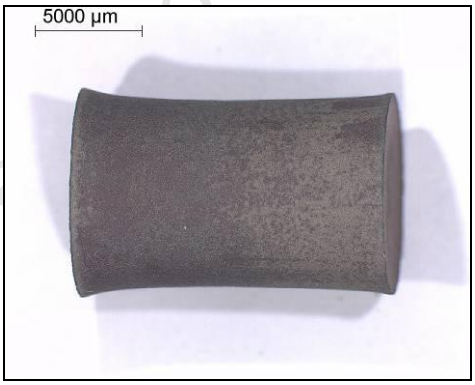

Figure 5.2.1.1 Sintered Ti sample with hourglass shape

The shape change could be due to a density gradient that occurs during the uniaxial pressing of the green compact. The force is applied along the vertical axis of the sample and no force is applied from the sides of the sample. The centre of the green compact is therefore denser than the outer regions and when the sample is sintered the reduction of the porosity causes the observed shrinkage of the sample.

5.2.2 Microstructure of the sintered samples

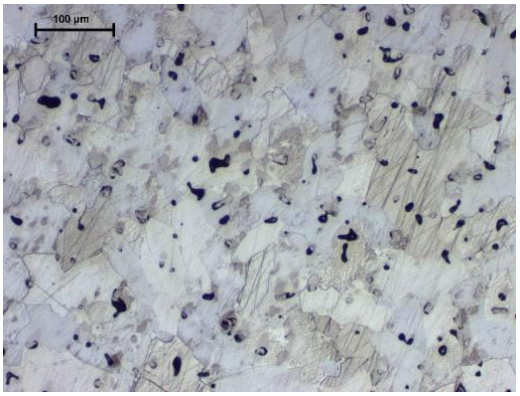

Figure 5.2.2.1 Sintered Titanium compact

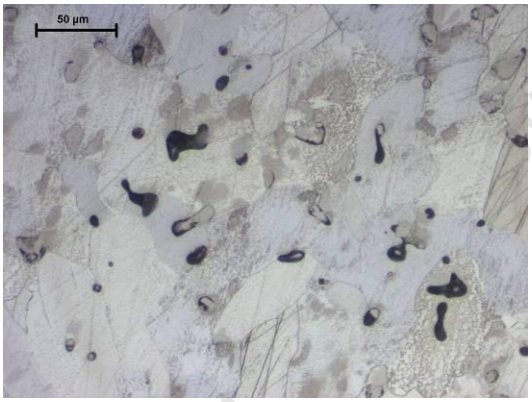

Figure 5.2.2.2 Pores in the sintered Titanium compact

5.2.3 Density of the sintered samples

The density of the samples after sintering has been determined using the Water Displacement Method as the hourglass shape of the sample makes determining the volume of the sample challenging. The mass of the sample is measured and then divided by the volume of the sample. The hourglass shape of the sample is due to the gradient in density through the centre of the sample during the initial uniaxial pressing of the powder into the green compact. The volume is determined by placing the one randomly selected sample inside a measuring cylinder filled with water. The volume increase when the sample is inserted is deemed to be the volume of the sample. The density of the sample before sintering was 3.06 g/cm^3 which is 68% of the full density and the sintered sample was determined to have a density of 4.011 g/cm^3 which is 89% of full density.

5.2.4 Volume fraction of porosity of the sintered samples

To confirm the density of the samples obtained from the Water Displacement Method another density measurement technique was employed i.e. the Point-counting Method.

The volume fraction of porosity in the sintered sample before hot compression was calculated using the point-counting method described in Section 4.3.1. The sum of the pores ($\sum P_\alpha$) in n = 10 fields is equal to 19.5 and therefore the point fraction (P_p) of pores equals 0.0195 and the volume fraction of the porosity (V_v) equal ± 2.0 %. There is a large difference in the values for the density obtained via the two methods. This is because the Water displacement method measures the density of the entire sample whereas the Point-counting method only determines the volume fraction of porosity for a small area captured on the micrographs. Point-counting also does not take into consideration the inhomogeneous density in the hourglass shaped samples. Therefore the Archimedes method is considered more accurate for samples where the material has a less homogenous nature because it considers the sample as a whole.

5.2.5 Bulk hardness of the sintered samples

The hardness of the sintered sample was measured using a bulk hardness testing machine. This was because of the porosity of the sample. When low loads are applied to the sample the hardness method measures the individual grain hardness whereas this is expected to be different to the bulk hardness in view of the influence of porosity (i.e. for a cast or wrought homogenous sample, the grain hardness is expected to represent the bulk hardness, whereas in a porous material, the hardness is influenced by the grain hardness and the “pore hardness”). The bulk hardness of the sintered titanium compact was found to be 279.5 ± 6.2 Hv.

5.3 Hot Compression testing of the Sintered Ti samples

5.3.1 Adjustments to testing parameters

The sintered titanium samples were less dense and had different dimensions than that of the wrought titanium samples. Therefore the setting on the remote heating station had to be adjusted to efficiently and accurately heat the sintered sample for compression. The varying geometry meant that the amount of deformation needed to produce the nominal amount of strain would also differ between the 3 batches. The wrought titanium samples require a large amount of force to deform them to the required fixed strains; this large force increases the risk of fracturing the ceramic platens and therefore limits the nominal strain to 0.5. The sintered titanium samples however require less force to deform them to the required fixed strains. The lower forces involved meant that the ceramics could safely handle the forces associated with the higher nominal strain and thus additional experiments at a nominal strain of 0.65 were added.

Determining the displacement required to obtain fixed strains

Nominal strain calculations are needed for sintered samples in Batch 1-15. The initial average height is 13.91mm and the average minimum diameter is 8.9mm. Therefore the calculated height change to achieve the nominal strain level (Δh) and the actual required machine cross-head displacement (ΔH) are as follows:

Table 5.3.1.1 Calculated displacements values for samples from batch 1-15 (formulae in section 5.1.1)

Nominal Strain	h_1 (mm)	Δh (mm)	ΔH (mm)
-0.2	11.4	2.5	3.0
-0.5	8.4	5.5	6.0
-0.65	7.3	6.5	7.2

The nominal strain calculations for sintered samples in Batch 16-31: The initial average height is 13.74mm and the average minimum diameter is 8.88mm. Therefore the calculated height change to achieve the nominal strain level (Δh) and the actual required machine cross-head displacement (ΔH) are as follows:

Table 5.3.1.2 Calculated displacements values for samples from batch 16-31 (formulae in section 5.1.1)

Nominal Strain	h_1 (mm)	Δh (mm)	ΔH (mm)
-0.2	11.3	2.5	3.0
-0.5	8.3	5.4	5.9
-0.65	7.2	6.6	7.1

The nominal strain calculations for sintered samples in Batch 32-35: The initial average height is 13.75mm and the average minimum diameter is 8.92mm. Therefore the calculated height change to achieve the nominal strain level (Δh) and the actual required machine cross-head displacement (ΔH) are as follows.

Table 5.3.1.3 Calculated displacements values for samples from batch 32-35 (formulae in section 5.1.1)

Nominal Strain	h_1 (mm)	Δh (mm)	ΔH (mm)
-0.2	11.3	2.5	3.0
-0.5	8.3	5.4	5.9
-0.65	7.2	6.6	7.1

The Stress vs. Strain curves for the various nominal strains are shown in Figure 5.3.1.1. It shows the stress required to achieve a preselected amount of compressive strain. We can see that the average yield stresses of the 3 curves are very similar which suggests that the sintered Ti samples behave in a homogenous manner.

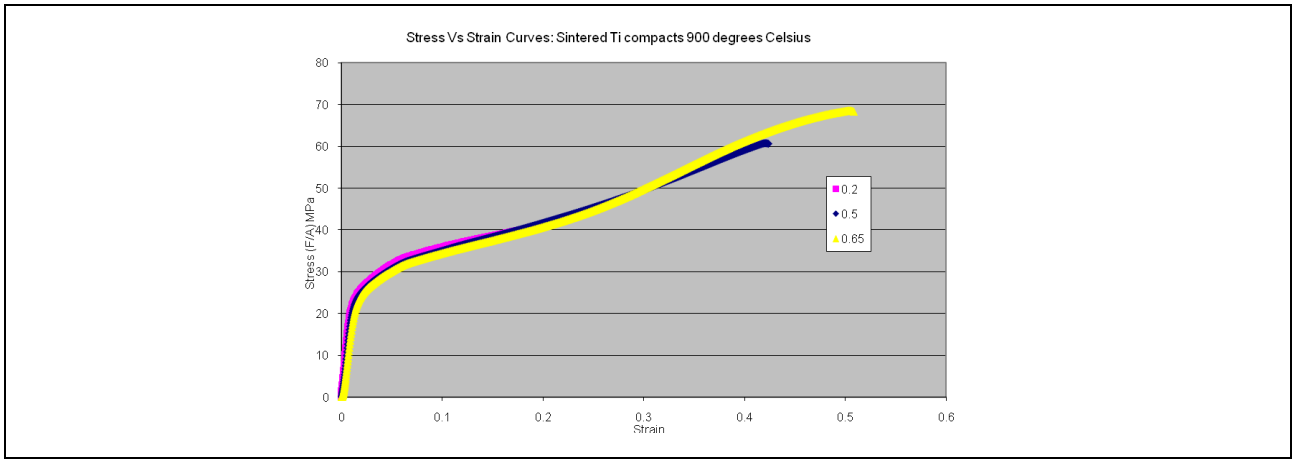

Figure 5.3.1.1 Stress vs. Strain curves for Wrought Ti at various nominal strains at a testing temperature of 900°C (initial strain rate = $0.1s^{-1}$)

From the graphs we can see that the actual strain experienced by the samples differs from the nominal value. For the nominal compressive strain of 0.2 the actual strain was found to be 0.22, for the nominal strain of 0.5 the actual strain was found to be 0.4 and for the nominal strain of 0.65 it was found to be 0.52.

Table 5.3.1.1 Results of hot compressing sintered Ti samples at 900°C for varying theoretical strains

Nominal Strain	Average Yield Stress (MPa)	Average stress at maximum strain (MPa)
0.2	19.52 ± 8.86	53.61 ± 16.48
0.5	18.75 ± 6.56	85.69 ± 22.48
0.65	21.16 ± 3.29	139.13 ± 23.09

5.3.2 Microstructure of hot compressed sintered Ti samples

Temperature =900°C and Nominal Strain = 0

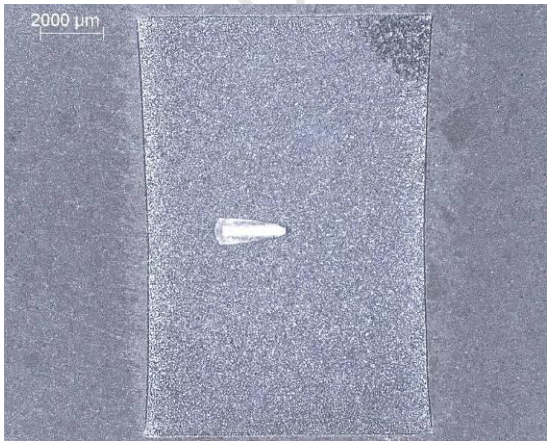

5.3.2.1(a) Cross-section through sample which has been heated at 900°C and strain = 0. This micrograph shows the basic shape of the sample as well as the position of the thermocouple within the sample.

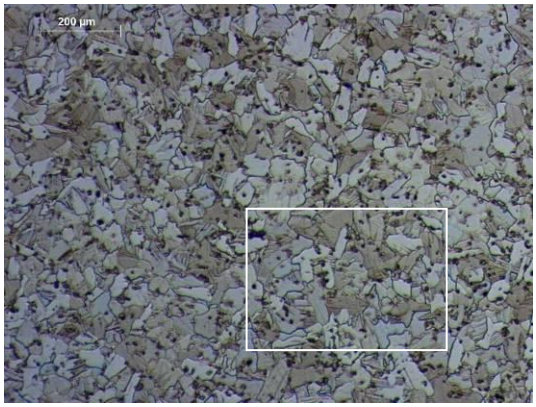

5.3.2.1(b) Cross-section through sample which has been heated at 900°C and strain = 0. This magnified image shows the prevalence of small pores within the sample. Area inside the white rectangle is magnified in Figure 5.3.2.1(c).

5.3.2.1(c) Cross-section through sample which has been heated at 900°C and strain = 0. Under further magnification the size of the grains and the shape of the pores can clearly be seen. The average grain size is ± 50µm and the pores are rounded. The rounded pores show that the sample is at an advanced stage in the sintering process.

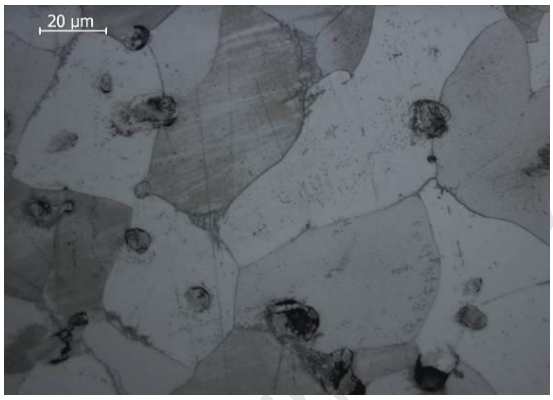

5.3.2.1(d) Cross-section through sample which has been heated at 900°C and strain = 0. Under high magnification the size of the grains and the shape of the pores can clearly be seen.

Interpretation of microstructures 5.3.2.1 (a) – (d):

This sample has not undergone compression testing. The microstructure is a result of the sintering and heating process rather than from the application of strain. Upon visual comparison between the micrographs in figure 5.3.2.1(c) and figure 5.2.2.2 (the as sintered sample), which are taken at the same magnification we can observe the following: There is a slight increase in grain size between the microstructure of the sample that has been sintered only and the sample that has been sintered and held at temperature. This increase is because of grain growth occurring in the sample at that temperature. The pores in the sample that has been held at temperature is also smaller, more rounded and the grain boundaries are more clearly defined.

Temperature = 900°C and Nominal Strain = 0.2

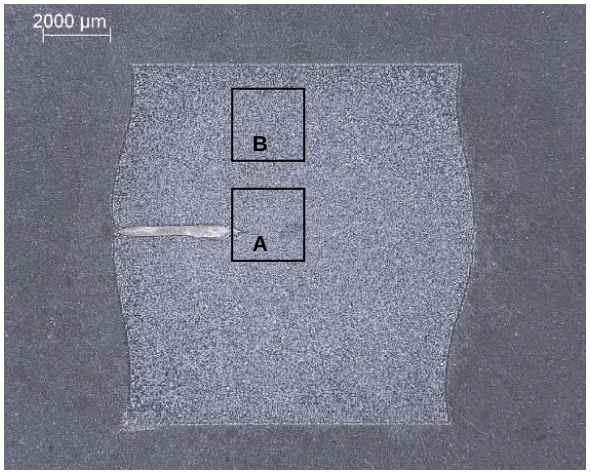

5.3.2.2(a) Cross-section through sample which has been heated at 900°C and underwent a nominal strain = 0.2 This micrograph shows the basic shape of the sample as well as the position of the thermocouple within the sample. The deformation of the sample can clearly be seen.

5.3.2.2(b) Cross-section through sample which has been heated at 900°C and underwent a nominal strain = 0.2 This micrograph is of the centre of the sample (Area A in 5.3.2.2 (a)) which experiences the highest amount of strain. The deformation of the grains is clearly visible.

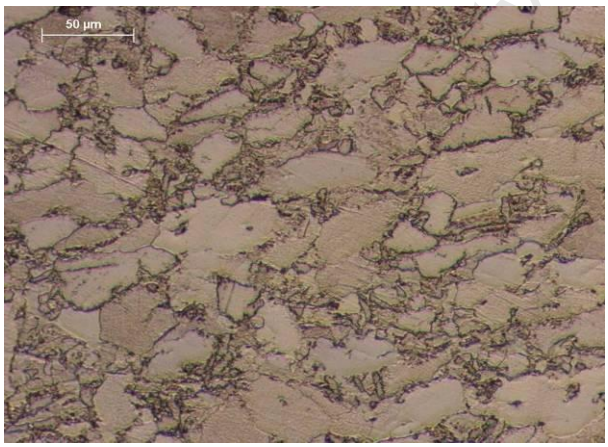

5.3.2.2(c) Cross-section through sample which has been heated at 900°C and underwent a nominal strain = 0.2.This a magnified micrograph of the centre of the sample. We can see that the grains have been deformed.

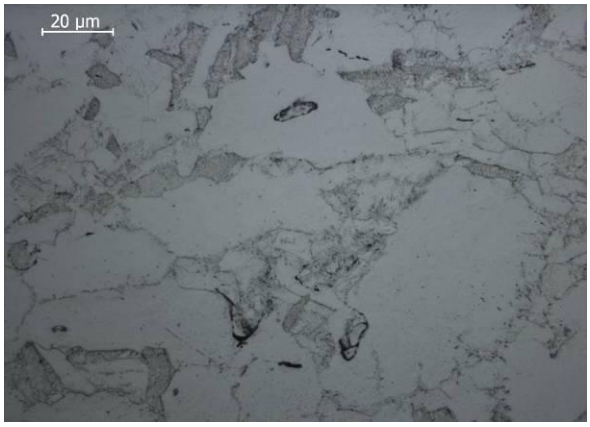

5.3.2.2(d) Cross-section through sample which has been heated at 900°C and underwent a strain = 0.2. Under high magnification the deformation of the grains can be observed. The grains are not as clearly defined as those along the edges of the sample.

5.3.2.2(e) Cross-section through sample which has been heated at 900°C and underwent a nominal strain = 0.2. This micrograph is of the edge of the sample (Area B in 5.3.2.2 (a)) which experiences a lower amount of strain. The deformation of the grains is less visible.

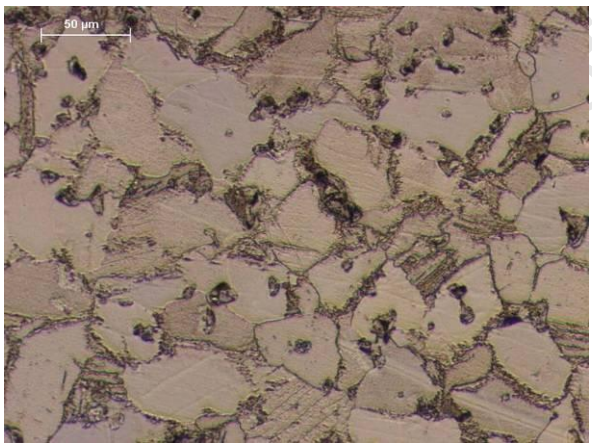

5.3.2.2(f) Cross-section through sample which has been heated at 900°C and underwent a nominal strain = 0.2. This is the magnified micrograph of the edge of the sample. We can see that the grains are still equiaxed. There are many pores still visible.

Interpretation of microstructures 5.3.2.2 (a) – (f):

In a direct comparison between the grains in the centre of the sample (see figure 5.3.2.2(c)) and the grains at the edge of the sample (see figure 5.3.2.2(f)) taken at the same magnification the following can be seen: The microstructure in the centre of the sample shows that the grains there have been deformed slightly more in the high retained strain region than at the edges which have a lower retained strain.

The grains in the centre of the sample appear marginally smaller than the grains around the edges of the sample. There is also much less porosity in the centre of the sample than in the edges of the sample

Temperature = 900°C and Nominal Strain = 0.5

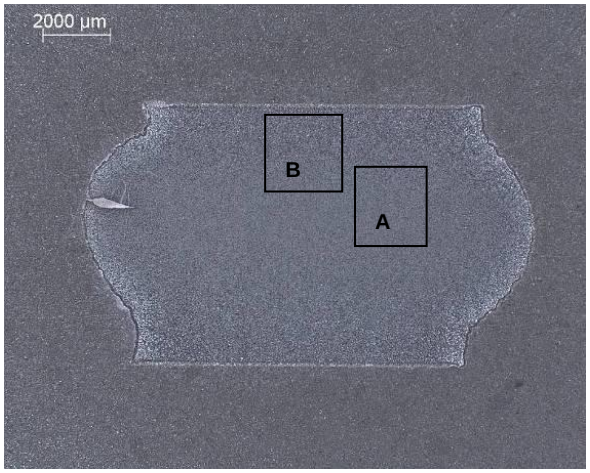

5.3.2.3(a) Cross-section through the sample which had been heated at 900°C and underwent a nominal strain = 0.5. This micrograph shows the basic shape of the sample as well as the position of the thermocouple within the sample. The deformation of the sample can clearly be seen.

5.3.2.3(b) Cross-section through the sample which had been heated at 900°C and underwent a nominal strain = 0.5. This is the micrograph of the centre of the sample (Area A in 5.3.2.3 (a)) which experiences the highest amount of strain. The deformation of the grains is clearly visible.

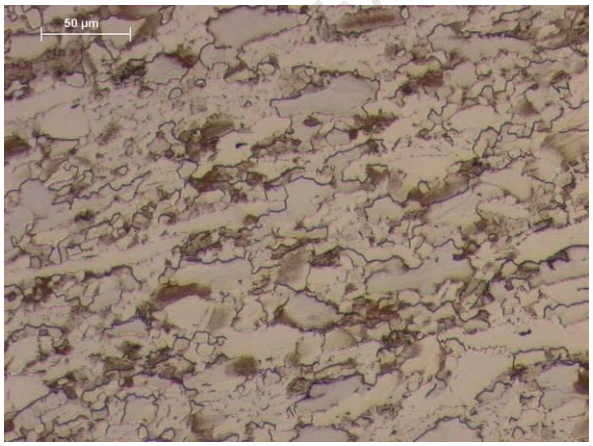

5.3.2.3(c) Cross-section through the sample which had been heated at 900°C and underwent a nominal strain = 0.5.This a magnified micrograph of the centre of the sample. We can see that the grains have been deformed and there are almost no pores visible.

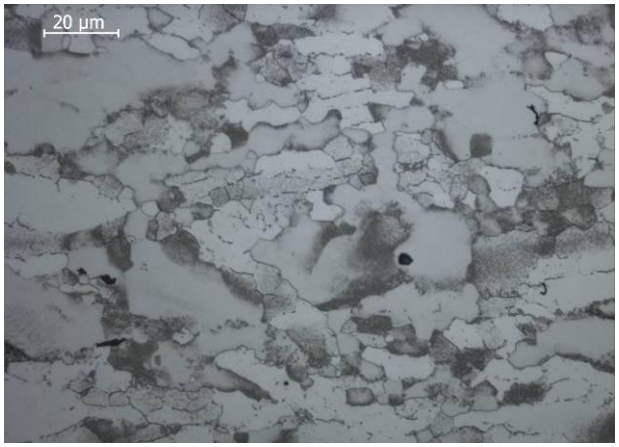

5.3.2.3(d) Cross-section through the sample which had been heated at 900°C and underwent a strain = 0.5. Under high magnification the highly deformed grains can be seen as well as smaller more equiaxed grains. The grains are more clearly defined than those at the centre of the nominal strain=0.2 sample.

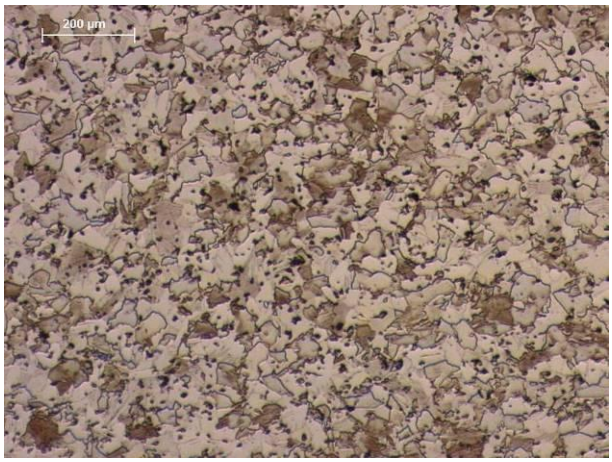

5.3.2.3(e) Cross-section through the sample which had been heated at 900°C and underwent a nominal strain = 0.5. This is the micrograph of the edge of the sample (Area B in 5.3.2.3 (a)) which experienced a lower amount of strain. The deformation of the grains is less visible than in Fig. 5.3.2.3(b).

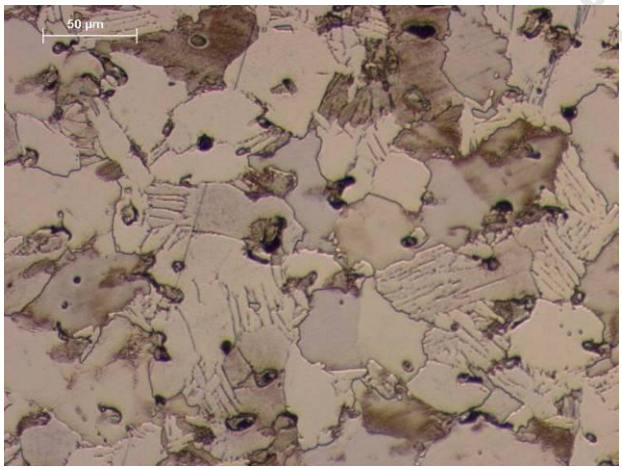

5.3.2.3(f) Cross-section through the sample which had been heated at 900°C and underwent a nominal strain = 0.5. This is the magnified micrograph of the edge of the sample. We can see that the grains are still equiaxed and there are many pores visible.

Interpretation of microstructures 5.3.2.3 (a) – (f):

The microstructure at the centre of the sample shows a definite increase in the amount of deformation in the grains when compared to that of the same region in the sample with nominal strain = 0.2. In figure 5.3.2.3(c) there is a more uniform distribution of deformed grains with a moderate degree of directionality perpendicular to the applied stress. Under much higher magnification we can see that the grain boundaries are irregular and smaller grains are also present. These smaller grains are thought to be newly recrystallized grains.

The sizes of the grains in the centre of the sample appear to be similar to those at the edges of the sample but the shape is much more deformed. When the amount of porosity is compared in figures 5.3.2.3(c) and 5.3.2.3(f) there is a noticeable decrease in porosity between the centre and the edge because of the high amount of retained strain in the centre region and the low amount of retained strain in the edge region.

Temperature = 900°C and Nominal Strain = 0.65

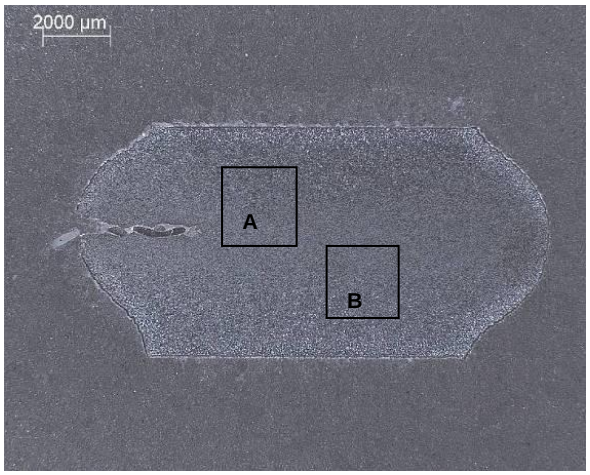

5.3.2.4(a) Cross-section through the sample which had been heated at 900°C and underwent a nominal strain = 0.65. This micrograph shows the basic shape of the sample as well as the position of the thermocouple within the sample. The deformation of the sample can clearly be seen.

5.3.2.4(b) Cross-section through the sample which had been heated at 900°C and underwent a nominal strain = 0.65. This is the micrograph of the centre of the sample (Area A in 5.3.2.4 (a)) which experienced the highest amount of strain. The grains are very deformed and show signs of directionality with respect to the applied strain.

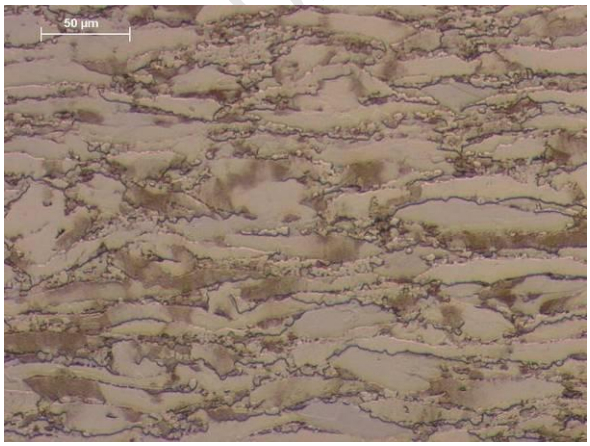

5.3.2.4(c) Cross-section through the sample which had been heated at 900°C and underwent a nominal strain = 0.65.This a magnified micrograph of the centre of the sample. We can see that the grains have been severely deformed and there are no pores visible.

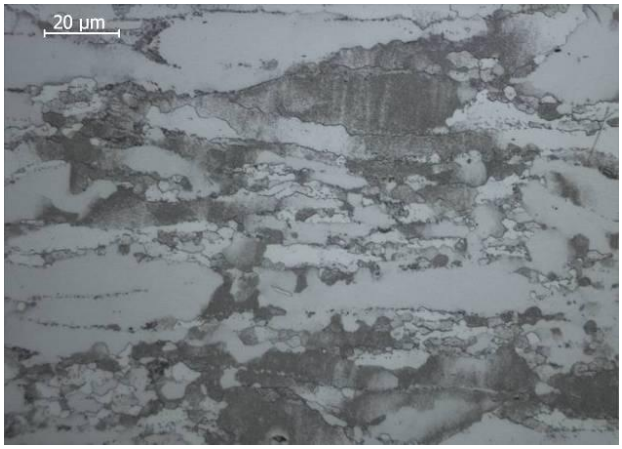

5.3.2.4(d) Cross-section through the sample which had been heated at 900°C and underwent a strain = 0.65. Under high magnification the highly deformed grains can be seen as well as smaller more equiaxed grains. The grain boundaries appear jagged.

5.3.2.4(e) Cross-section through the sample which had been heated at 900°C and underwent a theoretical strain = 0.65. This is the micrograph of the edge of the sample (Area B in 5.3.2.4 (a)) which experienced a lower amount of strain. The deformation of the grains is less visible.

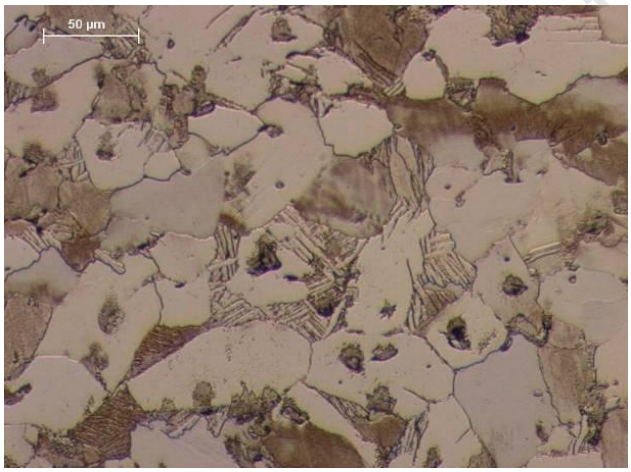

5.3.2.4(f) Cross-section through the sample which had been heated at 900°C and underwent a nominal strain = 0.65. This is the magnified micrograph of the edge of the sample. We can see that the grains are still equiaxed and there are still a few pores visible.

Interpretation of microstructures 5.3.2.4 (a) – (f):

The microstructure of the centre of the sample which has had a nominal strain = 0.65 is significantly more deformed than that of the sample which had a nominal strain of 0.5. The large grains have a more acicular shape and are surrounded by a thick band of smaller equiaxed recrystallized grains. The smaller equiaxed recrystallized grains in the sample which has had a nominal strain = 0.65 are much finer than those of the sample which has had a nominal strain = 0.5.

A comparison between the grains at the centre of the sample (see figure 5.3.2.4(c)) and those at the edge (see figure 5.3.2.4(f)) at a similar magnification show that the grains that are deformed were originally present in the bulk of the sample as represented by the micrograph of the edge of the sample. There is also much less porosity visible in the centre of the sample where there is a higher amount of retained strain than at the edge where there is a lower amount of retained strain. The grain boundaries of the larger deformed grains are very irregular and jagged (see figure 5.3.2.4(d)). The bulging of grain boundaries are thought to be a “prelude” to future recrystallization within the deformed sample. It can also be seen that no small equiaxed grains were present in the bulk of the sample before the deformation cycle but are present after the deformation cycle. From the comparison it can be concluded that the formation of the recrystallized grains is a direct result of the deformation cycle. The micrograph of the edge of the sample under high magnification (see Fig. 5.3.2.4 (f)) shows a few grains with a lamellar structure inside. This is possibly an indication of some transformation to β the at compression temperature followed by a reversion to α+β during cooling to room temperature.

5.3.3 Microhardness testing of hot compressed sintered Ti compacts

The hardness of the hot compressed sintered Ti samples was measured using microhardness at a force of 1000 gforce. Because the indentations are made through the centre of the sample which is much less porous, bulk hardness is not needed. Each sample has 5 indentations and there are 10 samples that are tested for each strain condition.

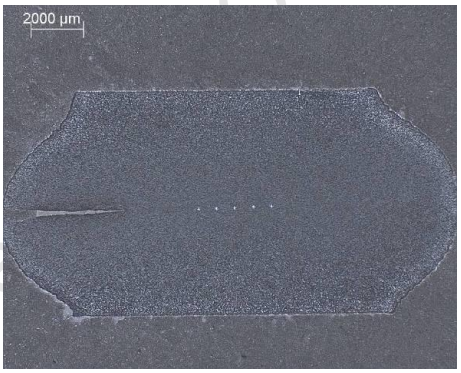

Figure 5.3.3.1 Location of microhardness indentations on a hot compressed sintered Ti sample

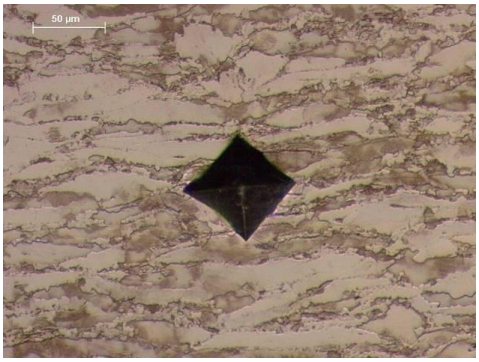

Figure 5.3.3.2 Magnified image of the indentation

Table 5.3.3.1 Hardness Values of sintered Ti samples hot compressed at 900°C for varying strains.

Nominal Strain	Average Hardness (Hv)	Standard deviation (Hv)
0	238.1	18.6
0.2	286.6	18.0
0.5	304.2	14.3
0.65	306.4	14.6

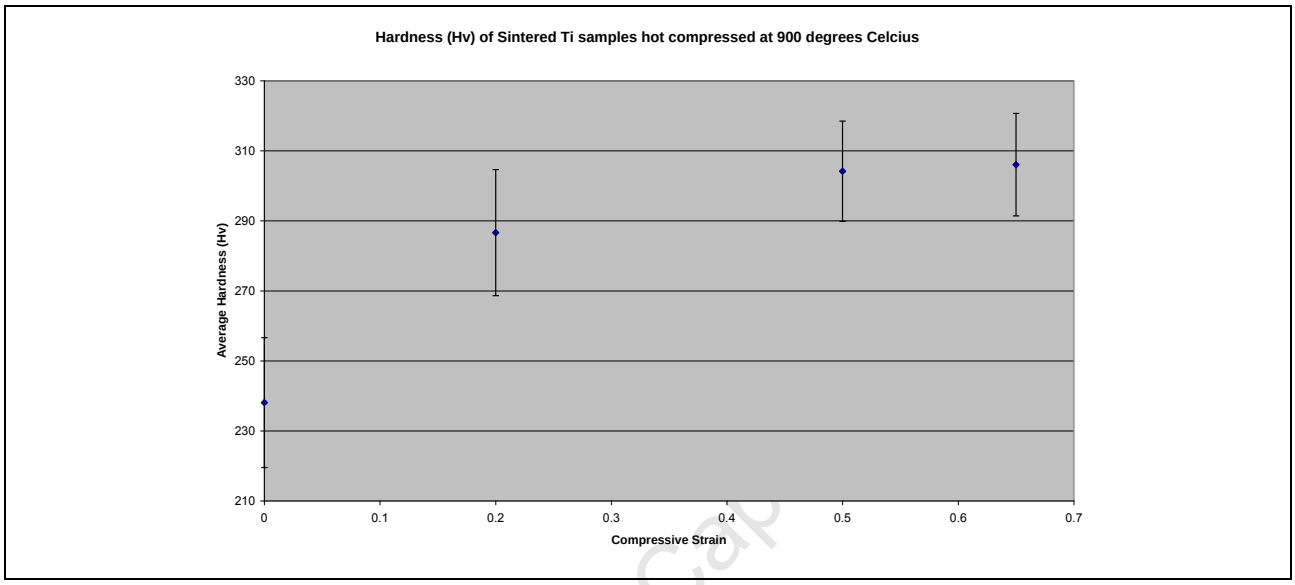

Figure 5.3.3.3 Graph of Average hardness of Sintered Ti samples that have been hot compresses at 900°C at varying nominal strains

The hardness of the sintered samples at various nominal strains closely models the stress vs. strain curves of the same samples (see Fig. 5.3.1.1), i.e. the hardness increases with increasing applied strain. The graph above (see figure 5.3.3.3) shows a similar general pattern to that of a stress vs. strain curve that is displaying work hardening. The accumulated plastic deformation caused by deforming the grains in the sample, contribute largely to the increase in the hardness of the samples after they have been hot compressed. The reduction in grain size also contributes to the increased hardness with increased measured stress but to a smaller degree than work hardening.

The graph for the average hardness at various nominal strains deviates from the stress vs. strain curve between a nominal strain of 0.5 and 0.65 but instead there is no real difference between the hardness. This is due to the sample now being almost fully dense and the effect of porosity reduction on the hardness is also diminished. Post deformation softening does occur during each test as the furnace cooling allows the sample to cool slowly from the elevated set point temperature to room temperature (±17°C/min).

However the softening effect is not the dominant factor influencing the hardness of the sintered Ti samples at 0, 0.2, 0.5 and 0.65 nominal strain conditions. The effects of work hardening and the reduction in porosity during deformation as well as the grain refinement caused by deformation and subsequent recrystallization causes the increase in hardness.

5.3.4 Post Deformation annealing of Sintered Ti samples

The annealing cycle is as follows: The sample is heated at 5°C/min to 870°C. It is then held at 870°C for 1 hr. Following the holding period the sample is cooled from 870°C to 600°C at a rate of 3°C/min. At 600°C the sample is allowed to furnace cool to room temperature (> 5°C/min).

Nominal strain = 0.2

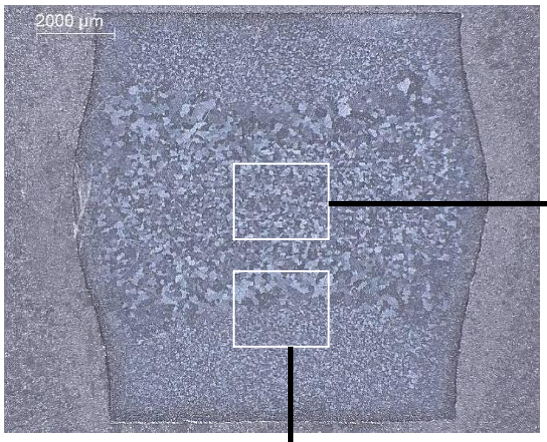

5.3.4.1(a) Overview low mag.

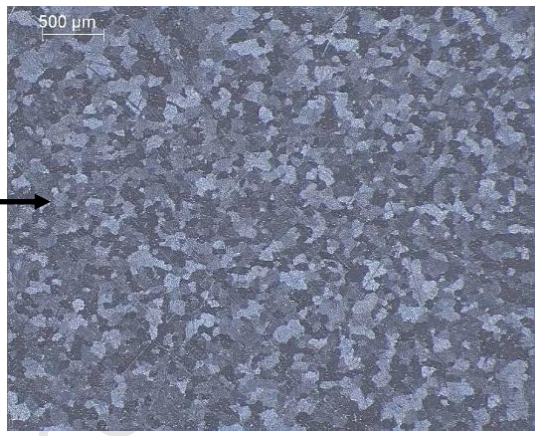

5.3.4.1(b) Centre low mag.

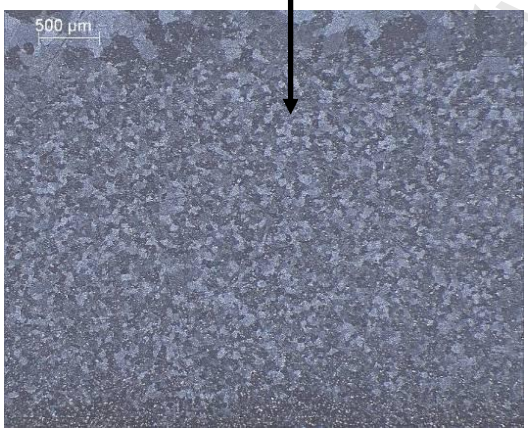

5.3.4.1(c) Edge low mag.

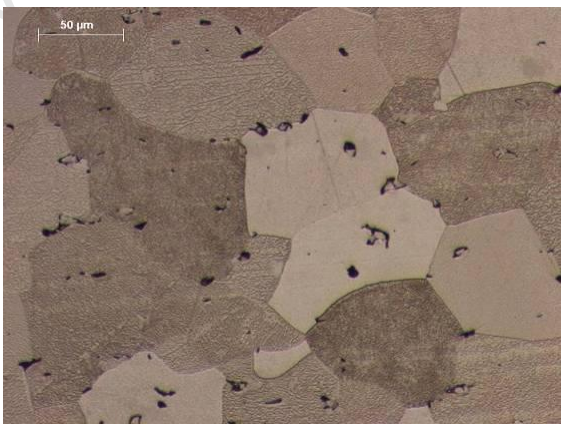

5.3.4.1(d) Centre higher mag.

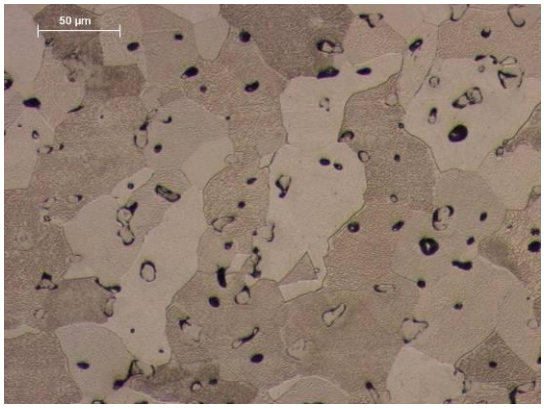

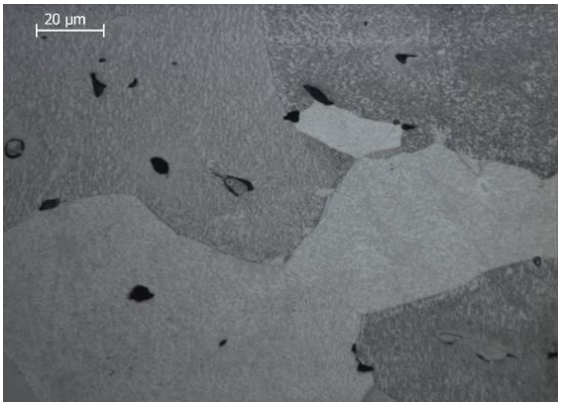

5.3.4.1(e) Edge higher mag.

5.3.4.1(f) Centre higher mag. view than (d)

Interpretation of microstructures 5.3.4.1(a)-(f):

We can identify that there are three distinct regions in the sample. Each region has a different average grain size. Small grains are located at the centre of the sample which experienced the higher amount of strain overall. As we move away from the centre the grain size has increased substantially, this area has experienced less strain than the centre but more strain than the edges. Near the edges where the lowest strain occurs (close to 0) the grains appear to be the smallest and are unaffected by the annealing, other than a small amount of grain growth and show no signs of further recrystallization. The three distinct regions are the result of metadynamic recrystallization occurring in the sample. In other words recrystallization initiated dynamically, but only propagated to a significant extent during post deformation annealing.

In the centre of the sample the smaller grains are formed when subgrains are created under strain during deformation. These form many nuclei for new grain development during recrystallization. This results in grains which are finer than the grains in the original deformed microstructure.

The larger grains in the area between the centre of the sample and the edges are formed due to a smaller strain gradient in this region and consequently fewer recrystallization nuclei form from the lower strain experienced during deformation. These few nuclei form new grains during recrystallization which absorb neighbouring subgrains with low angle grain boundaries as well as adjacent grains which do not have nuclei for recrystallization. This results in grains which are larger than the original grain structure.

Nominal strain = 0.5

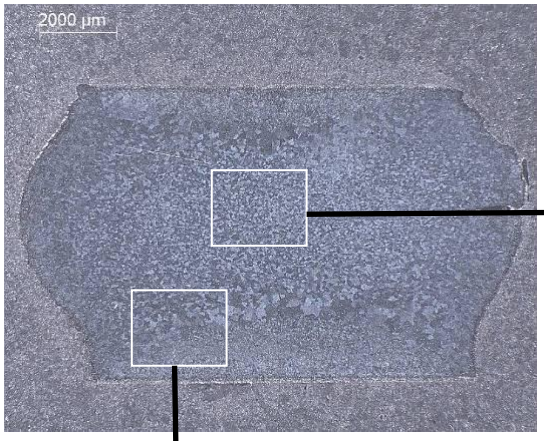

5.3.4.2(a) Overview low mag.

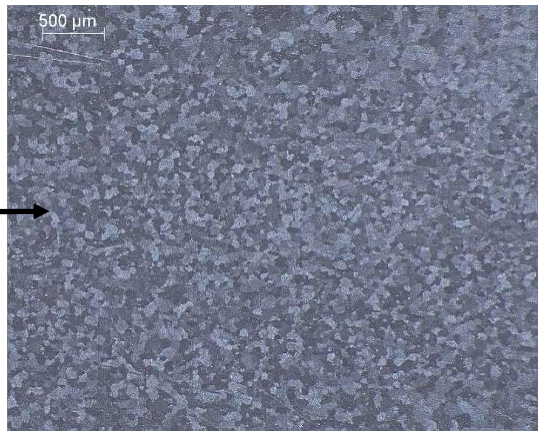

5.3.4.2(b) Centre low mag.

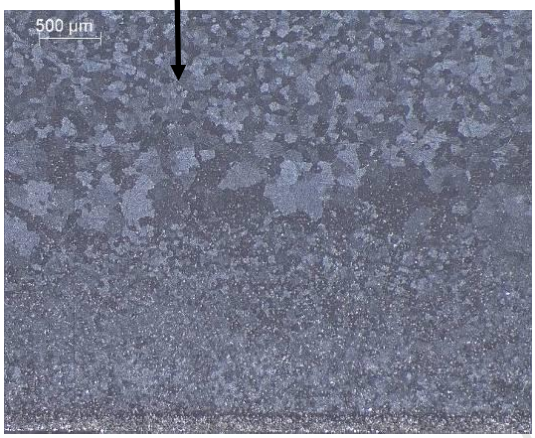

5.3.4.2(c) Edge low mag.

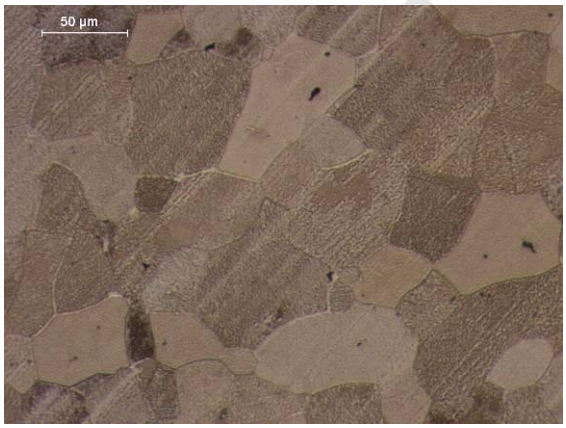

5.3.4.2(d) Centre higher mag.

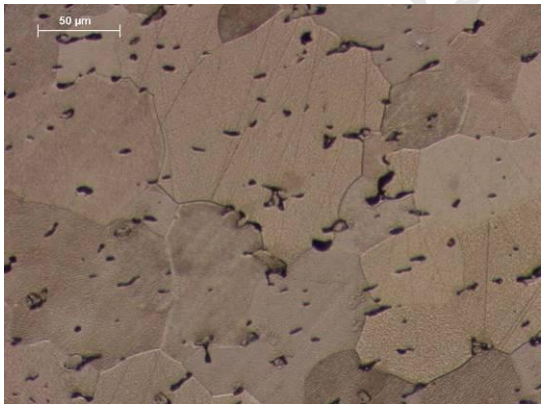

5.3.4.2(e) Edge higher mag.

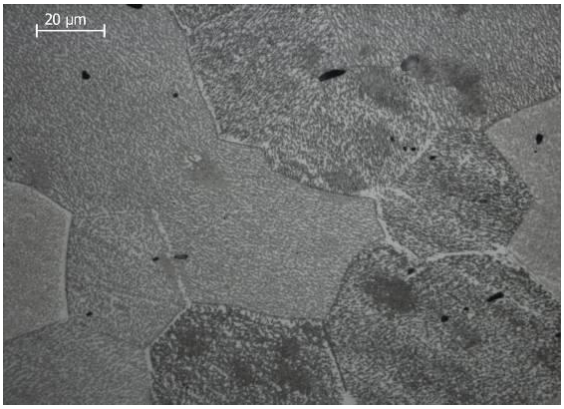

5.3.4.2(f) Centre higher mag. view than (d)

Interpretation of microstructures 5.3.4.2(a)-(f):

The volume in the centre of the sample which has the smaller recrystallized grains is larger than that of the sample which has undergone hot compression at a nominal strain of 0.2. The average size of the grains also appear smaller than those which underwent a nominal strain = 0.2. The intermediate strain volume is also reduced as well as the apparent size of the grains in this region when compared to those of the sample which had undergone a nominal strain of 0.2. The region which experienced the least amount of strain occurs along the edges of the sample and does not exhibit recrystallization during annealing, occupies a smaller volume than the sample which had undergone a nominal strain = 0.2.

Nominal strain = 0.65

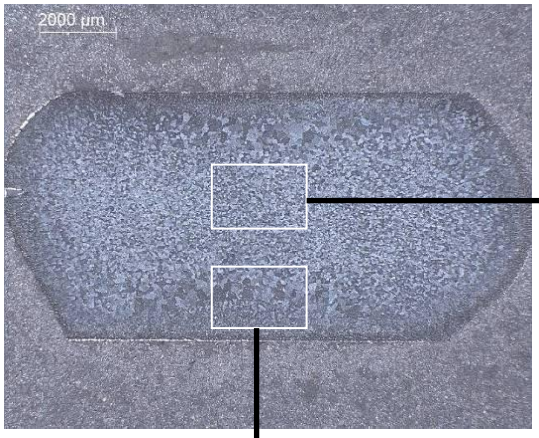

5.3.4.3(a) Overview low mag.

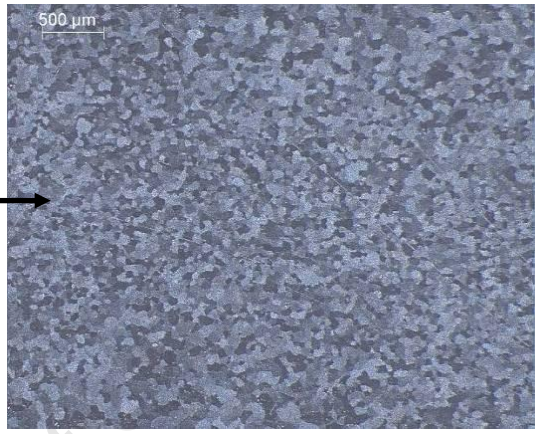

5.3.4.3(b) Centre low mag.

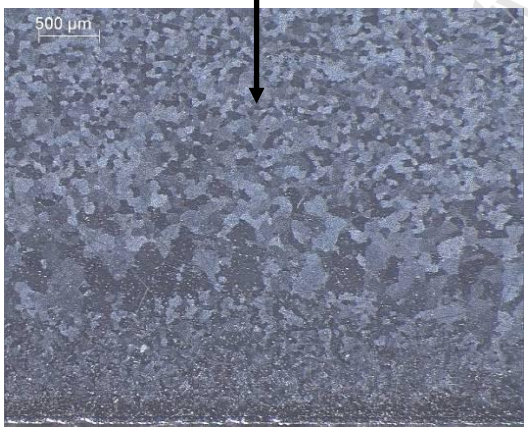

5.3.4.3(c) Edge low mag.

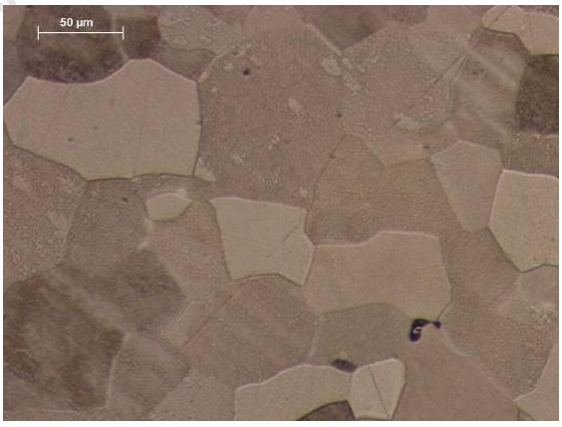

5.3.4.3(d) Centre higher mag.

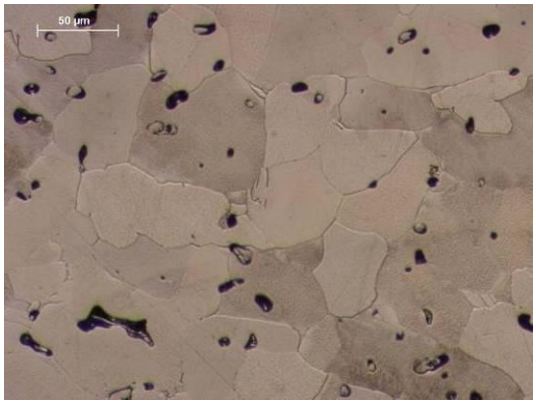

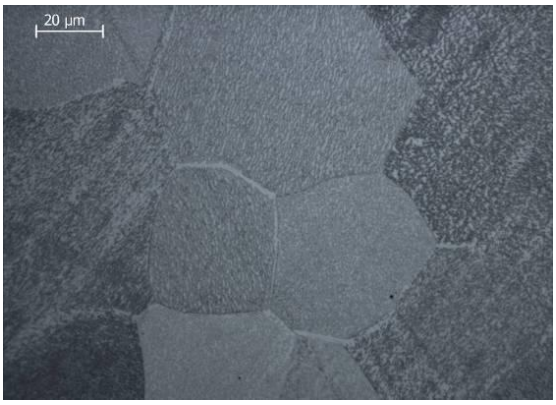

5.3.4.3(e) Edge higher mag.

5.3.4.3(f) Centre higher mag. view than (d)

Interpretation of microstructures 5.3.4.3 (a)-(f):

The area in the centre of the sample which contains the recrystallized grains has a larger volume than that of the sample which has undergone hot compression at a nominal strain of 0.5. The microstructure of the sample is now dominated by the recrystallized grains. The volume of the intermediate strain area is also reduced as well as the size of the grains in this region when compared to those of the sample which had undergone a nominal strain of 0.2 but are similar in both ways to those of the sample which has underwent a nominal strain =0.5. The region which experienced the least amount of strain occurs along the edges of the sample and does not exhibit recrystallization during annealing is occupying a smaller volume than the samples which had undergone nominal strains of 0.2 and 0.5.

5.4 Comparison of the microstructures of post deformation annealed wrought Ti with those of the post deformation annealed sintered Ti

The microstructure of the samples which have undergone hot compression testing at 900°C for nominal strains = 0.2 and 0.5 prior to post deformation annealing are assessed and compared in the sections below.

5.4.1 Wrought Ti vs. Sintered Ti at a nominal strain = 0.2

Sintered Ti has three distinct regions of varying grain size similar to the wrought Ti. Both samples have smaller grains at the edges of the samples where recrystallization did not occur during hot compression or during the post deformation annealing process. This is due to the edge regions having the lowest retained internal strain (almost zero) during hot compression. Under high magnification it can be seen that the grains in the centre of the wrought sample are larger than the original grains but have an irregular shape. Clearly the sample has not undergone recrystallization. This is the result of the sample having insufficient retained strain for nucleation and initiation of recrystallization.

During post deformation annealing, the irregular shaped grains grow rapidly due to the effect of the temperature on the sample. Grain growth is more dominant during the deformation cycle than during the post deformation annealing treatment for the wrought titanium as the maximum temperature during deformation is 900°C and the maximum temperature during annealing is 870°C. In the sintered sample recrystallization results in small equiaxed grains which are smaller than the grains in the centre of the sample and the middle region (between the centre and the edges) in the sintered sample.

In the sintered sample it can be noticed that the grain growth is inhibited resulting in a high degree of recrystallization with very little grain growth. The pores themselves actually prevent grain growth in the adjacent grains as the grains cannot grow into the pores as they are essentially empty space. Also Ti powders have a fine layer of oxide on the individual powder particles which act as interstitial atoms in the sintered metal pinning dislocations and preventing the migration of grain boundaries needed for rapid grain growth.

5.4.2 Wrought Ti vs. Sintered Ti at a nominal strain = 0.5

As in the sample which had undergone a nominal strain = 0.2, the sintered Ti has three distinct regions of varying grain size similar to that of the wrought Ti. Both samples have smaller grains at the edges of the samples where recrystallization did not occur before or during the annealing process. This is due to the edges being the regions that have the lowest retained internal strain in the entire sample. It can be observed that the volume of grains in the centre of the sample which has the highest amount of retained internal strain is larger in the sintered Ti sample than in the wrought Ti sample. Post deformation annealing reveals that recrystallization is the dominant restoration process for sintered Ti samples while grain growth is the dominant restoration process for the wrought sample. This is because in the sintered sample grain growth is inhibited resulting in a high degree of recrystallization with very little grain growth.

There are two important factors which are responsible for this phenomenon. The first is that the porosity inhibits grain boundary migration by acting as obstacles. The grains cannot grow into the empty space of the pores resulting in the pinning of the grain boundary. This contributes to the restriction of the grain growth of the sample during the compression cycle but as the porosity decreases this effect is diminished. Another factor that affects grain boundary migration is the presence of impurities on the surface of the powder particles. It is highly likely that oxides are present on the surface of the CP-Ti powder given titanium's affinity for oxygen. This results in interstitial oxygen contaminating the grain boundaries. This contamination is probably the primary cause of the inhibition of grain growth in the sintered Ti sample. This factor is also not affected by the reduction in porosity during hot compression. It is also possible that the amount of subgrains which act as nucleation sites for initial recrystallization are higher in the sintered sample than in the wrought sample but this can only be proved by Electron Backscattered Diffraction (EBSD) analysis of the as deformed wrought and sintered samples which have not undergone post deformation annealing.

6 CONCLUSIONS

The hot compression testing was used to investigate the effects of hot deformation on the sintered CP-Ti compacts. We found that by applying various strains at a temperature of 900°C we could reduce the porosity of the sample and deform its microstructure which increased the hardness of the sintered CP-Ti. We also found that partial recrystallization was occurring in samples which had undergone hot compression under nominal strains of 0.5 and 0.65. The resulting recrystallized microstructure has smaller grains than that of the parent sintered CP-Ti samples. Thus hot deformation e.g. hot compressing can be used to reduce porosity and refine microstructure leading to an improvement in the mechanical properties of the sintered CP-Ti made from direct reduction powders.

A series of more specific conclusions were drawn which formed the platform upon which the main conclusion could be made:

- A hot compression testing rig was successfully designed and built to accurately simulate the hot rolling process.

- Sintered titanium compacts that represent metal made by the Direct Powder Rolling method can made by uniaxial pressing and then sintered at 1200°C in a vacuum furnace, at a vacuum of 10^{-4} Torr.

- The critical strain (ε_c) needed to initiate recrystallization in wrought CP-Ti at 900°C has been determined to be a nominal strain of at least 0.5. This was determined by the hot compression of the wrought CP-Ti samples.

- The initiation of recrystallization cannot be clearly observed in the hot compression wrought CP-Ti samples due to the initial fine grain structure but can be observed once the samples have undergone post deformation annealing.

- The micro-hardness testing of the hot compressed wrought titanium samples show that at 800°C the increase in the hardness is due to work hardening but at 900°C and above the hardness testing shows no significant increase in the hardness of the samples which indicates that post-deformation softening has occurred in the samples which have undergone hot compression.

- In the wrought Ti samples deformed at 800°C to ε = 0.2 and 0.5, 900°C to ε = 0.5 and 1000°C to ε =0.5 and sintered Ti samples deformed at 900°C to ε = 0.2, 0.5 and 0.65; recrystallized grains which are equiaxed in shape could clearly be observed once they had undergone the post deformation annealing treatment.

- After post deformation annealing, the recrystallized grains in the sintered Ti sample which experienced a nominal strain of 0.5 are similar in size to those in the sample which had experienced a nominal strain of 0.65.

- In the as deformed sintered Ti samples, the deformed grains in the samples which had undergone a nominal strain of 0.5 and 0.65 have jagged looking grain boundaries which are thought to be a sign of the initiation of recrystallization.

- Hot compression greatly reduced the amount of pores and promoted the sintering process in the sample. At a nominal strain of 0.65 almost no pores are visible.

- Micro-hardness testing shows an increase in the hardness of the hot compressed sintered CP-Ti compacts with increasing nominal strain. This is mainly due to work hardening during hot compression with the collapse and subsequent reduction in porosity and/or the refinement of the grain structure by recrystallization also contributing to the increase in hardness.

- In the sintered Ti samples the post deformation annealing resulted in further recrystallization of the grains which were deformed during hot compression.

- The microstructures of both the wrought and the sintered Ti samples are observed having three distinct regions which are caused by the following factors:

i) Strain gradient – the sample has a gradient of retained strain with the highest retained strain present in the centre of the sample and decreasing to zero retained strain at the edges of the sample. Regions with the highest retained strain had the smallest recrystallized grains. The medium retained strain regions had larger recrystallized grains and the regions with the lowest retain strain had no recrystallized grains at all.

ii) Inhomogeneous temperature distribution – the heating of the samples is provided by an induction heating coil which only affects materials in which eddy currents can be induced i.e. metallic materials. The platens are ceramic in nature and are therefore not affected by the heating coil. The ceramic platens act as heat sinks drawing the heat out from the faces of the sample which are in contact with the platens. This results in the centre of the sample being the closest to the set point temperature and rest of the sample becoming cooler toward the surface of the sample. The temperature of the samples also effects the grain growth within the samples. The warmers regions have more grain growth than the cooler regions.

iii) The dead zone at the sample faces in contact with the platens – this effect is due to the barrelling of the cylindrical shaped sample during hot compression testing. The friction present during compression causes the surface of the sample in contact with the platens to continually fold over exposing new material to the platen. This prevents strain from building up at the faces of the sample creating a dead zone which has zero strain.

7 FUTURE WORK

The following recommendations are made in the anticipation that further investigation will be made into the effects of hot deformation on sintered titanium. The techniques and equipment used for this project can be used to further our present understanding of the microstructural evolution of the sintered titanium metal made by the Direct Rolling method of titanium powder metallurgy.

- Electron Backscatter Diffraction (EBSD) analysis on the deformed microstructures of both the wrought CP-Ti and the sintered CP-Ti could be conducted to measure the amount of high angle grain boundaries in the regions of the deformed microstructures which have the highest amount of retained internal strain. The aim would be to determine if the sintered samples have more nucleation sites for recrystallization in comparison with the wrought samples which have undergone the same deformation parameters.

- Higher nominal strains, above 0.65 could be introduced to the sintered CP-Ti samples to increase deformation and the degree of partial recrystallization that occurs under hot compression. When this step is followed by post deformation annealing it will result in the recrystallization of the entire sample. In order to increase the nominal strain, modifications will need to be made to the compression platens of the hot compression testing facility.

- CP-Ti is not as extensively used as the Ti-6Al-4V alloy which has better mechanical properties than the pure metal but is more expensive to produce. Therefore investigations into producing the Ti-6Al-4V alloy by mixing blended elemental powders and/or pre-alloyed powders, uniaxially compressing the powders into green compacts and then sintering would be beneficial.

- Sintering kinetics differs between the CP-Ti and the Ti-6Al-4V, which requires further sintering trials to produce a homogeneous alloy and reduce porosity. Modifications to the vacuum furnace used to sinter the CP-Ti will be needed as the alloy would require a higher sintering temperature beyond the current upper limit of the furnace. The microstructure of samples made with the blended elemental powders could be compared with sample made with pre-alloyed powders.

- The sintered Ti-6Al-4V would have different mechanical properties and would require different testing and heating parameters during hot compression testing. The induction heating and temperature controller would have to be recalibrated for the efficient and accurate heating of the Ti-6Al-4V alloy.

8 BIBLIOGRAPHY

1. Prof. S. Gleixner. “Characterization of particulate debris obtained from failed orthopaedic implants, Chapter 5 – Mechanical Metallurgy and Passivation of Titanium Implant Alloys”. San José State University, Charles W. Davidson College of Engineering. http://www.engr.sjsu.edu/WofMatE/srproject/srproj5.html (Last date visited: 02-06-2010)

2. “Grade 1 Commercially Pure Titanium”. Titaniumart. http://www.titaniumart.com/titanium-info-cp.html (Last date visited: 02-06-2010)

3. V.S. Moxson, V.A. Duz, J.W. Adams and W.N. Roy, **Low Cost Titanium Components for armour and structural applications**, *Titanium 2005*

4. M.J. Tan and X.J. Zhu, **Microstructure evolution of CP Titanium during high temperature deformation**, *Archives of Materials Science and Engineering*, Volume 28, Issue 1, January 2007, pages 5-11

5. R.C. Rice, J.L. Jackson, J. Bakuckas and S. Thompson, **Metallic Materials Properties Development and Standardisation (MMPDS) Scientific Report** January 2003, *National Technical Information Service*, Springfield (NTIS), Virginia 22161

6. H.K.D.H. Bhadeshia. “Metallurgy of titanium and its alloys”. University of Cambridge: Department of Material Science and Metallurgy. http://www.msm.cam.ac.uk/phase-trans/2004/titanium/titanium.html (Last date visited: 02-06-2010)

7. “Ti-6Al-4V (Grade 5), Annealed”. ASM Aerospace Specification Metals Inc. http://asm.matweb.com/search/SpecificMaterial.asp?bassnum=MTP641 (Last date visited: 02-06-2010)

8. F.H. Froes. “Developments in Titanium P/M”. Institute for Materials & Advanced Processes (IMAP), University of Idaho. http://www.webs1.uidaho.edu/imap/MPR%20Paper.pdf (Last date visited 02-06-2010)

9. F. Thümmler and R. Oberacker**, Introduction to powder metallurgy**, *The Institute of Materials Series on Powder Metallurgy*, series editors: I. Jenkins and J.V. Wood, 1993.

10. “Student information, C. Key steps in PM processing, 1. Manufacture of Metal Powders. Metal Powder Industries Federation. http://www.mpif.org/apmi/doc4.htm (Last date visited: 02-06-2010)

11. M. Mitkov and D. Božić, **Hydride-dehydride conversion of solid Ti-6Al-4V to powder form**, *Materials characterization* 37:53-60 (1996)

12. F.H. Froes, **The production of low cost titanium powders**, *Journal of Materials*, September 1998

13. S.J. Gerdemann, **Titanium process technologies**, *Advanced Materials & Processes*, July 2001

14. R.M. German, **Powder Metallurgy Science**, Second Edition, *Metal Powder Industries Federation*, 1994

15. "Zinc Stearate". chemBlink – Online Database of Chemicals from Around the World. http://www.chemblink.com/products/557-05-1.htm (Last date visited: 02-06-2010)

16. V.S. Moxson, V.A. Duz, J.W. Adams and W.N. Roy, **Low Cost Titanium Components for armour and structural applications**, *Titanium 2005*

17. V.A Druz, V.S. Moxson, R. Chernenkoff, W.F. Jandeska Jnr., and J. Lynn, **Blending an elemental approach to volume titanium manufacture**, *Journal of Materials*, November 2006.

18. F.H. Froes, S.J. Mashl, V.S. Moxson, J.C. Hebeisen and V.A. Duz, **The technologies of titanium powder metallurgy**, *Journal of Materials*, November 2004.

19. G. Greetham. "Powder Metallurgy – Component manufacture by Uniaxial Pressing". The A to Z of Materials. http://www.azom.com/details.asp?ArticleID=155 (Last date visited: 02-06-2010)

20. V.S Moxson, O.N Senkov and F.H Froes, **Innovations in titanium powder processing,** *Journal of Materials,* May 2000

21. *Metals Handbook*, Ninth Edition, **Volume 8 – Mechanical Testing**, pages 581-584

22. *Metals Handbook*, Ninth edition, **Volume 8 – Mechanical Testing**, pages 55-58

23. F.J. Humphreys and M. Hatherly, **Recrystallization and related annealing phenomena**, *Elsevier Science Limited*, 1995

24. P. Cotteril and P.R Mould, **Recrystallization and grain growth in metals,** *Surrey University press*, 1976, Chapter 9

25. M. Hayashi, H. Yoshimura, M. Ishii and H. Harada, **Recrystallization behaviour of commercially pure titanium during hot rolling,** *Nippon Steel technical report no.62,* July 1994

26. T. Furuhara, B. Poorganji, H. Abe and T. Maki, **Dynamic recovery and recrystallization in titanium allots by hot deformation,** *Journal of Materials,* January 2007

27. P. Johnson. "Understanding a PID controller". McShane Inc. http://mcshaneinc.com/html/Library_UnderstandingPID.html (Last date visited 02-06-2010)

28. "Temperature control – Tuning a PID (Three mode) Controller". Omega.com http://www.omega.com/temperature/z/pdf/z115-117.pdf (Last date visited: 02-06-2010)

29. L.X. Li, D.S. Peng, J.A. Liu and Z.Q Liu, **An experiment of the lubrication behaviour of graphite in hot compression tests of Ti-6Al-4V alloy**, *Journal of Materials Processing Technology* 112 (2001) 1-5

30. G.F. Vander Voort, **METALLOGRAPHY Principles and Practice**, *McGraw-Hill Materials Science and Engineering Series*, 1984, Chapter 6-6

31. K.P. Rao and E.B. Hawbolt, **Development of constitutive relationship using compression of a medium carbon steel**, *ASME J. Eng. Ind.* 114(1992)116

32. G. Fernández and V. Gerardo. "Constitutive relations to model the hot flow of commercial purity copper – 2 Experimental Procedure". TDX – Tesis Doctorals en Xarxa. http://www.tesisenxarxa.net/TESIS_UPC/AVAILABLE/TDX-0104105-092144//04Vggf04de11.pdf (Last date visited: 02-06-2010)

9 APPENDICES

9.1 Schematic showing the designed and manufactured components of the Hot Compression Testing Rig once assembled

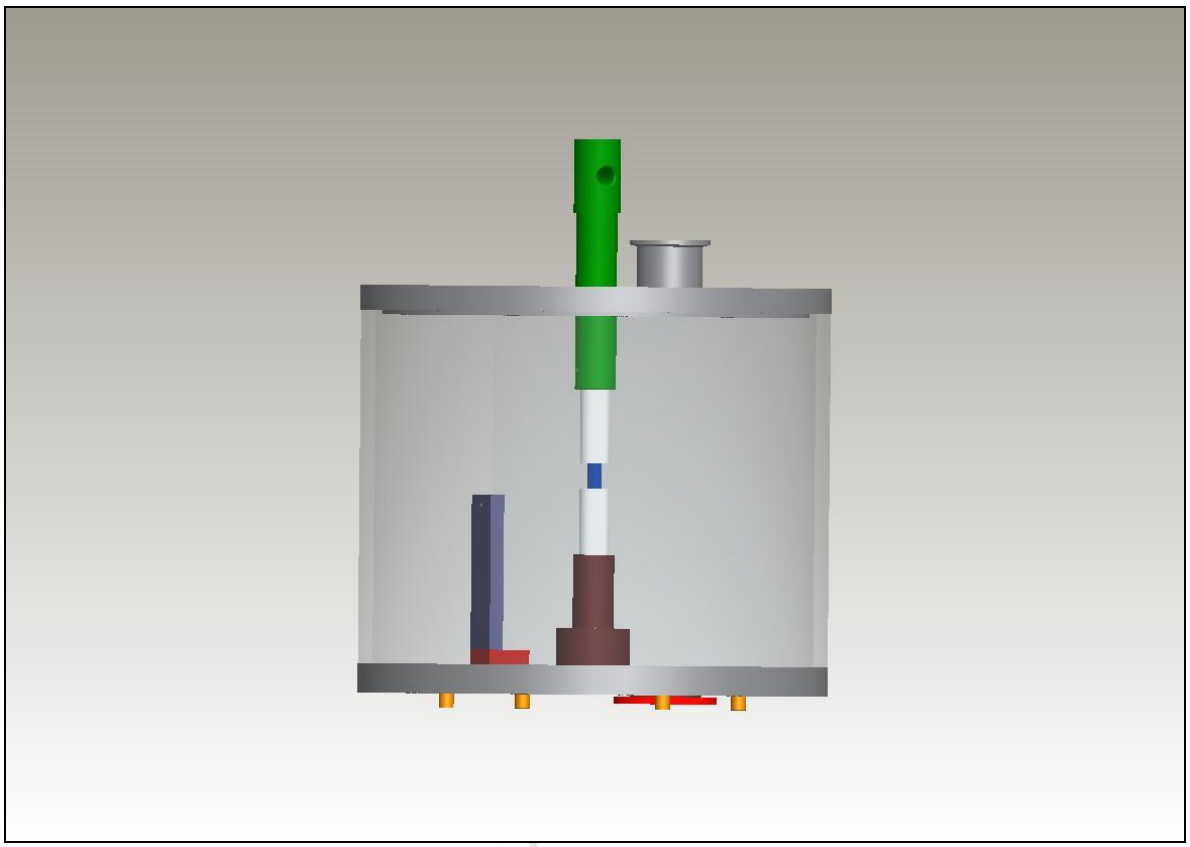

9.2 Technical drawings of the designed and manufactured components (drawings 1-13)